İSTANBUL TECHNICAL UNIVERSITY ★ INSTITUTE OF SCIENCE AND TECHNOLOGY

LASER SYSTEMS FOR BIOMEDICINE: INTRODUCING THE 980 NM DIODE LASER

Ph.D. Thesis by

Murat GÜLSOY, M.A., B.S.E.E.

(504920045012)

Date of submission : 26 January 2000

Date of defence examination: 01 May 2000

Supervisor (Chairman): Assoc.Prof.Dr. İnci ÇİLESİZ

Members of the Examining Committee Prof.Dr. Ertuğrul YAZGAN

Prof.Dr. Ercan TOPUZ

Assoc.Prof.Dr. Reşit CANBEYLİ (B.Ü.)

Prof.Dr. Sacit KARAMÜRSEL (İ.Ü.)

JANUARY 2000

İSTANBUL TEKNİK ÜNİVERSİTESİ ★ FEN BİLİMLERİ ENSTİTÜSÜ

BİYO-TIP İÇİN LASER SİSTEMLERİ: 980 NM DİYOT LASERİNİN SUNUMU

DOKTORA TEZİ
Murat GÜLSOY
(504920045012)

Tezin Enstitüye Verildiği Tarih : 26 Ocak 2000
Tezin Savunulduğu Tarih : 1 Mayıs 2000

Tez Danışmanı : Doç.Dr. İnci ÇİLESİZ
Diğer Jüri Üyeleri Prof.Dr. Ertuğrul YAZGAN
Prof.Dr. Ercan TOPUZ
Doç.Dr. Reşit CANBEYLİ (B.Ü.)
Prof.Dr. Sacit KARAMÜRSEL (İ.Ü.)

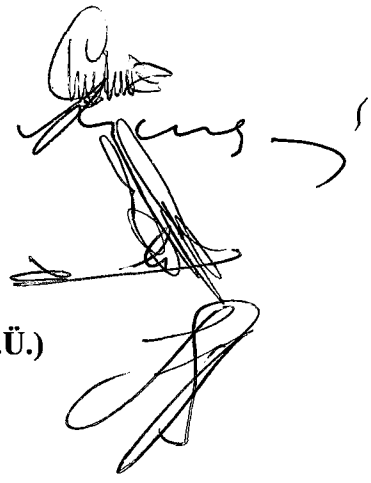

OCAK 2000

Acknowledgments

I would like to express my sincere gratitude to my supervisor Dr. İnci Çilesiz for her support throughout my graduate study. I must also thank Prof. Dr. Ertuğrul Yazgan, Tansu Çelikel, Adnan Kurt, Dr. Reşit Canbeyli, Dr. Alphan Sennaroğlu, Dr. Özlem Kurtkaya, Dr. Aydın Sav, Dr. Sacit Karamürsel, Dr. Kadir Durak for their contribution to my studies. I also want to emphasize the financial support of State Planning Organization (DPT Project ITU-97K121670), Istanbul Technical University Research Activities Secretariat, MITRA A.Ş., Teknofil Ltd. Şti., Koç University Physics Laboratory, Istanbul University Electrophysiology Laboratory, and Boğazici University Psychobiology Laboratory. I am also indepted to my wife Nazlı Ökten and my parents Selma and Turan Gülsoy for the morale support and encouragement.

TABLE OF CONTENTS

LIST OF ABBREVIATIONS

AC	: Alternative Current
ANOVA	: Analysis of Variance
CL	: Canine Irradiated Myocardium
CN	: Canine Normal Myocardium
DC	: Direct Current
EEG	: Electroencephalography
Er:YAG	: Erbium Yitrium Aliminum Garnet
HeNe	: Helium Neon
IMB	: Interceptal Middle Bottom Part
IMU	: Interceptal Middle Upper Part
IN	: Interceptal Nerve Bundle
IR	: Infrared
HA	: Human Cardiac Aneurism
HE	: Human Epicardium
HM	: Human Myocardium
KrF	: Krypton Flouride
LEP	: Laser Evoked Potential
Nd:YAG	: Neodyium Yitrium Aliminum Garnet
PDT	: Photodynamic Therapy
PMN	: Polymorphonuclear Neutrophil
PRP	: Pain Related Potential
TMLR	: Transmyocardial Laser Revascularization
UV	: Ultraviolet
VB	: Ventricule Bottom Part
VI	: Ventricule Inner Part
VM	: Ventricule Middle Part
VMB	: Ventricule Middle Bottom Part
VU	: Ventricule Upper Part
VUB	: Ventricule Upper Bottom Part

LIST OF TABLES

LIST OF FIGURES

Page No

LIST OF SYMBOLS

c	: Speed of light in vacuum
[c]	: Concentration of absorbing agents
cw	: Continuous Wave
d	: Thickness
e_i	: Energy Levels of Electrons
E	: Energy
E, E′and E″	: Electric field vectors of the incident, reflected, and refracted light
g	: Anisotropy factor
h	: Plank's constant
I	: Intensity
k′	: Extinction coefficient
λ	: Wavelength
μ_a	: Absorption Coefficient
μ_s	: Scattering Coefficient
υ	: Speed of light in a medium
n	: Index of refraction
p(θ)	: Probability Function
r	: Radius
θ	: Angle
W	: Watt
z	: Depth

LASER SYSTEMS FOR BIOMEDICINE: INTRODUCING THE 980 NM DIODE LASER

SUMMARY

The motivation of this study was to develop and study new surgical laser delivery systems for medical use. This manuscript consists of three main parts: the background chapter describing the basic physical principals of lasers (collimated, coherent and monochromatic nature of lasers), major parameters of laser-tissue interaction mechanisms (such as power, pulse duration, wavelength, absorption, scattering, propagation of light in biological tissue), laser-tissue interaction mechanisms (photochemical, thermal interactions, photoablation, plasma-induced ablation and photodisruption), recent medical applications of lasers; and secondly, chapters presenting and discussing the results of the studies (computer simulations performed; computer controlled laser beam delivery systems designed and developed; *in vitro* and *in vivo* experiments done, histologic examination procedures followed); and finally a conclusion chapter. In appendices, computer simulation technique applied; laser systems utilized (1064 nm Nd:YAG laser, 2094 nm Er:YAG laser; 980 nm diode laser) and power measurement methods were described. The original contributions of the present study are summarized below:

1. Different biological tissues were compared in terms of laser fluence distribution. The homogeneity of cardiac tissue due to Nd:YAG laser irradiation were pronounced. Experiments showed the coagulative effect of the widely known Nd:YAG laser and results provided evidence for the relevancy of Monte Carlo simulation technique.
2. Er:YAG laser was first applied on cardiac tissue and showed that it was a candidate for ablative purposes.
3. Original data were presented dealing with the effect of Er:YAG laser within cerebellar and cerebral tissues. Results were significant for the future applications of Er:YAG laser within brain tissue as an ablator.
4. The 980 nm diode laser was presented as a new surgical device for brain tissue. A computer controlled laser delivery system for the 980 nm diode laser was designed and developed. This surgical laser delivery system was adapted to stereotaxic surgical procedure and tested through *in vitro* and *in vivo* animal experiments. All possible aspects (laser dosimetry, different regimes of laser irradiation, histological examination of thermally altered tissue) of laser-tissue interaction implications were studied and the results providing concrete evidence for the benefits of this new laser system was reported first in the literature.
5. New possibilities of the 980 nm laser system were searched. It was tested for LEP (Laser Evoked Potential) studies as a pain stimulant. The experiments done on human subjects showed that this new laser system can be a better candidate than Nd:YAG laser for pain studies.

BİYO-TIP İÇİN LASER SİSTEMLERİ: 980 NM DİYOT LASERİNİN SUNUMU

ÖZET

Bu çalışmanın amacı, tıbbi uygulamalar için yeni cerrahi laser aktarım sistemleri geliştirmektir. Bu tez metni üç ana bölümden oluşmaktadır: laserlerin temel fiziksel ilkelerini (laserlerin dağılmadan düz gitme, tek renkli ve koheran olma özelliklerini), laser-doku etkileşim mekanizmalarının (güç, darbe süresi, dalgaboyu, soğurulma, saçılma ve biyolojik dokunun içinde ışığın yayılması gibi) başlıca parametrelerini, laser-doku etkileşim mekanizmalarını (fotokimyasal, ısıl etkileşimler, fotoablasyon, plazma kaynaklı ablasyon ve fotodisropsiyon), ve laserlerin tıptaki en son uygulamalarını açıklayan bir arkaplan bölümü; ikinci olarak yapılan çalışmaların (gerçekleştirilen bilgisayar benzetimleri, tasarlanıp geliştirilen bilgisayar denetimli laser ışını aktarma sistemleri, yapılan *in vitro* ve *in vivo* deneyler, izlenen histolojik inceleme süreci) sunulduğu ve tartışıldığı bölümler; ve son olarak bir sonuç bölümü. Eklerde uygulanan bilgisayar benzetim tekniği, kullanılan laser sistemleri (1064 nm Nd:YAG laser, 2094 nm Er:YAG laser; 980 nm diyot laser) ve güç ölçüm yöntemleri betimlenmiştir. Bu çalışmanın özgün katkıları aşağıda özetlenmiştir:

1. Farklı biyolojik dokular laser akısının dağılımı açısından karşılaştırılmıştır. Kardiyak dokunun Nd:YAG laser ışımasına göre homojenliği belirtilmiştir. Deneyler, yaygın olarak bilinen Nd:YAG laserinin koagülatif etkisini göstermiş ve sonuçlar Monte Carlo benzetim yönteminin uygunluğu yönünde kanıt sağlamıştır.
2. Er:YAG laseri kardiyak doku üzerinde ilk kez denenmiş ve ablasyon amaçları için aday bir sistem olduğu gösterilmiştir.
3. Er:YAG laserinin serebral ve serebellar dokulardaki etkilerine ilişkin özgün bulgular sunulmuştur. Sonuçlar, gelecekteki Er:YAG laserinin beyin dokusunda bir ablatör olarak kullanımı açısından önemli bulunmuştur.
4. 980 nm diyot laseri beyin dokusu için yeni bir cerrahi aygıt olarak sunulmuştur. 980 nm diyot laseri için bilgisayar denetimli laser aktarım sistemi tasarlanmış ve geliştirilmiştir. Bu aktarım sistemi stereotaksik cerrahi sürecine uyarlanmış ve *in vitro* ve *in vivo* hayvan deneylerinde sınanmıştır. Laser-doku etkileşim kapsamındaki tüm özellikler (laser dozimetrisi, laser ışımasının farklı rejimleri, ısıl olarak değişmiş olan dokuların histolojik incelenmesi) üzerinde çalışılmış ve bu yeni laser sisteminin yararı yönünde somut kanıtlar sağlayan sonuçlar literatürde ilk kez sunulmuştur.
5. 980 nm laser sisteminin yeni olanakları araştırılmıştır. LEP (Laserle Uyarılmış Potansiyeller) çalışmaları için bir ağrı uyarıcısı olarak denenmiştir. İnsan denekler üzerinde yapılan deneyler bu yeni laser sisteminin ağrı çalışmaları için Nd:YAG laserinden daha iyi bir aday olduğunu göstermiştir.

1. INTRODUCTION

The motivation of this study was to develop and study new laser delivery systems for medical use. The objectives of the study presented in this manuscript is summarized in the following:

a) Comparing the laser light propagation in different types of tissues.

b) Comparing the effects of various wavelengths of lasers in heart and brain tissues.

c) Studying the coagulation and ablation effects of various laser systems.

d) Design and development of a new medical laser delivery system.

e) Testing the new system via *in vitro* and *in vivo* experiments. Adapting the system to stereotaxic surgical procedure.

f) Searching other possible medical applications for the developed laser delivery system.

In the following parts of the background chapter, first the physical principles underlying laser phenomenon, collimated, coherent and monochromatic nature of laser light, classification due to the wavelength intervals are described. Second, major parameters of laser-tissue interaction are summarized; the optical and thermal characteristics of the tissue; the effects of the wavelength of laser beam, power or energy density of laser source; time duration of laser irradiation; and mode of laser system are discussed. Reflection, refraction, absorption and scattering phenomenons take place in biological tissue are defined. Then, main interaction categories of photochemical interactions, thermal interactions, photoablation, plasma induced ablation and photodisruption are explained. Finally, the new developments in medical applications of lasers are summarized.

In the preceding chapters, the results of the following studies are presented:

1. Design of a computer controlled laser delivery system.

2. Monte Carlo simulations of light propagation in different biological media such as human (bone, brain white matter, liver, prostate, epicardium, normal myocardium, lased myocardium) and canine (cardiac) tissues.
3. Coagulation of lamb heart tissue by the Nd:YAG laser.
4. Ablation of lamb heart tissue by the Er:YAG laser.
5. Ablation of rat brain tissue by the Er:YAG laser.
6. Application of the 980 nm Diode Laser in Stereotaxic Surgery.
    a) Predosimetry study of *in vitro* experiments
    b) Dosimetry study of *in vivo* experiments
    c) Experiments dealing with the effect of modulation of laser beam
7. Obtaining laser evoked potentials

Finally, the results of those studies are discussed.

2. BACKGROUND

2.1. Lasers Overview

The use of light in medicine had started just before the development of laser technology. The coagulative effect of xenon flash lamps had been investigated by Gerd Meyer-Schwickerath in 1956 in order to repair retinal detachments. After the first report on laser radiation by Maiman [1], lasers were applied in various areas of medicine starting with ophtalmology. Dentistry and other medical disciplines followed ophtalmology within years. Before dealing with the medical applications in detail, it would be useful to review the properties of lasers in general.

LASER is the acronym for Light Amplification by Stimulated Emission of Radiation. Laser light is monochromatic, collimated and coherent [2] as a result of stimulated emission (Figure 2.1.).

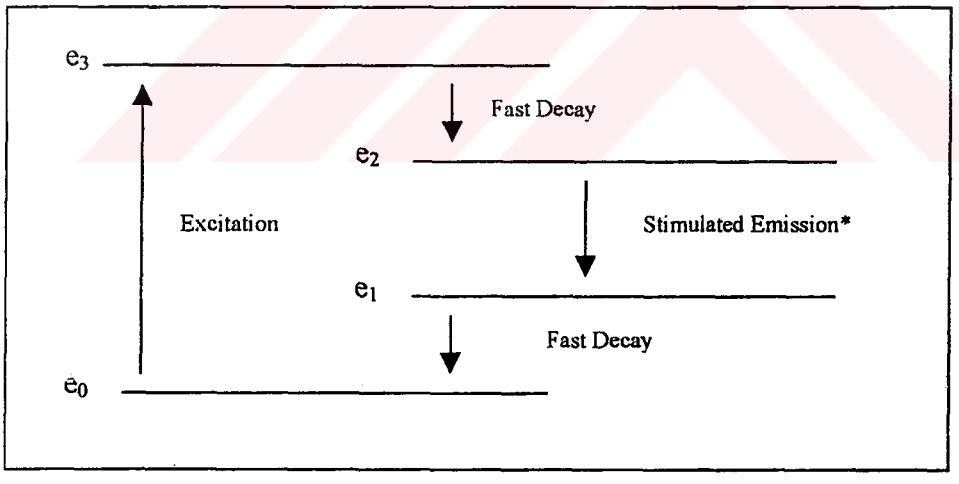

Figure 2.1. Stimulated emission of radiation in a four level energy diagram (A population inversion must exist between e_2 and e_1).

e_0 is the ground state and e_3 is the state that the energy of atom has been raised by an external excitation of a photon with an energy of e_3-e_0. Excited state e_3 is an unstable state and temporary. Thus, the excited atom relaxes back to a lower state either by conversion to thermal energy or by emission of light if population inversion takes place. The latter is called stimulated emission. External triggering is necessary to

excite atoms and to obtain photons in phase. If an atom is raised to an excited state, emission of a photon causes the energy of the atom drops to its original energy level. The emitted photon excites another atom like the first one. If there are many photons emitted then there will be many atoms excited and will be many emitted photons in phase and propagate in the same direction. If one can provide oscillation of photons in an optical medium, amplification can occur. In other words, if the lasing medium is contained within an optical cavity the repeated passes of the stimulated emission output can magnify the gain sufficiently to create a macroscopic electromagnetic mode which can build up to produce a coherent, monochromatic output. It is possible to pump the medium by an external source continually or by pulses. Thus a laser medium of finite length full of excited atoms and optical resonator make the laser output possible. The system that permits the generation of laser light consists of an optical cavity, a laser medium and two mirrors (Figure 2.2.). One of the mirrors must be partially transmitting in order to release the photons, namely laser light.

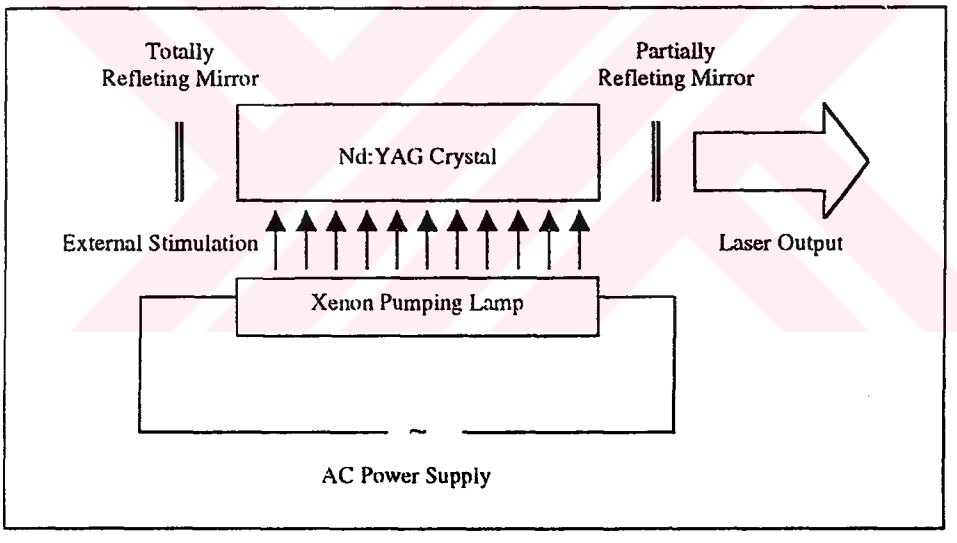

Figure 2.2. Schematic diagram of an Nd:YAG laser. In this example, laser medium is the Nd:YAG crystal itself. The crystal between two mirrors functions as an optical cavity also. External stimulation is provided by the xenon lamp. Laser output is obtained from the partially reflecting mirror.

Laser sources differ according to the type of the laser medium. The medium can be filled with gas (e.g. Ar^{++}, CO_2), dye or crystal (Nd:YAG, Erbium, Ruby). Semiconductor media are also available. The wavelength of laser radiation also varies with the material in the optical cavity. Medical lasers have wavelengths that extend from 193 to 10600 nm (Figure 2.3.). Lasers then can be classified according to the wavelength they radiate like UV (Ultraviolet), IR (Infrared), etc. Lasers can

also be identified by the type of the pumping function. In order to obtain a continuous wave laser output, laser medium needs to be pumped continuously. If the laser medium is pumped with pulses, then pulsed mode laser can be obtained. The range of pulse durations ranges from femtoseconds to several hundred microseconds.

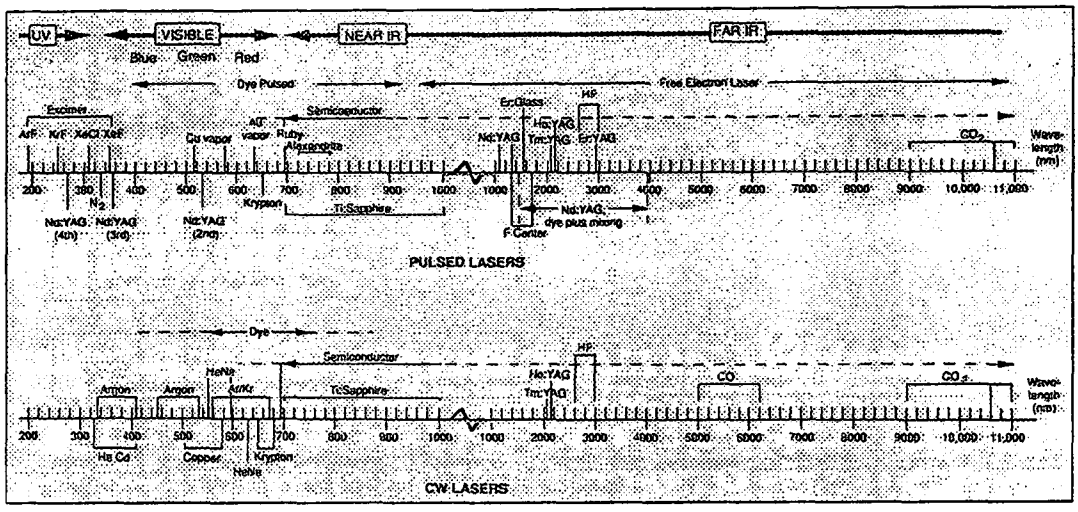

Figure 2.3. Spectrum of commercially available lasers [3].

The special properties of lasers can be summarized as:

(1) Spatial coherency.

(2) High intensity in both continuous wave and pulsed modes of operation.

(3) Monochromaticity.

(4) Short (controllable) pulse duration.

Spatial coherency refers to the fact that all of the laser light is in phase. Laser light intensity is very high when compared to other light sources. One of the reasons is that laser light is collimated and its divergence is low. Laser light is a monochromatic electromagnetic radiation; namely, it contains a single wavelength. The wavelength is associated with the energy difference between e_2 and e_1 (Figure 2.1.); in other words, it is related to the energy difference and can be denoted by the formula 2.1. where h is the Planck constant and λ is the wavelength:

$$E = \frac{hc}{\lambda} \qquad (2.1)$$

Biomedical laser applications can be classified as follows [4]:

(1) Laser diagnostics based on resonant and nonresonant laser-matter interaction.

(2) Laser therapy based on laser-induced molecular processes consequent upon excitation of certain molecules.

(3) Laser surgery based on laser induced destructive macroeffects. Only the third one is covered within the scope of this thesis.

2.2. Major Parameters of Laser-Tissue Interaction

Laser beam causes chemical, thermal and optical changes in the irradiated tissue. In this part, these interaction mechanisms are summarized in order to prepare a theoretical background for understanding the effect of Er:YAG, Nd:YAG and diode lasers on cardiac and brain tissues.

The interaction mechanisms are dependent on several parameters such as:

1. the optical and thermal characteristics of the tissue;
2. the wavelength of laser beam;
3. power or irradiance of laser source;
4. time duration of laser irradiation;
5. the mode of laser system.

Many studies have been done on laser-tissue interactions since the early medical applications of lasers [5-10]. The interaction mechanisms are classified as [10]:

a) photochemical,

b) thermal,

c) photoablation,

d) plasma-induced ablation and photodisruption.

First, the parameters related to laser-tissue interaction will be defined, then fundamentals of interaction mechanisms will be covered in the following sections.

The optical and thermal responses of tissue are the resultant changes to laser irradiation and are related to laser source characteristics as well as the optical and thermal properties of tissue [2].

When laser beam is incident on a slice of tissue, reflection, refraction, absorption and scattering take place (Figure 2.4.).

Reflection is the returning of incident light by the surface. Reflection angle (θ') equals the incident angle (θ) and they are on the same plane (plane of incidence) with the normal of the reflecting surface. Reflection phenomenon is dependent on the smoothness of the surface; if it is smooth enough specular reflection takes place, if the roughness of the surface is larger then the wavelength of radiation there exists diffuse reflection. This means that some of the reflected rays do not lie in the plane of incidence. Diffuse reflection occurs at surfaces of all tissues.

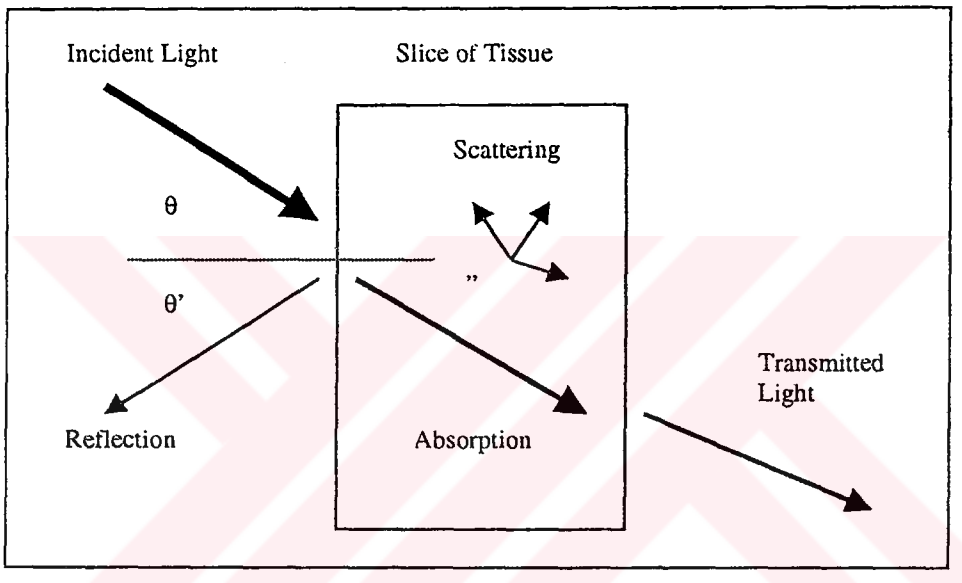

Figure 2.4. Reflection, refraction, absorption and scattering of light within a slice of tissue.

Refraction occurs if two media separated by the reflecting surface have different indices of refraction. There is a change in speed of light due to the difference in indices of refraction. Snell's law gives the mathematical relation due to refraction [10]:

$$\text{Sin}\,\theta \,/\, \text{Sin}\,\theta'' = \upsilon \,/\, \upsilon' \qquad (2.2)$$

where θ is the angle of incident beam, θ'' is the angle of refraction, υ is speed of light in the first media, and υ' is speed of light in the second media. If indices of refraction is defined as

$$n = c/\upsilon \text{ and } n' = c/\upsilon' \qquad (2.3)$$

where, c is the speed of light in vacuum. Then Snell's law can be expressed as:

$$n \sin\theta = n' \sin\theta'' \tag{2.4}$$

Reflectivity and reflectance are measures of the amount of reflected light and corresponding intensities, respectively, and they depend on the angle of incidence, the polarization of light and the indices of refraction. Fresnel's laws define the relations for reflectivity and refraction.

$$\frac{E_S'}{E_S} = -\frac{\sin(\theta-\theta'')}{\sin(\theta+\theta'')} \tag{2.5a}$$

$$\frac{E_P'}{E_P} = \frac{\tan(\theta-\theta'')}{\tan(\theta+\theta'')} \tag{2.5b}$$

$$\frac{E_S''}{E_S} = \frac{2\sin\theta''\cos\theta}{\sin(\theta+\theta'')} \tag{2.5c}$$

$$\frac{E_P''}{E_P} = \frac{2\sin\theta''\cos\theta}{\sin(\theta+\theta'')\cos(\theta-\theta'')} \tag{2.5d}$$

E, E′ and E″ are amplitudes of the electric field vectors of the incident, reflected, and refracted light, respectively. Subscripts s and p denote the two planes of oscillation with s being perpendicular to the plane of incidence and p being parallel to the plane of incidence.

Biological tissues contain water in high percentages (60-80%) [11]. Thus, the response of water plays a significant role in the optical response of the biological tissue especially in the IR ($\lambda > 1500$ nm). Indices of refraction and reflectances of water change with the wavelength of the light (Table 2.1.).

When electromagnetic radiation passes through a medium, light energy is converted into heat due to excitation of molecules, which is called resonance absorption [2]. This process results in attenuation of incident energy. The absorbance of a medium is defined as the ratio of absorbed and incident intensities. Absorption is a wavelength dependent property of materials. Since, the rate of heat generation depends on the rate of absorption and scattering takes place, it is one of the significant factors in laser-tissue interaction process.

Table 2.1. Indices of refraction and reflectance of water [10].

Wavelength (μm)	Index of Refraction	Reflectance	Wavelength (μm)	Index of Refraction	Reflectance
0.2	1.396	0.027	2.9	1.201	0.008
0.3	1.349	0.022	3.0	1.371	0.024
0.4	1.339	0.021	3.1	1.467	0.036
0.5	1.335	0.020	3.2	1.478	0.037
0.6	1.332	0.020	3.3	1.450	0.034
0.7	1.331	0.020	3.4	1.420	0.030
0.8	1.329	0.020	3.5	1.400	0.028
0.9	1.328	0.020	4.0	1.351	0.022
1.0	1.327	0.020	5.0	1.325	0.020
1.6	1.317	0.019	6.0	1.265	0.014
2.0	1.306	0.018	7.0	1.317	0.019
2.6	1.242	0.012	8.0	1.291	0.016
2.7	1.188	0.007	9.0	1.262	0.013
2.8	1.142	0.004	10.0	1.218	0.010

Absorption is described by the relations called Lambert-Beer's law:

$$I(z) = I_o \exp(-\mu z), \qquad \text{Lambert's law} \qquad (2.6)$$

$$I(z) = I_o \exp(-k'[c]z), \qquad \text{Beer's law} \qquad (2.7)$$

$$z = 1/\mu \ln[I_o / I(z)], \qquad \text{Lambert-Beer's law} \qquad (2.8)$$

where z denotes the path on the optical axis, I(z) is the intensity at a distance z, I_o is the incident intensity, μ is the absorption coefficient of the medium, [c] is the concentration of absorbing agents, and k′ denotes the extinction coefficient dependent on internal parameters.

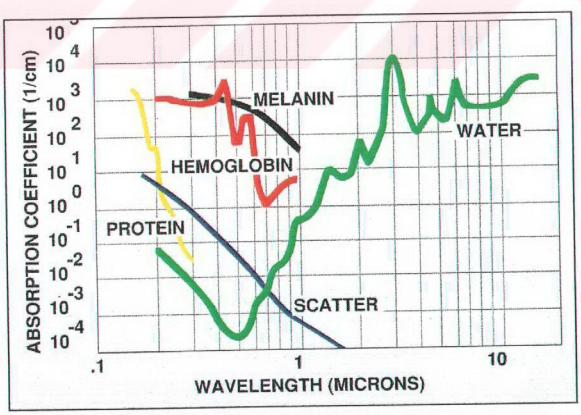

Figure 2.5. The absorption spectra of water, pigments, melanin and hemoglobin with respect to the wavelength of radiation. Horizontal axis corresponds to the wavelength and vertical axis corresponds absorption coefficient (1/cm).

For biological tissues absorption is determined by the absorption of water and macromolecules such as proteins and pigments. Figure 2.5. shows the absorption spectra of water, pigments, melanin and hemoglobin [12].

Scattering is another phenomenon that takes place in the irradiated tissue. It occurs at frequencies not corresponding to the natural frequencies of particles at which those of the particles resonate with the applied electromagnetic waves. The portions of scattered light reflected from or transmitted through tissue depend upon internal reflectances and absorption properties of the tissue.

Two types of scattering are defined: elastic and inelastic scattering. If the incident and scattering photons have the same energy, it is called elastic scattering. Widely known Rayleigh scattering is a kind of elastic scattering. In that case, scattering particles are smaller than the wavelength of incident radiation. Scattering is inversely proportional to the fourth power of wavelength:

$$Is \sim 1 / \lambda^4 \text{ or} \tag{2.9}$$

$$Is(\theta) \sim [1+Cos^2(\theta)] / \lambda^4 \tag{2.10}$$

In Figure 2.6., it is observed that Rayleigh scattering is therefore reduced within the visible spectrum with increasing wavelength [10].

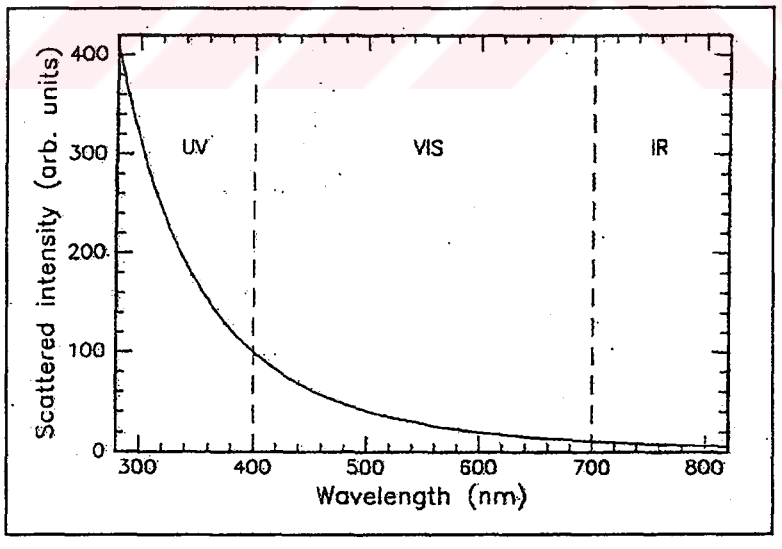

Figure 2.6. Rayleigh scattering due to wavelength.

Another type of scattering is Mie scattering which differs from Rayleigh scattering in two aspects. First, Mie scattering preferably occurs in the forward direction and

second, Mie scattering has less dependence on wavelength ($\sim \lambda^{-x}$ with $0.4 \leq x \leq 0.5$) compared to Rayleigh scattering ($\sim \lambda^{-4}$).

Unfortunately, neither Rayleigh nor Mie scattering can exactly describe the scattering that takes place in biological tissues. Because, scattering in tissue is mostly in forward direction (Rayleigh scattering can not describe this condition) and it depends strongly on wavelength (Mie scattering can not predict this condition). In order to explain the scattering phenomenon, a probability function $p(\theta)$ of a photon is defined. If $p(\theta)$ does not depend on θ, it is called isotropic scattering. If it depends on θ, it is called anisotropic scattering. The coefficient of anisotropy g, is a measure of anisotropy and is defined as:

$$g = \frac{\left[\int 4\pi\, p(\theta) \cos\theta \, dw\right]}{\left[\int 4\pi\, p(\theta)\, dw\right]} \qquad (2.11)$$

(Special cases: g = 1 purely forward scattering; g = 0 isotropic scattering; g = -1 purely backward scattering)

2.3. Laser-Tissue Interaction Mechanisms

Main interaction categories will be discussed in this part. Those are photochemical interactions, thermal interactions, photoablation, plasma induced ablation and photodisruption [10]. In the scope of the thesis, thermal interactions and photoablation will be emphasized.

In Figure 2.7. different effects of laser radiation on biotissue are demonstrated. It is a double logarithmic graph which has the x axis as the exposure time in seconds and y axis as the power density in W/cm^2. The characteristic energy density varies from 1 J/cm^2 to 1000 J/cm^2 as illustrated within the two diagonals, in the figure. As shown, there are five major ranges for exposure time:

(1) greater than 1 sec for photochemical interactions,

(2) 1 minute to 1ms for thermal interactions,

(3) 1 ms to 1 ns for photoablation, and

(4 and 5) less than 1 ns for plasma induced ablation and photodisruption.

Certainly the power densities corresponding to those of the exposure times are increasing as shown in the Figure 2.7.

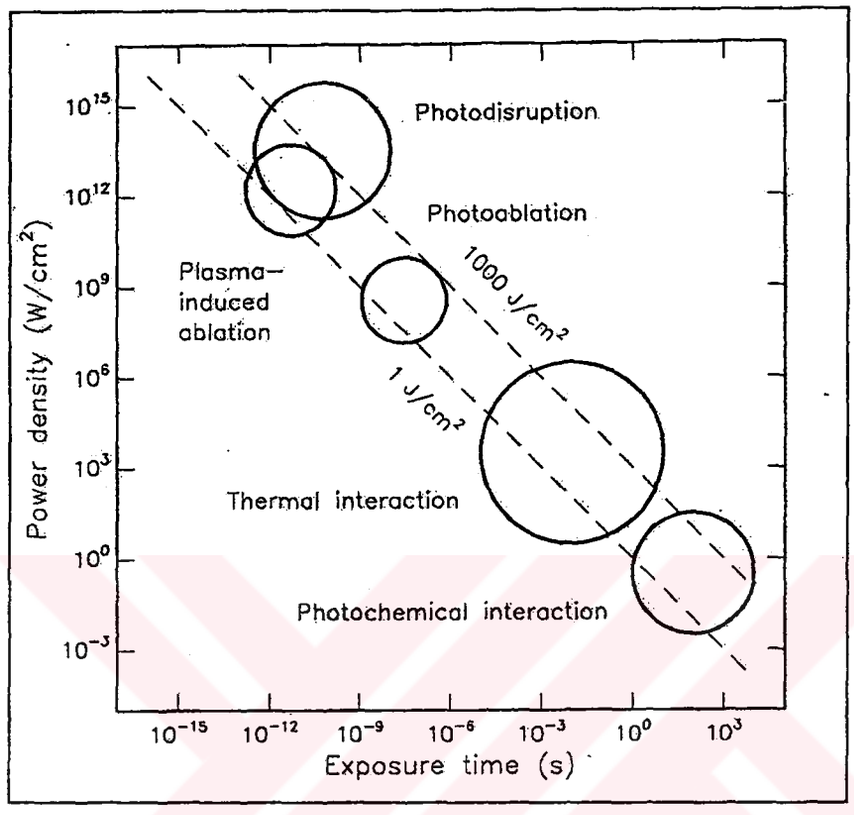

Figure 2.7. Various regimes of laser pulse interaction with tissue [10].

2.3.1. Photochemical Interactions

Photochemical interactions occur at very low irradiances and long exposure times. Typical irradiance is 1 W/cm^2. This type of interaction takes place during photodynamic therapy which is one of the significant applications of medical lasers.

Monochromatic irradiation is applied to the selectively sensitive chromophores injected into tissue in order to create a chemical reaction. Those extrinsic chromophores are called photosensitizers and trigger the release of cytotoxic reactants upon irradiation resulting in an irreversible oxidation of cell structures (also called photosensitized oxidation). Tumor treatment is the principal application of photodynamic therapy. Red dye lasers and diode lasers are used for PDT [13-28]. Typical irradiances vary between 0.01 to 50 W/cm^2.

2.3.2. Thermal Interactions

The thermal effects of various wavelengths are the subject of many researchers since the initial applications of lasers on biological tissues [3,7,13, 29-41]. The structural and chemical changes in tissue due to the increase of temperature can be classified as coagulation, vaporization, carbonization and melting. Thermal effects of laser irradiation according to the temperature of the tissue is demonstrated in Table 2.2.

Table 2.2. Thermal effects of laser irradiation [10].

Temperature	Effect
37°C	Normal
45°C	Hyperthermia
50°C	Reduction in enzyme activity, cell immobility
60°C	Denaturation of proteins and collagen, coagulation
80°C	Permeabilization of membranes
100°C	Vaporization, thermal decomposition (ablation)
>150°C	Carbonization
>300°C	Melting

Hyperthermia onset ranges from 42°C to 50°C (45°C average). The main indications are bond destruction and membrane alterations. If temperature exceeds 50° C, there exist reduction in enzyme activity, as a result of this, reduction of energy transfer within the cell and immobility of the cell can be observed. Necrosis starts at 60°C with the denaturation of proteins and collagens. Coagulation can be visually observed as whitening of the tissue. At temperatures greater than 80°C, membrane permeability is increased. At 100°C, tissue water starts to vaporize. Buble formation can be observed at this stage. At temperatures greater than 150°C carbonization starts as blackening of the irradiated tissue. Beyond 300°C melting may start depending on tissue type.

Depending on laser parameters and tissue characteristics, several thermal effects occur together. Due to heat transfer and diffusion of light there exists a temperature gradient within tissue (Figure 2.8.).

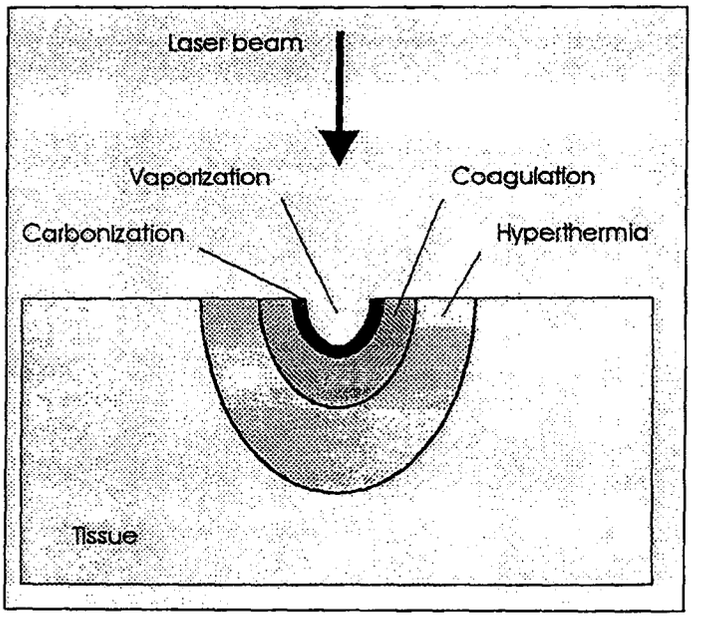

Figure 2.8. Various thermal zones within tissue [10].

2.3.3. Photoablation

Srinivasan and Mayne-Banton [42] described photoablation first and they called this phenomenon ablative photodecomposition, which means that material is decomposed when exposed to intense laser irradiation. If there is sufficient heat generation within the target tissue, then vaporization occurs without thermal demage around the ablated zone. Precise tissue removal can be done by this technique. The volume of ablated tissue per pulse is a function of the penetration depth of the laser light, duration of the pulse, and the spatial parameters of the beam.

The photoablative process is defined as a disruption of the covalent bond between two atoms by the absorption of photon energy. It can be summarized as a two step process:

(1) Excitation: $AB + hf \longrightarrow (AB)^*$ (2.12)

In this step, as a result of absorption of a photon energy hf, the molecule AB promote to an excited state $(AB)^*$.

(2) Dissociation: $(AB)^* \longrightarrow A + B + E_{kin}$ (2.13)

The molecule promoted to an excited state may dissociate, in other words bond disrupts.

Table 2.3. Dissociation energies of selected chemical bonds [10].

Type of Bond	Dissociation Energy (eV)
C = O	7.1
C = C	6.4
O - H	4.8
N - H	4.1
C – O	3.6
C – C	3.6
S – H	3.5
C – N	3.0
C - S	2.7

The mechanism of this process is totally different from thermal interaction. In thermal interactions, the photon energy is not high enough for the molecule to be promoted the excited state but only to a vibrational state within the ground level. Vibrational excitation relaxes by generation of heat resulting in a temperature gradient around the irradiated molecule. In order to obtain photoablation, the photon energy must exceed the dissociation energy of the covalent bond of the molecule. In Table 2.3. dissociation energies of some important chemical bonds are shown.

Table 2.4. Photon energies of selected laser systems [10].

Laser Type	Wavelength (nm)	Photon Energy (eV)
ArF	193	6.4
KrF	248	5.0
Nd:YLF (4ω)	263	4.7
XeCl	308	4.0
XeF	351	3.5
Argon ion	514	2.4
Nd:YLF (2ω)	526.5	2.4
HeNe	633	2.0
Diode	800	1.6
Nd:YLF	1053	1.2
Nd:YAG	1064	1.2
Ho:YAG	2120	0.6
Er:YAG	2940	0.4
CO_2	10600	0.1

When compared to the photon energies of certain laser types (Table 2.4), it can be seen that photoablation is limited with ArF, or limited with high energy UV photons. Corneal shaping is the most significant application of photoablation [43-54]. Typical power densities for photoablation are 10^7 - 10^8 W/cm^2.

2.3.4. Plasma-Induced Ablation and Photodisruption

If laser irradiance is on the order of 10^8 or 10^9 W/cm^2 optical breakdown occurs, i.e. plasma formation takes place. The primary parameter of plasma-induced ablation is the local electric field strength E. E is related to the power intensity by the following equation:

$$I(r, z, t) = 1/2\ \varepsilon_0\ c\ E^2 \qquad (2.14)$$

If irradiance exceeds a certain value, then electric field E becomes strong enough to create a plasma and generate shock waves. After the plasma formation occurs, the intreaction parameters change because the main absorber of the medium becomes plasma itself. This feature renders possible an energy deposition not only in pigmented tissue but also in weakly absorbing media.

The result of plasma induced ablation is a very clean ablation, associated with audible report and blueish plasma sparking. Nd:YAG, Nd:YLF and Ti:Sapphire are the lasers used for plasma induced ablation. Typical pulse durations are between 100fs-500ps. Irradiances are between 10^{11} to 10^{13} W/cm^2. Refractive corneal surgery is the main application area [55-56].

Besides plasma-induced ablation, shock wave generation and cavitation effects occur. Those mechanical effects are used for fragmenting and cutting of tissue. Lens fragmentation [51,56] and lithotripsy [58-61] are main application areas.

2.4. Medical Applications of Lasers

2.4.1. Ophtalmology

In ophtalmology, lasers are being used for diagnostic or therapeutic purposes. As a diagnostic tool, confocal laser microscopy is used for detecting retinal changes. Mostly, laser systems are used as therapeutic devices. Retina is possibly the only tissue that can be effectively and noninvasively healed by laser sources. Retinal

holes, retinal detachment, diabetic retinopathy, central vein occlusiun, senile macula degeneration and retinal tumors are major areas of laser treatment. Retinal coagulation is the method for dealing with those impairments. Meyer-Schwickerath was the first researcher who performed retinal coagulation (with sunlight in 1949 and with xenon lamp light in 1956)[62]. After the development of laser technology, Ruby laser was used by Zaret et al. in 1961 [63]. Then Argon ion laser found functional especially for stopping bleeding which could not be done by Ruby laser. Krypton ion laser [64] and diode lasers [65-68] became very important in 1970s and in 1988, respectively, for the treatment of retina.

Cataract surgery of the lens is another important laser treatment in ophtalmology [69]. In cataracts, transparency of lens is reduced. In order to get acceptable vision, lens interior must be removed and this operation can be done by the Nd:YAG laser. The picosecond Nd:YLF laser is another source for lens surgery (fragmentation of lens).

When the drainage of aqueous humor from the rear to the front chamber of eye is obstructed (acute block glaucoma), it is possiple to perforate the iris to obtain an additional passage for the aqueous humor. This operation is called laser iridotomy and can be performed with either argon ion lasers or pulsed Nd:YAG lasers [70]. Another type of glaucoma (open-angle glaucoma) is cured by the laser treatment called trabeculoplasty. Argon ion laser is applied to the surface of trabeculum [71].

The most widely known surgical treatment in ophtalmology is performed on cornea in order to reshape it to correct vision. Corneal surgeries can be classified as: removel of any pathologic conditions and refractive corneal surgery. ArF excimer and short pulsed neodymium lasers are used for those surgical purposes. Alteration of the cornea's refractive power is another application area. Radial keratotomy, radial keratectomy and photorefractive keratectomy are the techniques using laser sources to reshape corneal tissue. Excimer laser is found very succesful for those operations [44,45,48,51,54,72-78].

2.4.2. Dentistry

In dentistry, there are two major laser applications. One of them is the removal of infected substances from hard dental tissue. It is conventionally done by mechanical drils. This method creates pain due to the sensitivity of tooth nerves to vibration and

temperature change. Unfortunately those problems could not be solved by laser systems. CO_2, Er:YAG and Ho:YAG lasers were used and the ErYAG laser seemed to be the most promising because of its efficiency in ablating hard dental tissue via thermomechanical interaction [79-85]. Yet, recently, some data were collected regarding microcracks induced by the Er:YAG laser "shock". The most recent development is the application of the Nd:YLF laser system. It is found that its mechanical impacts are negligible.

Second major laser application in dentistry is laser treatment of soft dental tissue. CO_2 lasers are widely used in the treatment of malignant, premalignant and benign lesions of the oral mucosa. Excision and vaporization are two techniques the surgeon can perform.

Endodontics (treatment of infections of the root canal), laser treatment of filling materials, laser-welding of dental bridges and dentures are the other application areas in dentistry which are still under investigation. CO_2 and ArF lasers were studied for endodontics. For the treatment of filling materials Nd:YLF and Er:YAG lasers are used [86]. CO_2 and Nd:YAG lasers are found advantageous for laser-welding since the reflectivity of metals used in the soldering material is very high in the infrared spectrum.

2.4.3. Gynecology and urology

In gynecology, lasers found a very significant application area, namely the treatment of cervical intraepithelial neoplasia. The CO_2 laser is the most widely used laser source in the treatment of cervical intraepithelial neoplasia and vaginal intraepithelial neoplasia. Selection of temporal mode (cw radiation, chopped pulse or superpulse) and decision of mode of focusing (defocused for coagulation, partially focused for vaporization and tightly focused for deep excision) are important factors that determine the outcome of laser treatment.

In urology, CO_2, argon ion, Nd:YAG and dye lasers are utilized. CO_2 laser is used for cutting whereas argon ion and Nd:YAG is used for coagulation of highly vascularized tissues. Dye lasers are recently applied in lithotripsy. In short, there are number of applications in urology [87-93]:

-Condylomata acuminata (Nd:YAG or CO_2)

-Hemangiomas of external genitals (Nd:YAG)

-Carcinoma (Nd:YAG)

-Recanalization of urethal stenoses (Ho:YAG)

-Tumors of the bladder (Nd:YAG, or photodynamic therapy, red dye laser)

-Lithotripsy (dye lasers and Nd:YAG)

-Benign proztatic hyperplasia (Nd:YAG, diode lasers)

2.4.4. Dermatology

In dermatology, coagulation and vaporization are two widely used laser applications [94-103]. Argon ion, dye, CO_2, Nd:YAG and ruby lasers are being used in clinical practice. Argon laser is suitable for superficial treatments of highly vascularized skin because of the high absorption of the argon ion laser's wavelength by hemoglobin and melanin. Lasers in dermatology became a significant tool because of the succesful treatment of port wine stains. Argon ion lasers are being widely used for the aim of coagulating port wine stains. Besides argon lasers, dye lasers also became efficient alternatives for port wine stain removal because of less painful operation procedure. However its price is a disadvantage for dye lasers.

CO_2 lasers are used for vaporization. Precise tissue remove was done by the CO_2 laser especially for external ulcers and refractory warts. CO_2 lasers are also used in removing tattoos besides argon ion lasers [100-103].

Because of its greater penetration depth, Nd:YAG is used for the coagulation of deeply located hemangiomas and semi malignant skin tumors.

2.4.5. Orthopedics

In orthopedics, depending on the chemical composition of bone, CO_2, Er:YAG and Ho:YAG lasers are suitable for the treatment of bone [33, 104-114]. However, it is observed that there exists severe thermal side effects of CO_2 applications. The Ho:YAG laser is another candidate for treatment of bone, but investigations showed that the Er:YAG laser is more efficient because of minimal thermal effects. In arthroscopy, the Ho:YAG, Er:YAG and Er:YSGG lasers are under investigation.

2.4.6. Gastroenterology

In gastroenterology, lasers can be used efficiently if the target tissue is accesable with endoscopy. cw Nd:YAG laser is the most important tool for the coagulation in the treatment of gastrointestinal hemorrhages and benign, malignant, or non-neoplastic stenoses [20, 24, 116-124]. Photodynamic therapy (PDT) is another laser application at early stages of cancer. It has some advantages in spite of the fact that PDT can not provide a complete cure.

2.4.7. Otorhinolaryngology and pulmology

In otorhinolaryngology and pulmology, CO_2, Er:YAG, Er:YSSG and Nd:YAG lasers are being used or under investigation [125-137]. CO_2 laser is applied to remove benign and malignant lesions of the glottis (the vocal cords) and for the treatment of highly vascularized tumors such as hemangiomas or premalignant alterations of the mucosa. Er:YAG or Er:YSGG lasers are found advantegeous for laser-assisted stapedotomy. The Nd:YAG laser is capable of performing efficient treatment in the coagulation of tracheobroncial tumors.

2.4.8. Neurosurgery

In neurosurgery, lasers have great advantages since they can cut, vaporize and coagulate tissue without mechanical contact [138-163]. In addition, simultaneous coagulation of blood vessels and sterilizing are very important for the surgeon when dealing with highly sensitive tissues.

The CO_2 laser is found a good tool for cutting brain tissue but is not appropriate for coagulating blood vessels. On the other hand, studies concluded that the Nd:YAG laser functions well for both coagulating brain tissue and blood vessels. However, there is one important drawback of coagulation; that is to say, the coagulated tissue remains inside and causes edema or other serious complications. Moreover, thermal alteration of adjacent tissues can occur due to heat diffusion.

Ablation and vaporization are other methods for removing lesions or tumors in the brain. After the availability of suitable fibers, the Er:YAG laser became a surgical tool because its radiation at 2.94 mm is highly absorbed in water. However, the studies on ablation of brain tissue by the Er:YAG laser are new and rare. It is same

for the picosecond Nd:YLF laser which may succesfully perform non-thermal ablation of tissue.

Finally, the CO_2 laser was investigated for spinal surgery but those studies are very new and far from a convenient conclusion.

2.4.9. Cardiology

In cardiology, researchers tried to apply different laser sources for angioplasty like argon ion, Nd:YAG, XeCl excimer and Ho:YAG lasers [164-177]. The aim of angioplasty is to remove atherosclerotic plaque in order to recanalize the blood vessel. Laser light is transmitted through fibers and radiate from different types of fiber tips. Unfortunately all of the methods applied did not work properly (since the lack of studies dealing with tissue characterization and dosimetry) and they caused severe complications after the operations. It can be said that laser angioplasty was rejected recently.

Ablation of myocardial tissue is another application area in cardiology. For the treatment of tachyarrythmias, it is necessary to destroy the arrhythmogenic part of the mydcardium, without causing tissue defects or perforation. Intraoperative laser ablation and catheterization techniques become important alternatives to transcatheter direct current (DC) electrical shock ablation method in the surgical therapy for arrhythmia because of several reasons:

(1) Laser energy can be transmitted through optical fibers easily.

(2) Energy can be controlled and graded to the desired effect.

In spite of those advantages, procedures are still under investigation for better results. The Nd:YAG laser is widely used but other laser wavelengths (Er:YAG, Excimer) are also experimented with.

Transmyocardial laser revascularization (TMLR) is another laser application. The CO_2 laser is applied to the heart tissue to provide channels originating from the epicardium for additional blood supply to the heart. Most of the researchers report the effect of revascularization. However, results are far from being conclusive.

Medical applications of lasers and disciplines are summarized in Table 2.5.

Table 2.5. Clinical use of lasers.

Area	Laser Type
Ophtalmology	Nd:YAG, Nd:YLF, Ar^{++}, Excimer, Kr^{+}
Dentistry	CO_2, Er:YAG, Ho:YAG, Nd:YLF, ArF
Gynecology	CO_2, Nd:YAG, Ho:YAG, dye
Dermatology	CO_2, Nd:YAG, dye, Ar^{++}, ruby
Orthopedics	CO_2, Er:YAG, Ho:YAG, Er:YSGG
Gastroenterology	Nd:YAG, Ar^{++}
Otorhinolaryngology and Pulmology	CO_2, Er:YAG, Nd:YAG, Er:YSGG
Neurosurgery	CO_2, Er:YAG, Nd:YAG, Nd:YLF, Diode
Cardiology	CO_2, Ho:YAG, Nd:YAG, Excimer

2.4.10. Summary

Although only 40 years or so on the market, lasers have found many applications in medicine, and some such as in retinal detachment are the preferred method of treatment worldwide.

3. COMPUTER SIMULATIONS OF LASER TISSUE INTERACTIONS

The transport of an infinitely narrow photon beam incident on an infinitely wide tissue in the cylindrical coordinates (r,z) was simulated by Monte Carlo Simulation Program (Appendix A). The program calculates the statistical distribution of photon propagation at a specific wavelength by simulating the the random walk of a finite number of photons. The photon fluence (irradiated power per unit area) is obtained by convolving the photon absorption. Results of two sets of simulations were presented in national and international symposia [181,182].

3.1. Monte Carlo Simulation of the Nd:YAG Laser Fluence Distribution in Human Tissue

In this study [181], diffusion of Nd:YAG laser fluence in biological tissues was investigated via Monte Carlo Simulation method described in Appendix A. The aim of this study was comparing the fluence distribution within the different human tissues: bone (skull), brain (white matter), liver, myocardium, and prostate.

Semi-infinite tissue layer described by the following parameters: thickness (d = 0.1cm), refractive index (n = 1.3), absorption coefficient (μ_a), scattering coefficient (μ_s), and anisotropy factor (g).

Table 3.1. Parameters of the Monte Carlo Simulation of Nd:YAG Laser Fluence Distribution in Human Tissue.

Tissue	μa	μs	g	Reference
Bone (Skull)	0.50	120.0	0.900	Roggan et al.[5]
Brain(WhiteMatter)	0.40	110.0	0.950	Roggan et al.[5]
Liver	0.30	150.0	0.930	Roggan et al.[5]
Myocardium	0.40	175.0	0.970	Splinter et al.[6]
Prostate	0.40	110.0	0.960	Roggan et al.[5]

Besides the parameters describing the tissue, the following data are input parameters of the program:

• Number of photons, (1 000 000)

• Grid line separations ($\Delta r = \Delta z = 0.002$ cm)

• Number of grid elements ($\#\Delta r = \#\Delta z = 50$, $\#\Delta a = 30$).

The parameters of the first simulation were summarized in Table 3.1. Optical parameters of bone (skull), brain (white matter), liver, and prostate were measured by Roggan et al. [183]; the values for myocardium were measured by Splinter et al. [184]. Those measurements were performed for human tissues *in vitro*.

The fluence distribution of 0.1 cm diameter 1 J laser beam was calculated by the convolution program.

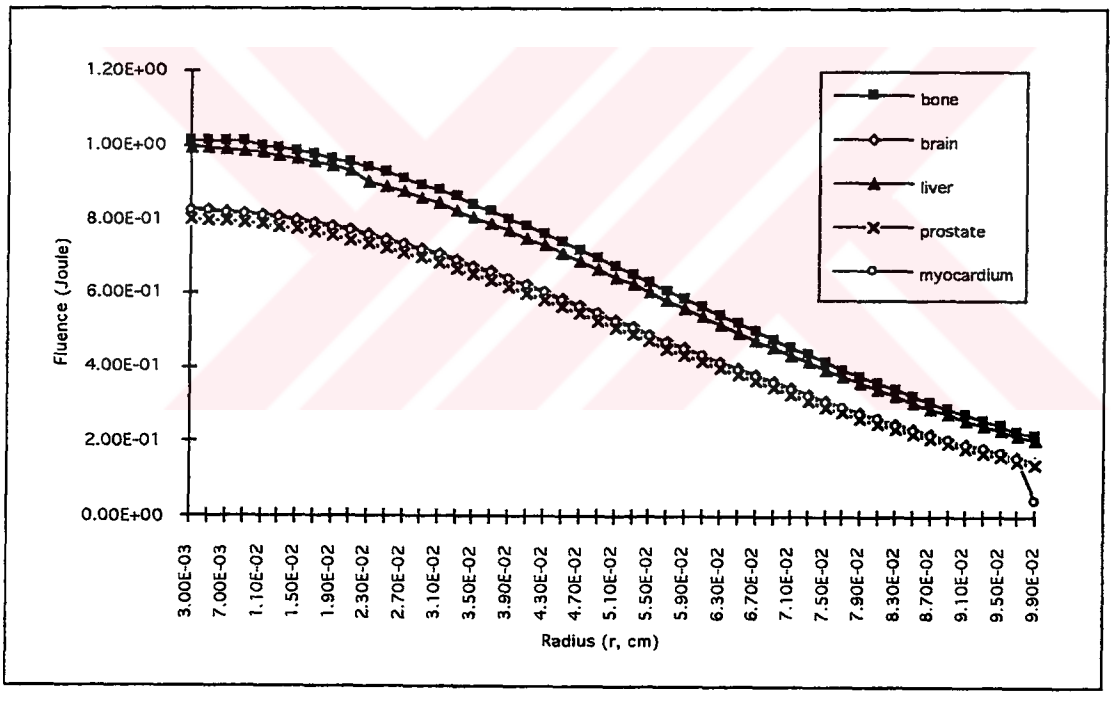

Figure 3.1. Laser fluence distribution in radial dimension.

The fluence distribution on the radial axis for all tissues were compared statistically and significant differences were found between bone and prostate, and between liver and prostate (double sided *t*-test, $p < 0.05$). The distribution has significant differences between 0.001 cm and approximately 0.068 cm (Figure 3.1.). Actually, for that region significant differences were found between bone and brain (double side *t* test, $p < 0.01$), bone and myocardium (double sided *t*-test, $p < 0.01$), brain and

liver (double sided t-test, $p < 0.05$), liver and prostate (double sided t-test, $p < 0.01$), liver and myocardium (double sided t-test, $p < 0.01$).

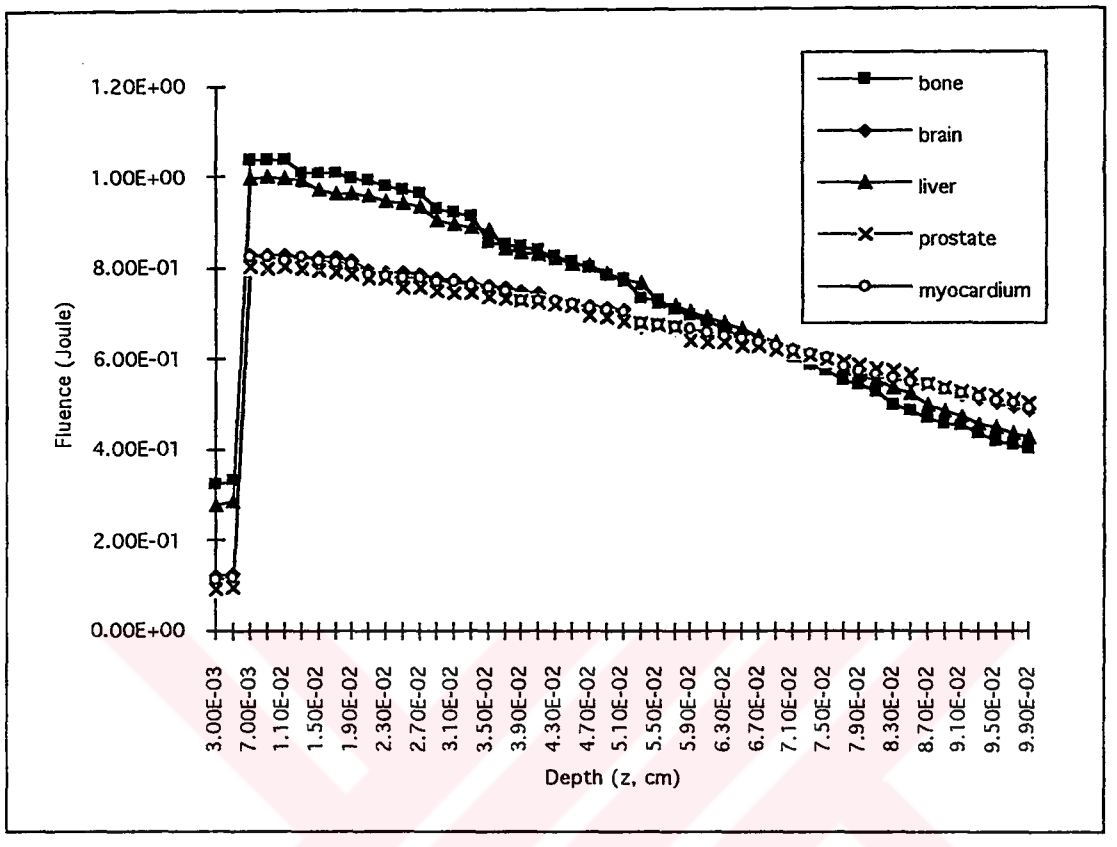

Figure 3.2. Laser fluence distribution in axial dimension.

Fluence distribution on the axial dimension for all tissues were compared statistically and significant differences were found between bone and brain (double sided t-test, $p < 0.01$), bone and prostate (double sided t-test, $p < 0.01$), bone and myocardium (double sided t-test, $p < 0.01$), brain and liver (double side t test, $p < 0.05$), liver and prostate (double sided t-test, $p < 0.01$), liver and myocardium. Fluence distribution differences can be observed in Figure 3.2.

Finally, isofluence lines are indicated in Figure 3.3. Laser beam is applied from the left upper corner. X axis corresponds to radial axis and Y axis corresponds to depth. The differences can also be seen for bone and liver when compared with others.

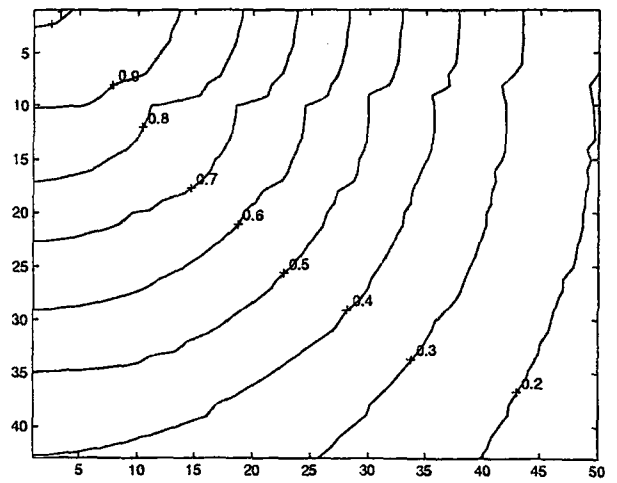

(a) Bone (Skull)

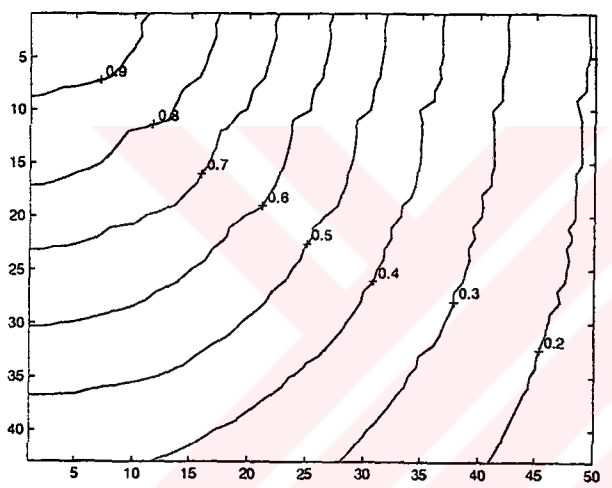

(b) Liver

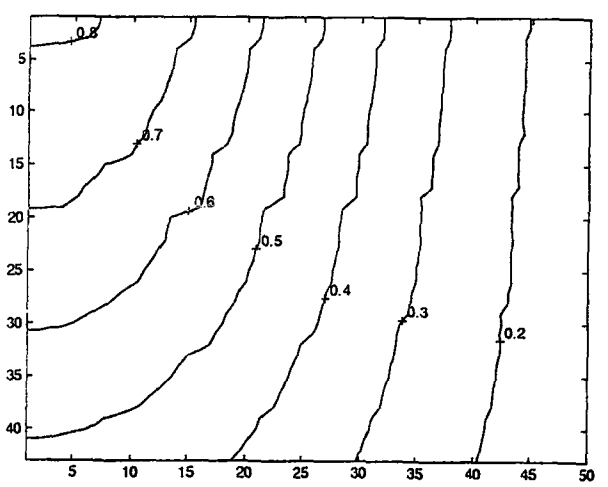

(c) Brain (White Matter)

Figure 3.3. (a) Fluence distribution within bone (skull); (b) Fluence distribution within liver; (c) Fluence distribution within brain (white matter);

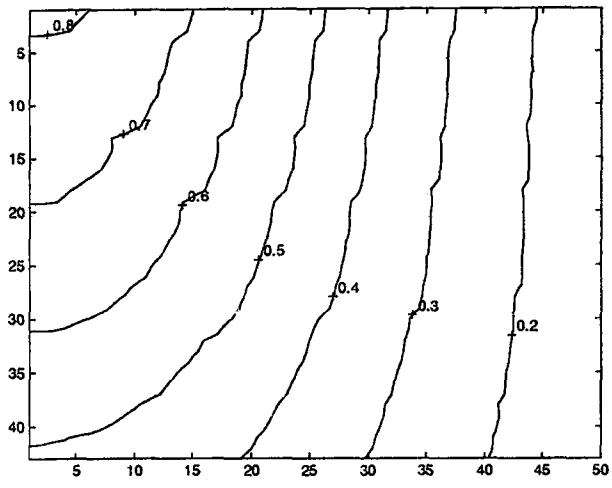

(d) Myocardium

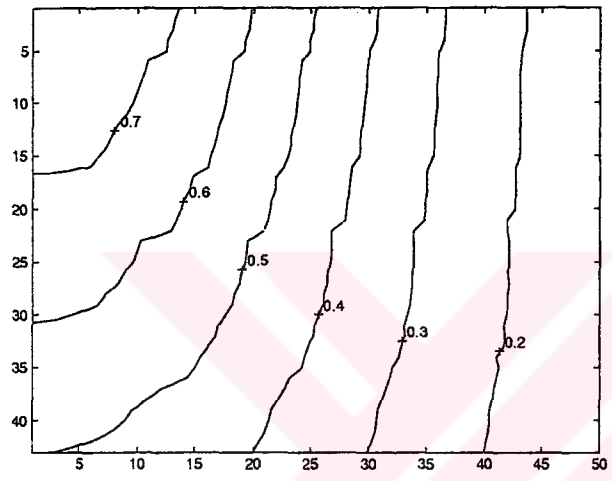

(e) Prostate

Figure 3.3. (Continued) (d) Fluence distribution within myocardium; (e) Fluence distribution within prostate. X axis corresponds to radial axis and Y axis corresponds to depth. Fluence values in Joules are denoted on isofluence lines.

Isofluence lines demonstrate the relative distribution of laser fluence in different tissues. In Figure 3.3., tissues are presented in increasing order in terms of fluence distribution. The significant difference between bone (skull) and prostate supports the idea of the fluence distribution of laser fluence at 1064 nm heavily depends on water content of tissues. Bone is the tissue with the least water content (12-15%). On the contrary prostate is the one with the relatively richest water content (83.3%) [11]. Other tissues analyzed in this study have values in increasing order from bone to prostate; and penetration depths are also in the same order.

3.2. Monte Carlo Simulation of the Nd:YAG Laser Fluence Distribution in Cardiac Tissues

In this study [182], diffusion of Nd:YAG laser fluence in cardiac tissues was investigated via Monte Carlo Simulation method described in Appendix A. The aim of the study was to compare the fluence distribution within the different cardiac tissues of human and canine: Normal canine myocardium (CN), irradiated canine myocardium (CL), human normal myocardium (HM), human epicardium (HE), and human cardiac aneurism (HA).

Table 3.2. Parameters of Monte Carlo Simulation of Nd:YAG Laser Fluence Distribution in Cardiac Tissues

Tissue	μa	μs	g
Canine / Normal Myocardium	0.40	173.5	0.974
Canine Lased Myocardium	0.35	245.9	0.956
Human Normal Myocardium	0.30	177.5	0.964
Human Epicardium	0.21	127.1	0.933
Human Cardiac Aneurism	0.40	137.0	0.975

Besides the parameters describing the tissue, the following data are input parameters of the program:

- Number of photons, (1 000 000)
- Grid line separations ($\Delta r = \Delta z = 0.002$ cm)
- Number of grid elements ($\#\Delta r = \#\Delta z = 50$, $\#\Delta a = 30$).

The parameters of the first simulation were summarized in Table 3.2. Optical parameters were measured by Splinter et al. [184]. Those measurements were performed for human and canine tissues *in vitro*.

The fluence distribution of 0.1 cm diameter 1 J laser beam was calculated by the convolution program.

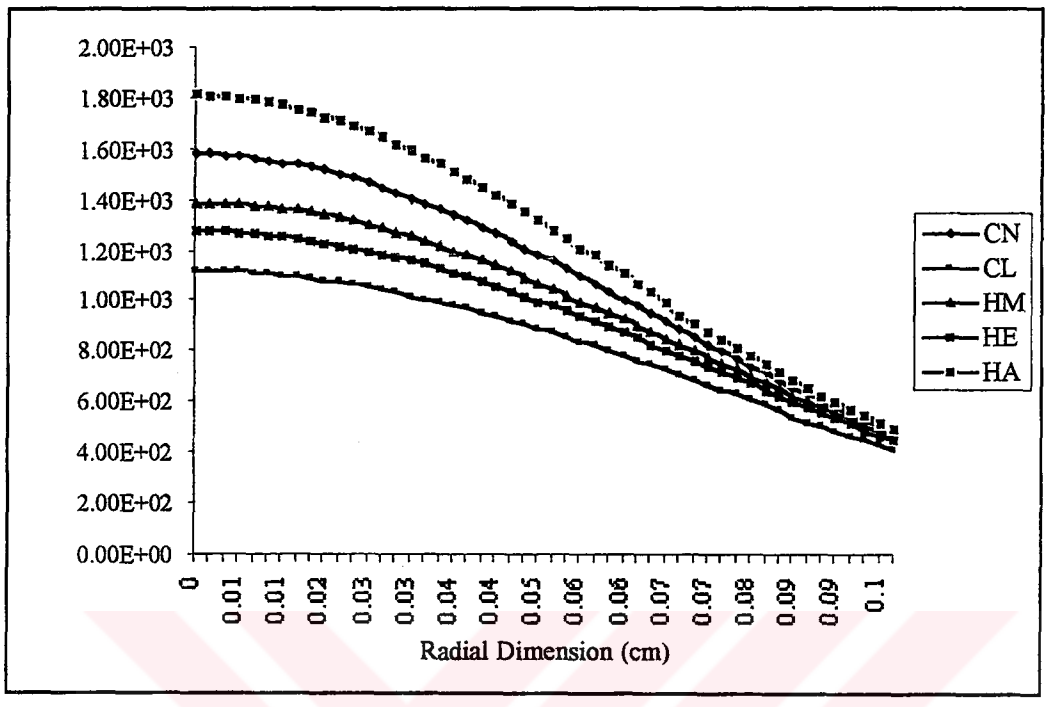

Figure 3.4. Laser fluence distribution in radial dimension (CN, Canine Normal Myocardium; CL, Canine Lased Myocardium; HM, Human Myocardium; HE, Human Epicardium; HA, Human Cardiac Aneurism).

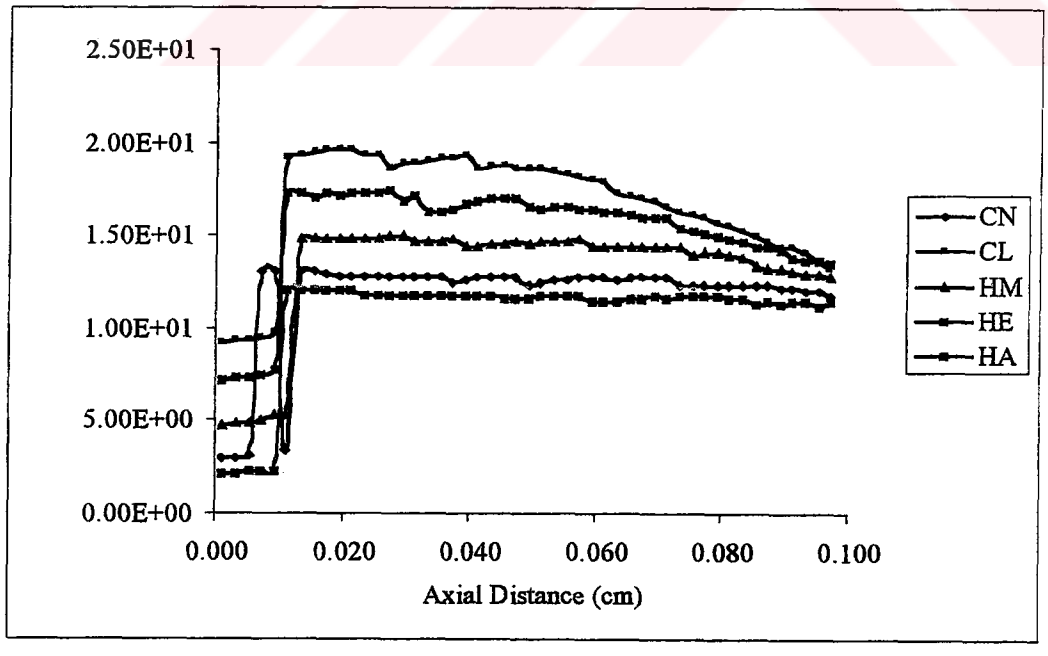

Figure 3.5. Laser fluence distribution in axial dimension (CN, Canine Normal Myocardium; CL, Canine Lased Myocardium; HM, Human Myocardium; HE, Human Epicardium; HA, Human Cardiac Aneurism).

The fluence distribution on the radial axis (Figure 3.4.) for all tissues were compared statistically and significant differences were found between CN and CL; between CN and HE; between CL and HM; between CL and HA; between HM and HA and between HE and HA (double sided t-test, $p < 0.01$). On the contrary, differences between CN and HM; CN and HA; CL and HE; HM and HE were not found statistically significant.

Scond, fluence distribution on the axial dimension (Figure 3.5.) for all tissues were compared statistically and significant differences were found between CN and HM; between CN and HA (double sided t-test, $p < 0.01$).

Finally, isofluence lines are indicated in Figure 3.6. Laser beam is applied from the left upper corner. Horizontal axis corresponds to radial axis and vertical axis corresponds to depth. The differences can also be seen between CL and others. This was the tissue irradiated beforehand. The results of this study showed that:

1. Distribution of light within human tissues did not show significant differences, those tissues (myocardium, epicardium and aneurism) can be assumed to be similar in terms of optical properties.
2. Distribution of light within canine normal myocardium did not show significant difference when compared to human tissues. This result indicates an interspecies homogeniety in terms of optical properties.
3. However, irradiated canine myocardium was found significantly different than others. This results indicates the change of optical properties during and after irradiation influences the optical properties of the target tissue and course of the lasing operation can change due to this alteration.

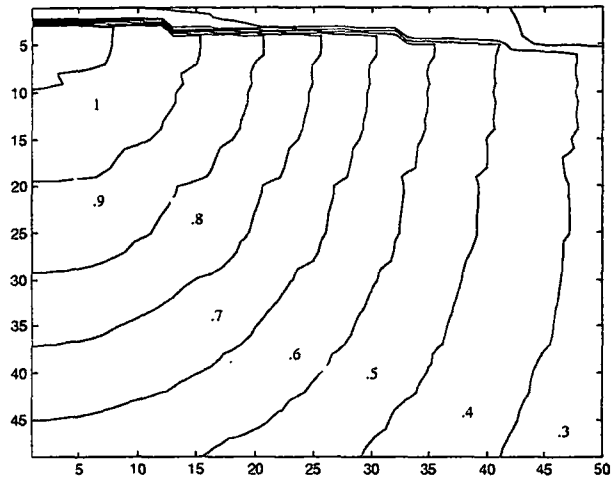

(a) Human Epicardium

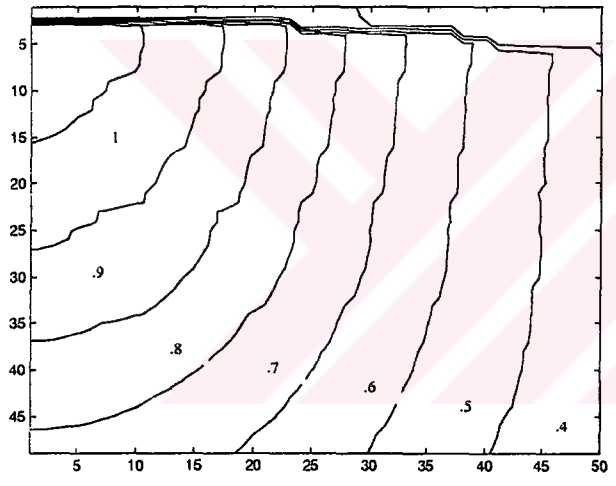

(b) Human Myocardium

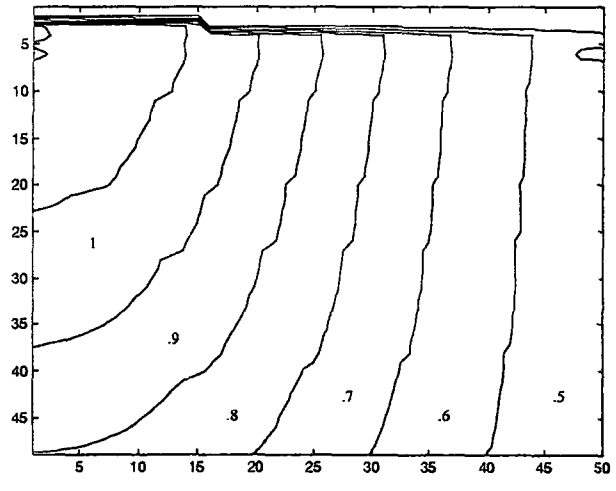

(c) Canine Myocardium

Figure 3.6. Fluence distribution witin (a) Human Epicardium, (b) Human Myocardium, (c) Canine Myocardium.

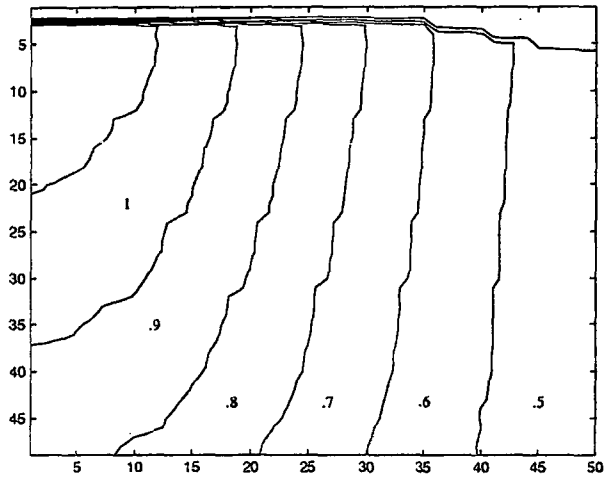

(d) Human Aneurism

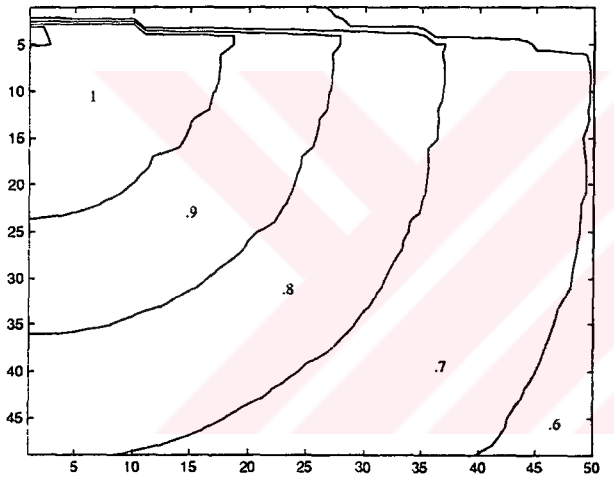

(e) Canine Lased Myocardium

Figure 3.6. (Continued) Fluence distribution witin (d) Human Aneurism, (e) Canine Lased Myocardium. X axis corresponds to radial axis and Y axis corresponds to depth. Fluence values in Joules are denoted on isofluence lines.

3.3. Discussion

In this section the results of the Monte Carlo Simulation results of the distribution of Nd:YAG laser fluence within biological tissues with different optical characteristics will be discussed.

The great fluence penetrations in soft tissues such as brain, myocardium and prostate support the coagulative applications of Nd:YAG laser source. In other words, relatively less energy can create greater coagulation in those tissues. This result

implies the constraints for cardiovascular applications such as coagulation of tachicardia focii. Larger penetration depth may cause undesired hazards in adjacent tissues. Nevertheless, those results provide evidence for the hyperthermia applications for soft tissues.

Our simulations underline another aspect of laser-tissue interaction mechanism: the differences of fluence distribution due to radial and axial dimensions. Dramatic changes with respect to different optical characteristics occur in the axial dimension. This dimension determines the penetration depth which is critical in laser applications.

Moreover, the results pointed out the homogeneity of human cardiac tissue (myocardium, epicardium and aneurism) as well as interspecies homogeneity (canine normal myocardium). On the other hand, the differences found for canine lased myocardium indicated the significance of the change of optical characteristics under laser irradiation. This result underlines the significance of temperature control systems during laser operation in order to obtain predictable laser ablation and coagulation.

Our study was based on the optical parameters measured *in vitro*. Fluence distribution can be affected and/or be changed in *in vivo* conditions mainly because of perfusion of tissues. Blood circulation would be a major factor influencing the heat transfer. In order to estimate proper dosimetry parameters, the simulation results must be compared and be tested with the experimental data.

4. LASER APPLICATIONS WITHIN CARDIAC TISSUE

In this section the results of two series of experiments on cardiac tissue are presented [185,186]. The aim of those experiments was to investigate the effect of different wavelengths (Nd:YAG and Er:YAG lasers, at 10.6μm and 2.94 μm, respectively) on different cardiac tissues.

The use of lasers in cardiovascular applications was summarized earlier in section 2.4.9. Creating lesions within the cardiac tissue is preferred for the following applications[187]:

1. Ablating cardiac tissue in order to isolate myocardial tissue responsible for the initiation of ventricular tachycardia.
2. Transvenous catheter ablation of the atrioventricular junction for modification of atrioventricular conduction.
3. Laser angioplasty

4.1. Coagulation of Cardiac Tissue by the Nd:YAG Laser

The Nd:YAG laser was found suitable for deep, uniform tissue coagulation because of tissue optical characteristics at 1064 nm and relatively great forward scattering that allows the energy penetrate deeply [7]. Since 1980s numerous studies were performed investigating the effect of the Nd:YAG laser on cardiac tissue [184-191]. In the following experiments the laser coagulations done on different ventricular tissues were compared.

4.1.1. Materials and Methods

Experiments were performed on fresh lamb hearts. They were kept in physiological saline solution for 24 hours. Three pieces were taken from each heart wall: ventricular bottom (VB), ventricular middle (VM), and ventricular upper (VU). Four levels of laser power were applied to every tissue, 4W, 5W, 6W and 7W, respectively (Appendix B.1.). Exposure durations were 10s, 15s, 20s, and 25s. The diameter of the laser beam was 1 mm. 2 minutes after each laser irradiation,

diameters of lesions were measured by micrometer (Figure 4.1.). Then lesions were cut cross-sectionally and coagulation depths were measured (Figure 4.2.).

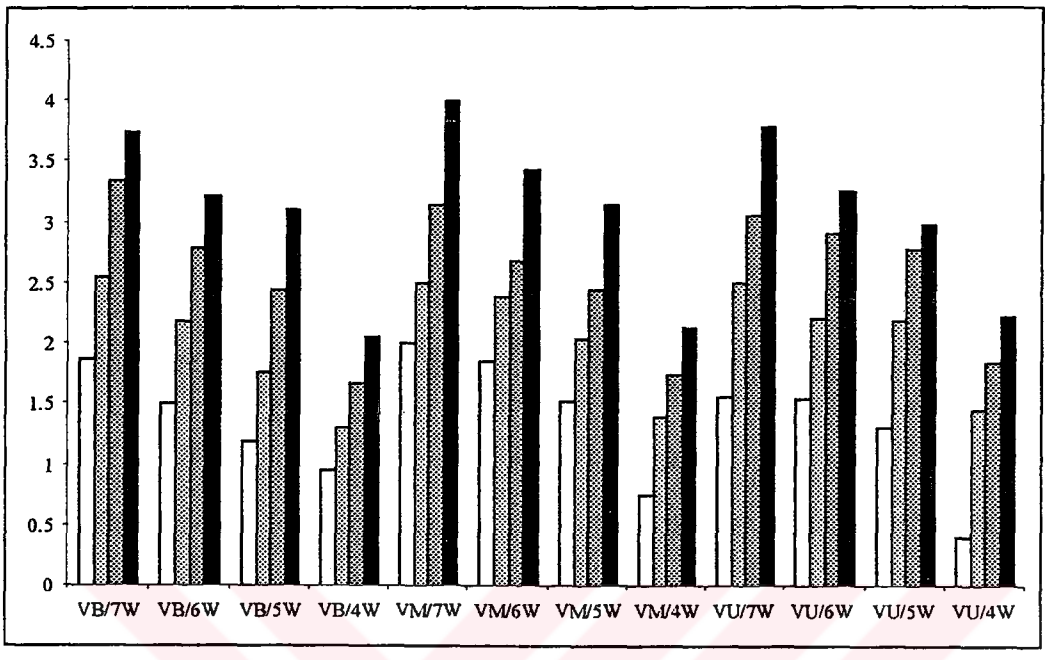

Figure 4.1. Diameters of lesions (in mm) created by Nd:YAG laser at 10, 15, 20, and 25 s lasing duration.

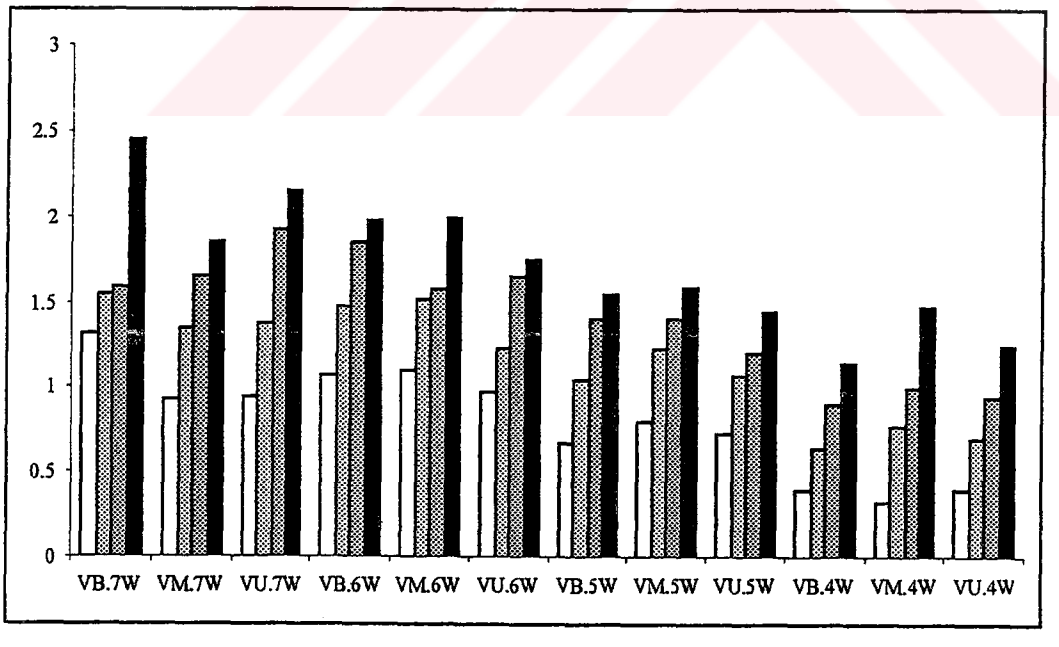

Figure 4.2. Depths of lesions (in mm) created by Nd:YAG laser at 10, 15, 20, and 25 s lasing duration.

4.1.2. Results

Statistical analysis (analysis of variance) was carried out and significant differences were found for:

1. diameters of coagulations created by 4 W irradiance ($p < 0.002$) with respect to tissue types;
2. depths of coagulations created by 5 W ($p < 0.04$) and 6 W ($p < 0.05$) with respect to tissue types;
3. diameters of coagulations at VB ($p < 0.001$) with respect to laser power levels applied;
4. diameters of coagulations at VM ($p < 0.001$) with respect to laser power levels applied;
5. diameters of coagulations at VU ($p < 0.001$) with respect to laser power levels applied;
6. depths of coagulations at VB ($p < 0.001$) with respect to laser power levels applied;
7. depths of coagulations at VM ($p < 0.001$) with respect to laser power levels applied;
8. depths of coagulations at VU ($p < 0.001$) with respect to laser power levels applied.

Finally, ventricular myocardium can be taken homogenous because different types of ventricular tissue did not show significant differences in optical behavior at 1.06 μm laser irradiation. On the other hand, level of power and irradiation duration are the significant variables for coagulation processes.

4.2. Ablation of cardiac tissue by the Er:YAG laser

The aim of this experiment was to investigate the ablation effect of the Er:YAG laser which radiates at 2.94 μm which overlaps with one of the greatest absorption peaks of water ($\mu_a \sim 10^4$ cm^{-1}). With the availability of suitable optical fibers which can transmit laser light at this wavelength, it became worthy to investigate the possible cardiovascular applications for the Er:YAG laser.

4.2.1. Materials and Methods

In order to investigate the effect of this wavelength, the Er:YAG laser (Appendix B.2.) was applied to tissue samples cut from fresh lamb hearts. They were kept in physiological saline solution for 24 hours and seven pieces were then taken from each heart: ventricular bottom (VB), ventricular middle bottom (VMB), and ventricular upper bottom (VUB), interceptal middle bottom (IMB), interceptal middle upper (IMU), interceptal nerve bundle (IN), ventricular inside (VI). Laser pulses have the energy levels of 0.3, 0.5, and 1.0 J as set by the manufacturer; exposure time per pulse was 150 μs. The diameters of the elliptical spotsize were 0.75 mm x 1.35 mm. The corresponding average power densities were 37.7 J / cm^2, 62.9 J / cm^2, and 125.8 J / cm^2, respectively.

4.2.2. Results

The ablation craters had conical shapes. 2 minutes after each laser shot, diameters of ablation craters were measured by a micrometer. The area of the conical base of lesions were calculated (Figure 4.3). Then lesions were cut cross-sectionally and ablation depths were measured (Figure 4.4.). Volumes of ablated tissues were calculated by combining both data.

Statistical analysis (analysis of variance) was carried out and significant differences were found for:

1. crater areas with respect to levels of energy ($p < 0.0001$);
2. crater areas with respect to types of tissues ($p < 0.006$);
3. crater depths with respect to levels of energy ($p < 0.0001$);
4. crater depths with respect to types of tissues ($p < 0.001$).

Additionally:

1. The crater areas showed an increasing tendency along ventricular tissues from bottom to upper sites (VB, VMB, and VUB).
2. The crater areas created at interceptal sites (IMB, IMU, IN) showed notable differences.
3. The crater areas of ventricular tissues (VB, VMB, VUB, and VI) showed notable differences.
4. The crater depths showed a decreasing tendency along ventricular tissues from bottom to upper sites (VB, VMB, and VUB).

5. The crater depths created at interceptal sites (IMB, IMU, IN) showed notable differences.

6. The crater depths of ventricular tissues (VB, VMB, VUB, and VI) showed notable differences.

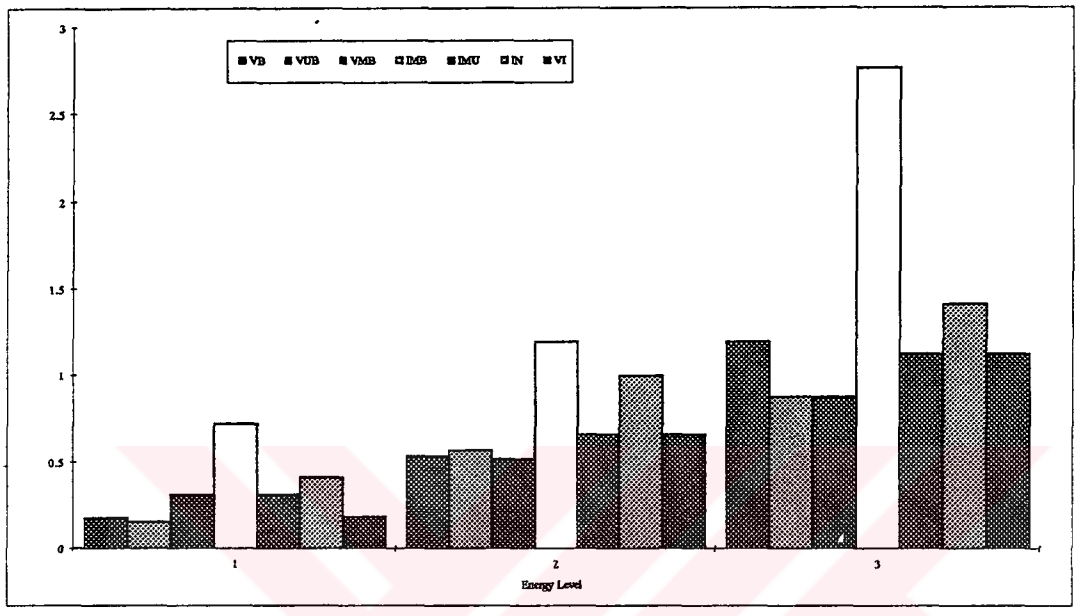

Figure 4.3. Crater areas of lesions created by Er:YAG laser at three energy levels of 0.3, 0.5 and 1J.

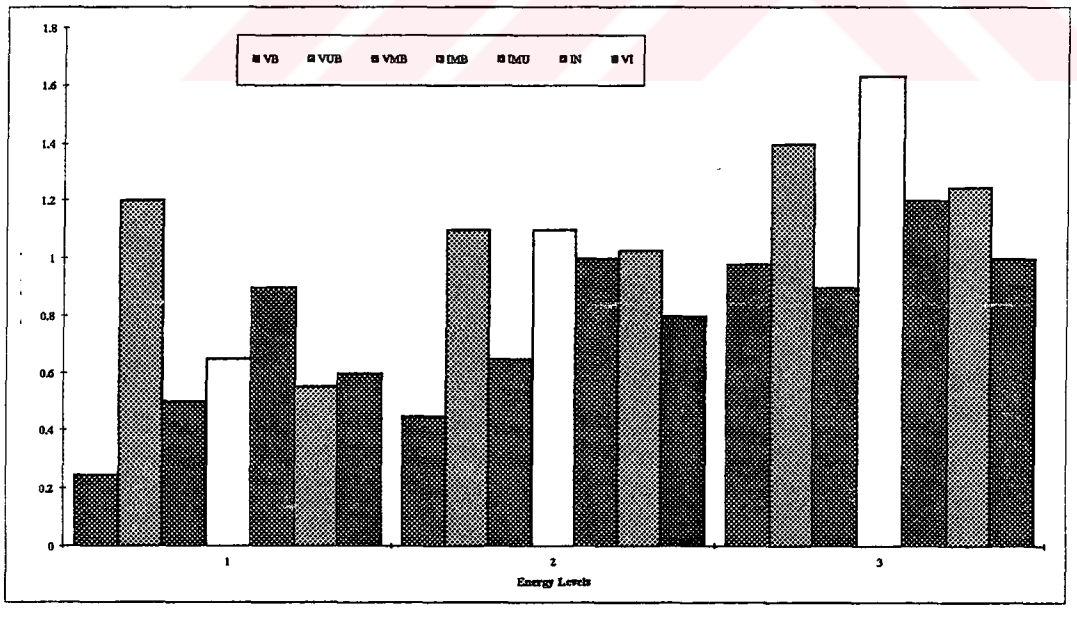

Figure 4.4. Crater depths of lesions created by Er:YAG laser at three energy levels of 0.3, 0.5 and 1 J.

4.3. Discussion

In our study different parts of cardiac tissue (ventricular bottom, ventricular middle, ventricular upper for Nd:YAG and ventricular bottom, ventricular middle bottom, ventricular upper bottom, interceptal middle bottom, interceptal middle upper, interceptal nerve bundle, ventricular inside for Er:YAG) were used. The coagulation and ablation process were described as a function of power and irradiation duration.

One of the significant results of those experiments was the homogeneity of cardiac tissue at 1.064 μm Nd:YAG irradiation. This result is consistent with the results of computer simulations (given in Chapter 3), even that lamb tissue was used in the experiments: computer simulations provided evidence for interspecies homogeneity. Second, simulation results indicated homogeneity of cardiac tissue at 1.064 μm irradiation. Experimental results also supported this prediction.

As a conclusion, ventricular myocardium can be taken homogenous because different types of ventricular tissues did not show significant differences at 1.064 μm laser irradiation. On the other hand, power and irradiation duration are significant variables in coagulation processes.

In the case of the Er:YAG laser application, the dimensions of ablation craters were found significantly different as a function of tissue type as well as level of energy delivered. In other words, cardiac tissue is not homogeneous at 2.94 μm. Second, Er:YAG laser ablation craters were found acceptable for cardiac applications with no thermal damage around.

The main difference between the results of both experiments was the thermal response of cardiac tissue with respect to wavelength of laser irradiation. The differentiation of tissue types with respect to 2.94 nm was notable whereas no significant difference was observed for 1.064 nm. This result highlights the significance of laser wavelength as a laser-tissue interaction parameter.

Both laser wavelengths were found worthy to be tested for cardiac applications such as coagulation and ablation processes.

5. Er:YAG LASER ABLATION OF CEREBELLAR AND CEREBRAL TISSUE

5.1. Background

Since they can be used for cutting, vaporizing and coagulating tissues with and without mechanical contact, lasers may have great potential advantages in neurosurgery [156]. Brain tumor removal is one of the major surgical laser applications. The primary goal in those applications is minimal thermal damage to adjacent healthy tissues. Thus far, various laser wavelengths and operation modes have been investigated [192, 10, 138, 193]. The CO_2 laser was found to be a good tool for cutting brain tissue, but it was not suitable for coagulating blood vessels [156]. On the other hand, the Nd:YAG laser, operating at 1064 nm, was adopted for coagulating both the brain tissue and blood vessels. However, there is one important drawback in use of Nd:YAG lasers in coagulation: adjacent tissue is thermally altered due to heat conduction (high scattering and poor absorption in tissue at 1064 nm) [143, 153-154]. High power diode laser's applicability in neurosurgery was investigated and clinical experiences and animal studies were reported very recently [161, 181, 193]. Diode lasers in the near infrared (NIR) region were found practical and efficient compared to the 1064 nm Nd:YAG laser. On the other hand, Er:YAG lasers had been known for years and used for superficial ablation in many medical applications. However, studies on ablation of brain tissues by the Er:YAG laser are recent and limited [162-163]. Since the Er:YAG laser wavelength overlaps with one of the absorption peaks of water in the IR, its optical absorption coefficient for organic tissues is higher than that of the other available laser sources. As a result, the 2.94 μm light only penetrates a few microns into the tissue. The associated thermal relaxation time is on the order of microseconds. Thus, there is minimal heat transfer to adjacent tissues during the laser pulse. The ablation process removes the heated tissue. Consequently, the 2.94 μm Er:YAG laser may be used as a source of precise ablation. With the availability of suitable fibers, the Er:YAG laser may become an indispensable tool for invasive neurosurgical applications.

The aim of this study was to investigate the ablative effect of Er:YAG laser pulses on different cortical tissues using different energy levels and to compare the features of the resulting lesions.

5.2. Materials and Methods

30 female Wistar rats weighing 180-220 gr. bred in the Animal Facility of the Psychobiology Laboratory at Bogaziçi University were used for experiments. They were housed in cages (8±1 animals per cage) in a temperature controlled vivarium kept at 22±2°C with a 12:12 hours light:dark cycle. Food and water were available *ad libitum*. Before surgery subjects were placed in individual cages and were euthanized by an overdose of ketamine (6 cc/kg, intraperitoneally). The skull was dislocated from the body and brain specimens were prepared within 3 minutes *post mortem*. Using an Er:YAG laser (TULAMASHZAVOD, Russia, Appendix B.2.), two sets of bilateral cerebral and one set of bilateral cerebellar lesions were created at three different pre-set energy levels.

Irradiation parameters were as follows: laser energy levels: 0.3, 0.5, and 1.0 J as set by the manufacturer; exposure time per pulse: 150 μsec as set by the manufacturer; number of pulses per lesion: 1. On each hemisphere, two sets of lesions were created 8 mm apart. The lesions created *in vitro ex situ* were at locations corresponding to 1 mm anterior to bregma and 1 mm posterior to lambda. In addition, one set of bilateral lesions was created on cerebellar cortex 1 mm from midline. Laser was focused on the target tissue by a cylindrical lens (Figure B.2.). Thus it was a non-contact lasing situation. The diameters of the eliptical spotsize were 0.75mmx1.35mm. The corresponding average irradiances were 37.7 J/cm^2, 62.9 J/cm^2, and 125.8 J/cm^2, respectively.

Surgical procedures were completed within 5 minutes *post mortem*. Immediately after laser procedures, diameter and depth of ablation craters were measured. Since our study was performed *in vitro ex situ* and was directed towards the estimation of the real dimensions of ablation craters, no histologic examinations were carried out.

5.3. Results

A total of 188 lesions were created *in vitro ex situ* on excised rat brain specimens. 52 lesions were created on the cerebellar cortex at 0.3 J. On the cerebral cortex, 44

lesions were created at 0.3 J, 46 lesions at 0.5 J, and 46 lesions at 1.0 J. We were able to create ablation craters in the cerebellum at the lowest energy setting of our laser at 0.3 J as seen in Figures 5.1. and 5.2. At increased energy levels (0.5 and 1.0 J), we "drilled" holes through the cerebellum. We also attempted to create a limited number of ablation craters in the spinal cord at 0.3 J and observed that the depth of ablation could not be controlled at the pre-set energy levels of our laser. Even at the lowest energy setting of 0.3 J, the ablation depths were much larger than the thickness of the spinal cord.

Cerebral lesion dimensions (ablation crater diameter and crater depth) created at 0.3 J were smaller than the cerebellar lesion dimensions (Figures 5.1. and 5.2.). Moreover, we did not observe "full thickness" ablation craters, i.e., "drilled" holes, in cerebral specimens.

When the lesion dimensions created in the cerebellum and the cerebrum were compared, we observed a significant difference in crater diameters ($p < 0.001$, paired t-test) and the crater depths ($p < 0.001$, paired t-test) at 0.3 J. All lesions had a conical form; and lesions created in the cerebellum had greater diameter/depth ratio when compared to lesions in the cerebral cortex.

In general, crater dimensions were a linear function of applied laser energy. However, as seen in Figures 5.1., the crater depth increased much faster than the crater diameter with increasing laser energy. Therefore, the ablated volume calculated assuming conical geometry was not a linear function of applied energy and the difference between cerebellar and cerebral lesions became more pronounced as seen in Figure 5.2.

Finally, subjective binocular observations revealed that cortical ablation lesions were not surrounded by coagulation zones.

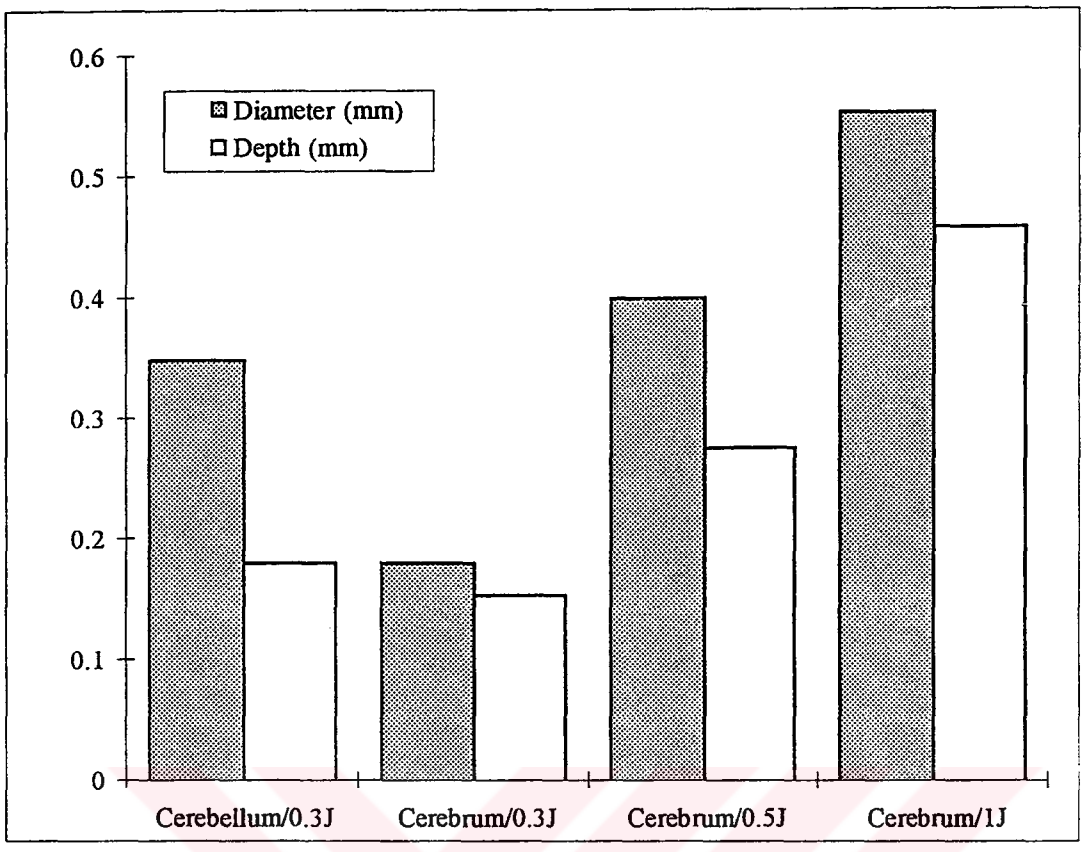

Figure 5.1. Ablation dimensions with respect to tissue types and laser energy levels.

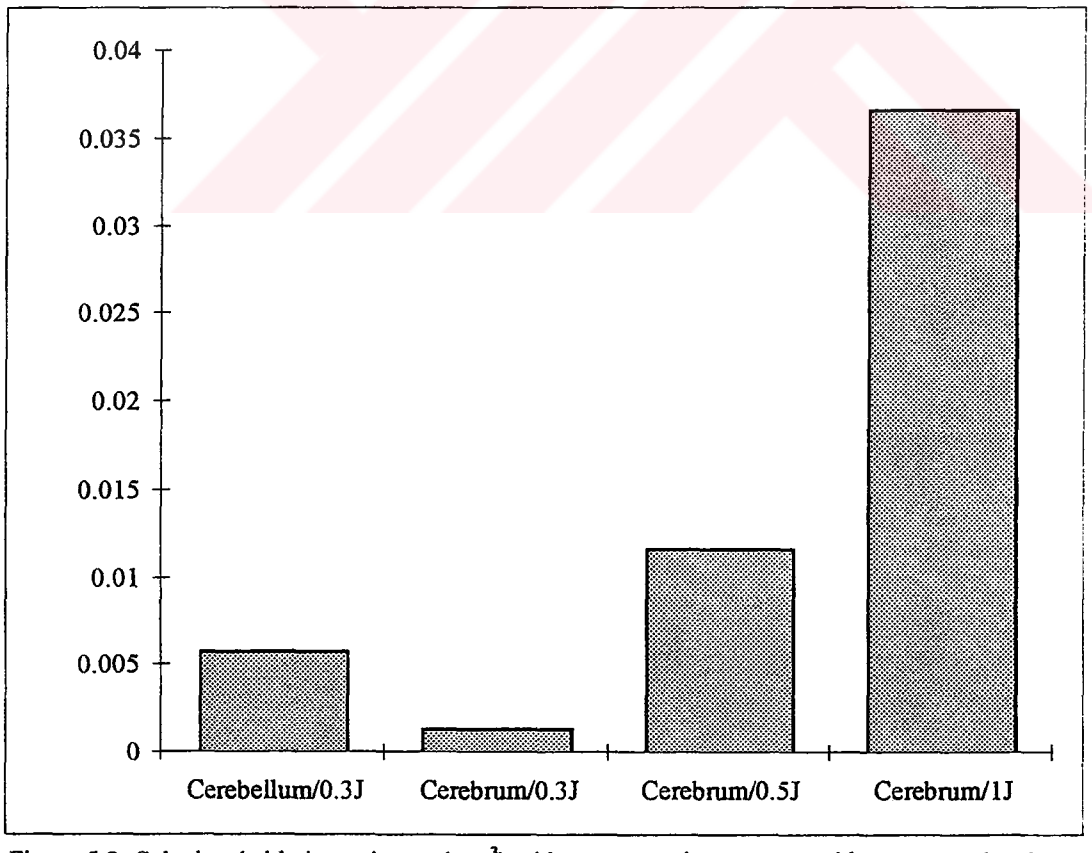

Figure 5.2. Calculated ablation volumes (mm^3) with respect to tissue types and laser energy levels.

5.4. Discussion

The primary goal of this study was to investigate the applicability of the Er:YAG laser in neurosurgery for ablation/tissue removal purposes. Results of previous studies by Cubeddu and associates showed that the 2.94 μm irradiation could ablate soft tissues without coagulating surrounding tissues. The damage created by the Er:YAG laser was evaluated using histochemical methods and negligible thermal but mechanical alteration of adjacent tissues was observed [162-163]. The results in our study also provided evidence of minimal thermal effect to adjacent tissues and efficient photoablation. The irradiance parameters and the resulting ablation craters in the present study and the previous ones [162-163] were similar.

Our *in vitro* results showed that the Er:YAG laser radiation, that is very strongly absorbed by tissue water, could be used to ablate neuronal/cortical tissues. However, the response of cerebral and cerebellar tissues to Er:YAG laser irradiation were significantly different. In both tissues, ablation craters had a conical form; yet, lesions created in the cerebellum had greater diameter/depth ratio when compared to those in the cerebral cortex. The differences observed in the response of cerebral and cerebellar cortical tissues may be due to the anatomical (the thickness of cortex in both regions) and chemical (water, lipid and protein contents) differences or due to the superposition. The key element here would be water content because of its higher percentage in brain tissue (approximately 75%) and thus greater absorption at IR wavelengths. It is known that there are differences in water content between different brain regions. Early studies [212] reported that the water content of the gray matter (83-86%) was higher than that of the white matter (68-77%) and increased from the frontal to the occipital and from the parietal to the basal cortex. Since the thickness of cortical tissue in cerebrum is remarkably greater than in cerebellum, laser energy absorbed in cerebral cortex must be greater than the energy absorbed in cerebellar tissue. The penetration depth is inversely proportional to the absorbed energy. Consequently, the penetration depth in cerebrum would be smaller than the penetration depth in cerebellum as in the case of lesions reported in the present study.

In previous studies, cavitation effects as a result of the explosive ablation process were observed. It was speculated that cavitation effects could be prevented by adding water to the surface of tissue to enhance ablation efficiency. In this study, we had similar observations; nevertheless, deep ablation channels were created in the cerebellum (at 0.5 and 1.0 J) and the spinal cord (at all energies applied), *but not* in the cerebral cortex. The observed differences in lesion formation were speculated to be indicators of different laser-tissue interaction processes, which are a function of applied energy and optical properties of the brain tissue at 2.94 μm.

In spite of its potential advantages in removing tissue, the Er:YAG laser with irradiation parameters as the ones used in this study, might not be a useful tool in removal of brain stem astrocytomas and intraspinal tumors. In order to create shallower ablation craters with better precision, Er:YAG laser systems with lower energy levels should be used.

The differences observed in the response of cerebral and cerebellar cortical tissues were dependent on the anatomical and chemical differences.

With the availability of fibers, the 2.94 μm Er:YAG laser promises to become an important surgical tool in brain surgery involving removal of tumorous tissues. Since the Er:YAG laser has great potential for use in neurosurgery, tissue characterization, simulation of laser-tissue interactions, and comprehensive dosimetry studies should be carried out to investigate the possible uses of this laser in medicine.

6. DESIGN OF A COMPUTER CONTROLLED LASER DELIVERY SYSTEM

In this part, the design of the medical delivery system for the 980 nm diode laser is described. The aim of the study was to design a reliable and practical control system and to develop a user-friendly interface. It was performed in two steps:

1. Before developing a complex controller it was necessary to test the reliability and potential of this new wavelength; thus a fast solution was needed. The best way to solve such a problem was to develop a virtual instrument that had the desired capabilities. GWI data acquisition unit and Superscope II software were utilized to monitor and control the laser parameters.
2. After the experimental studies, a microcomputer based controller was designed and developed for clinical usage.

In the following, the development of those control systems will be explained in detail. First, in 6.1. the structure and the function of the virtual controller will be explained. In 6.2. the design of the microcomputer based circuit will be discussed.

6.1. Controlling Laser Irradiance: Virtual Instrument Solution

A real time SCSI peripheral unit (MacADIOS adio), a personal computer (Apple Macintosh LC) and a program developed in Superscope II environment were the tools used for construction of virtual controller. Laser diode system (Appendix B.3.) permits the user to control the laser parameters via its remote control unit or from external signals through 25 pin connector. For faster design, it was decided to control the diode laser current knobe voltage on the remote control unit. The system is described in Figure 6.1.

Analog output signal (0-5 V) of MacADIOS provides control signal for the diode current knobe. That signal can be on and off at a frequency of 30 Hz (was limited by the frequency range of diode laser system). This feature allowed the controller to deliver laser energy in pulses with a desired waveform besides cw regime. Thus the

user can select the output power, mode of operation (cw or modulated), modulation waveshape (square, sine, triangle) and lasing duration. Those parameters can also be monitored and be stored throughout the experiments.

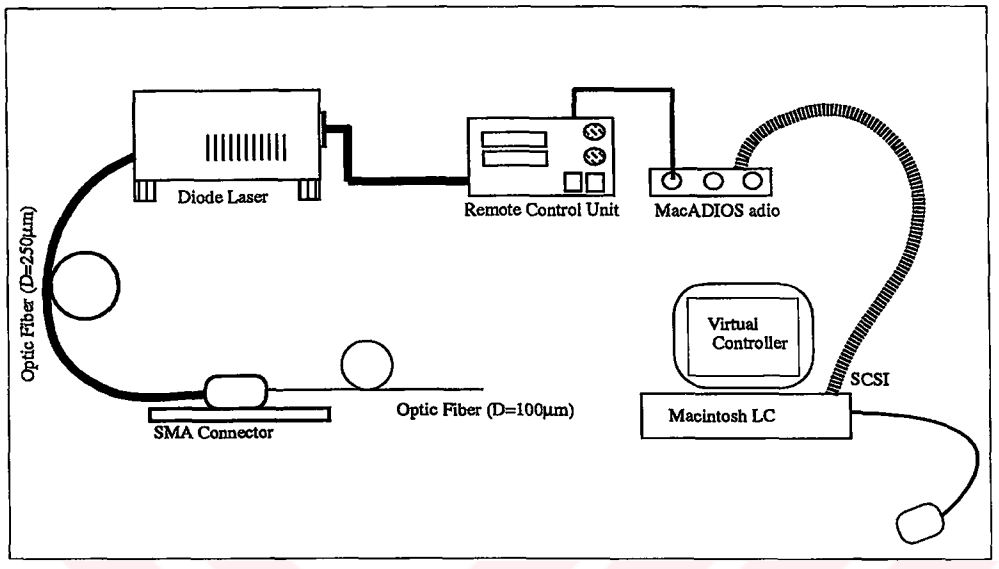

Figure 6.1. Block diagram of laser sysytem virtual controller.

Virtual controller was developed in Superscope II which is an object oriented programming environment. Therefore, the programming procedure is called construction rather than programming. There are numerous objects and functions defined in Superscope II environment. In the following, the objects used for virtual controller will be explained. The flow of the experimental process guided the design of the instrument. The user needs to choose the laser parameters, to monitor and to save data during the experiment. The front panel (Figure 6.2) of the virtual controller was developed with this motivation. The objects used are defined in the following:

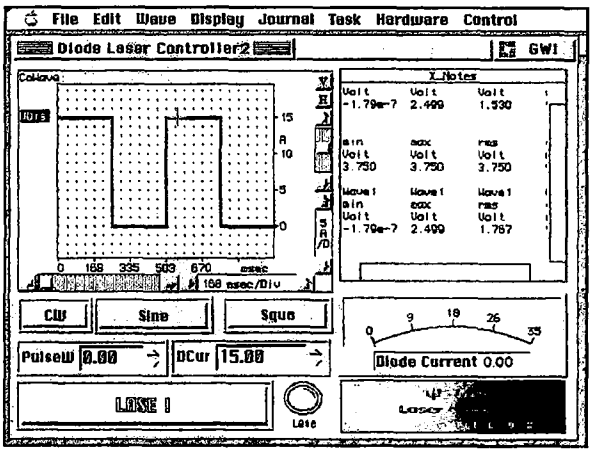

Figure 6.2. Front panel of the virtual controller.

A. Buttons

1. **Control Signal:** This control button allows the user to choose important laser parameters. When user presses this button with a cursor, a dialog box (Figure 3.3.) appears. Lasing duration can be set from Length option in terms of points (7200 points were set to 1 sec), type of modulation can also be set from this screen. If 'periodic' is selected as Sine, Square or Triangle, then the control voltage will be modulated with chosen Period. Alternatively, the user can select 'constant' function which corresponds to cw regime. This screen can also present other wave types as Ramp, Gaussian, or Uniform noise.

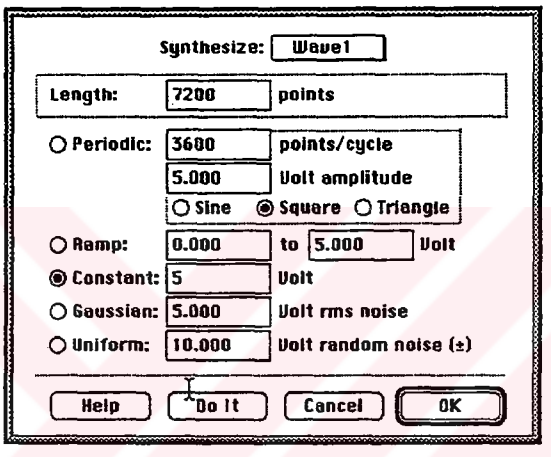

Figure 6.3. The dialog box that allows the user to choose the modulation parameters

2. **Set Diode Current:** This control unit is used for setting the value of diode current by typing the value or adjusting it from the arrows beside.

3. **Lase! :** This button is for starting the experimental session. When it is pressed, control signal with selected properties is delivered to the laser system.

B. Displays

1. **Cowave:** It indicates the shape of control signal in time domain. This display can be scrolled and/or be scaled from the vertical and horizontal scrollbars.

2. **X-Notes:** This is an object called Journal in Superscope II environment. The chosen properties of the signal delivered appear on this display. Minimum, maximum and rms values of control voltage are reported as well as the time duration.

3. **Diode Current:** The diode current set by the user is also monitored through this analog meter type display during the laser is on.

4. **Lase:** It is a virtual lamp which alerts the user when laser is on.

The program behind this virtual controller consists of two routines. The first one named SinT is composed of the control voltage according to the selected parameters:

```
Task Begin
    Wave Wave1 = 0.00000
    Variable Curre = Control Cur / 30.00
    Choose Synthesize... Wave1 Under Wave
    Wave1 = Wave1 + 2.50000
    Wave1 = Wave1 * variable Curre
    Statistics on Wave1 (min to X_Notes; max to X_Notes; rms to X_Notes; etc)
    Wdisp = Wave1 * 6.00000
```

Control voltage which is defined as Wave1 is set to 0 V at the beginning. Then it is adjusted between 0 and 5 Volts by shifting the wave by adding 2.5 Volts and multiplying it with a variable (variable curre) proportional to selected diode current. The statistical values of the wave (as min, max, rms and time duration) are also written on Journal display X_Notes and the wave is plotted on wave display by the last two lines of the program.

The second program routine (Task:T2) is smaller than the first one and it performs the task of digitizing the trace of wave within the adjusted trace properties:

```
Task Begin
Trace Loop Begin (2 traces)
    Digitize Trace (96 pts/trace, 192.00 pts/sec)
    Clear & Update
    Trace Loop End
```

6.2. Microcomputer Based Controller

The results of the experiments (Chapter 7) described the laser tissue interaction mechanism and it was concluded that the 980 nm diode laser energy can have great potential for medical applications. Thus it was decided to build a real controller system. This new system controls the diode laser (Appendix B.3.) via a 25-pin connector externally. The schematic diagram is showed in Figure 6.4..

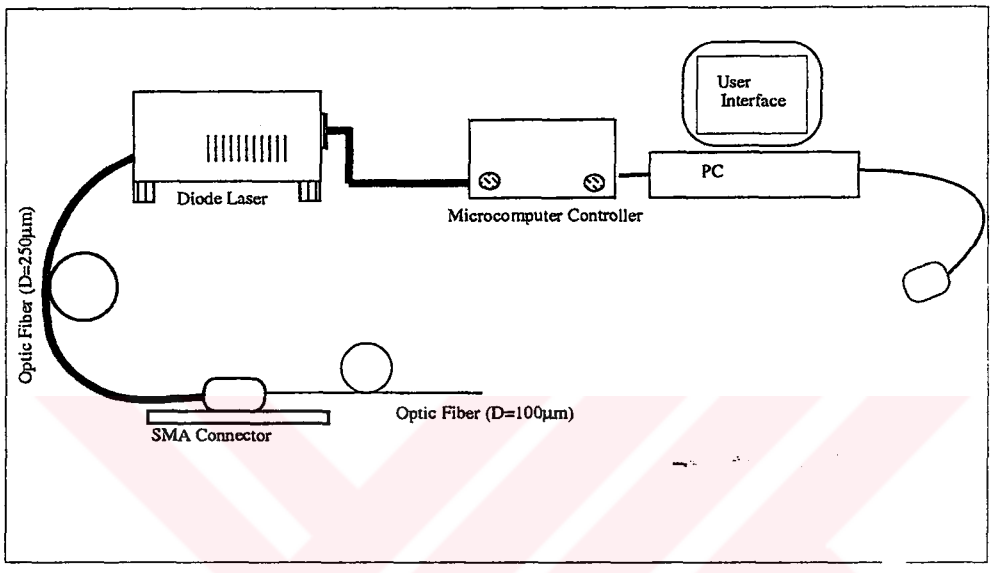

Figure 6.4. Schematic diagram of microcomputer based laser controller

Our diode laser has one analog input (Control Voltage), 2 analog outputs (Diode Current and Diode Temperature), 4 digital inputs (Power Reset, Laser On/Off, Ready in, Standby), 2 digital outputs (Emission and Ready out). The input/output characteristics and pin numbers are summarized in Table 6.1.

A microcomputer (PIC16C84) was chosen as the central processing unit. Pins #12 and #13 are used for collecting digital output from the diode laser; and pins #6 and #7 are connected to MAX232 chip which performs communication with the personal computer which runs the user interface program. Analog outputs of the diode laser (Diode current and Diode temperature) are converted by an analog to digital converter (ADC1034) and then received by PIC16C84 through pins #1 and #2 respectively. Digital outputs are obtained by using 74HC595 shift registers. Four digital outputs are reserved for relay control. Analog input of diode laser is provided by converting the digital signal generated by microcomputer through DAC714 circuitry. The ORCAD capture circuitries are showed in Figure 6.5. The ORCAD layouts showing top and bottom surfaces of the board are shown in Figure 6.6.

Table 6.1. Pin Descriptions of the 25-pin connector

Pin Number	Function	Specification
Diode Laser Inputs		
14	0-5V Control Voltage	Sets laser diode current from 0 to max. Mod freq 30 Hz (max) [Ref. Pin 2, Analog ground]
19	Power Reset	Resets the system to Standby mode when a TTLhigh is applied to powerup[Ref. Pins 8&9, +5V (Digital) &Digital ground]
20	Laser On/Off	Turns diode on when TTL is low, and off when it is high. [Ref. Pins 8&9, +5V (Digital) &Digital ground]
22	Ready in	Negative edge triggered TTL pulse turns on the diode power supply and places the system in Ready mode. [Ref. Pins 8&10, +5V (Digital) &Digital ground]
23	Standby	Negative edge triggered TTL pulse turns on the diode power supply and places the system in Standby mode. [Ref. Pins 8&10, +5V (Digital) &Digital ground]
Diode Laser Outputs		
15	Diode Current	Output voltage equal to the actual diode current. 0-1.75V = 0-35A (or 50mV/A). [Ref. Pin 1, Analog ground]
16	Diode Temperature	Output voltage equals actual diode temperature: 10 mV/°C with 250 mV = 25°C. Max/min range is 20 to 35°C. [Ref. Pin 1, Analog ground]
18	Emission	TTL high when system is ready and Laser On/Off is high. [Ref. Pins 8&9, +5V (Digital) &Digital ground]
21	Ready Out	TTL high when system is in Ready mode, low when in Standby mode. [Ref. Pins 8&10, +5V (Digital) &Digital ground]

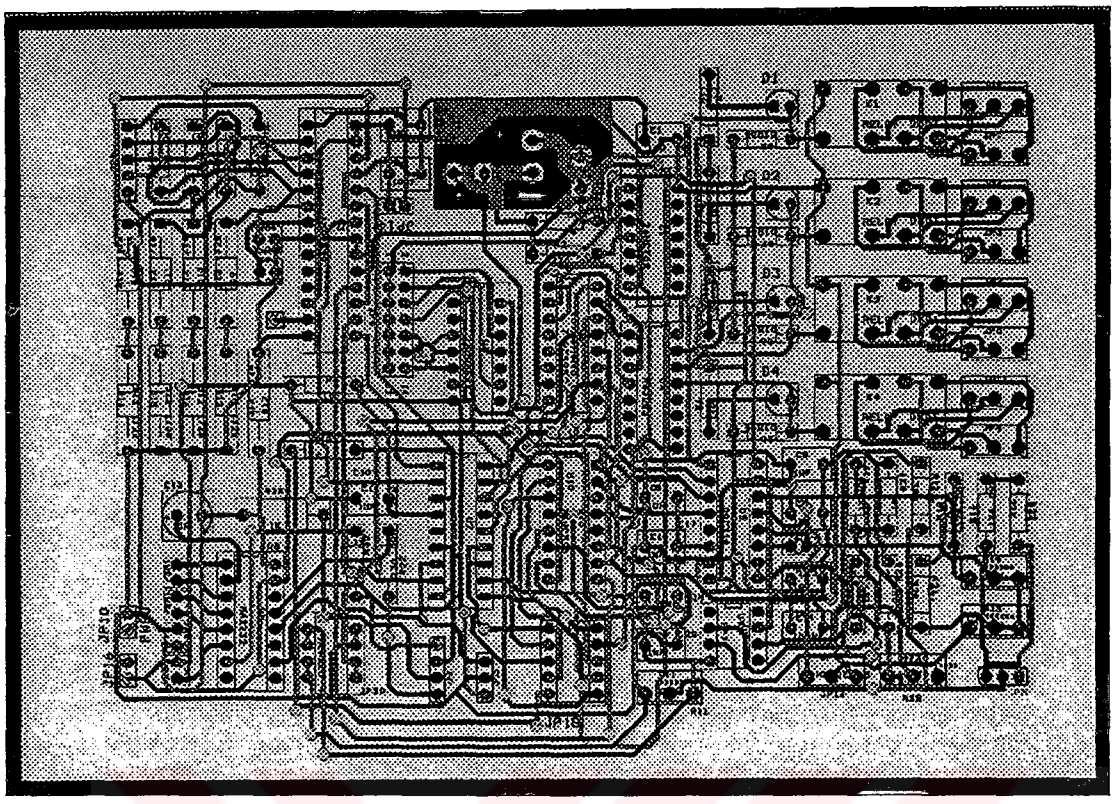

Figure 6.5. The ORCAD layout of the microcomputer based controller.

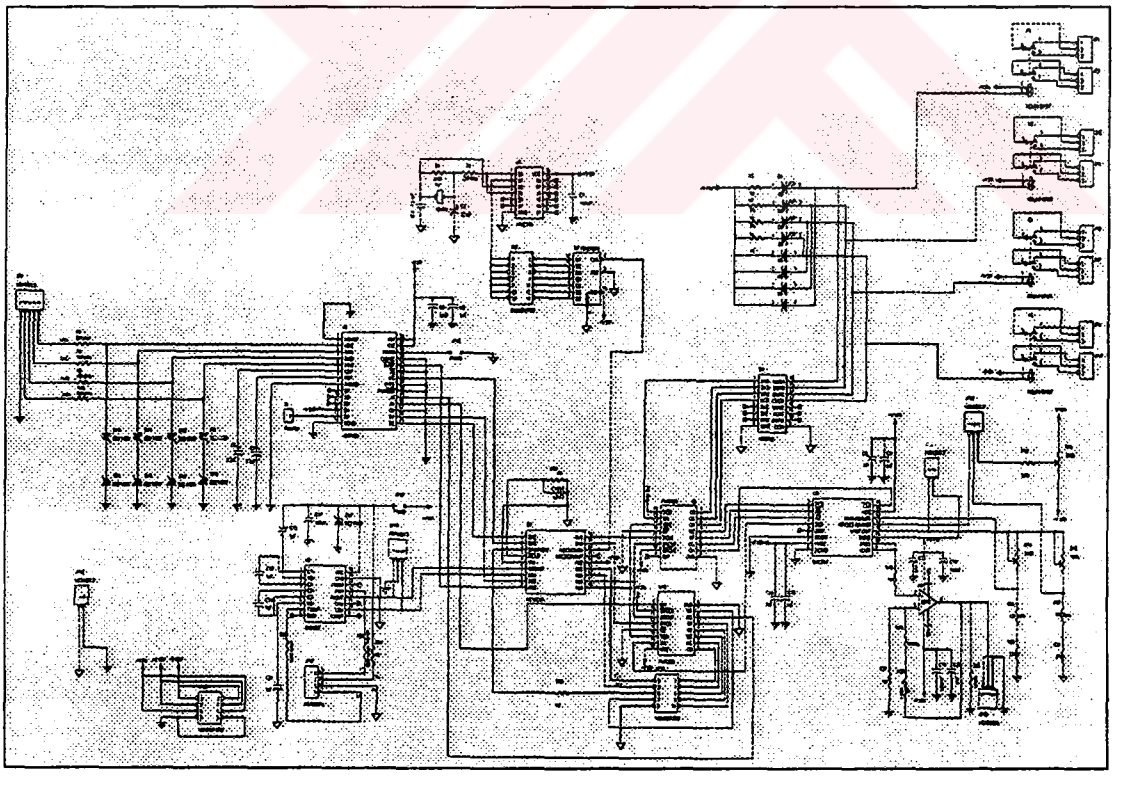

Figure 6.6. The ORCAD capture of the microcomputer based controller.

7. THE 980 nm DIODE LASER APPLICATIONS IN NEUROSURGERY

7.1. Introduction

The aim of the series of experimental studies presented below was to investigate the applicability of the 980 nm diode laser in stereotaxic neurosurgery.

In neurosurgery, electrocoagulators have been widely used to coagulate or ablate neuronal tissues. Recent studies showed that laser sources could create similar lesions with less damage to the periphery of target tissues when compared to electrocoagulators [194]. Lasers have great advantages since they could be used for cutting, vaporizing and coagulating tissues without mechanical contact [156]. Various energy sources and instrumentation systems have been under investigation for decades in order to develop better tools for cutting, ablating or coagulating target tissues without causing damage to the surrounding healthy tissues. Tissue damage due to laser irradiation is a result of laser-tissue interaction mechanisms determined by several factors including laser irradiation parameters (wavelength, output power, beam diameter, exposure time and mode); optical and thermal characteristics of target tissues (wavelength dependent coefficients of absorption and scattering, thermal conductivity and specific heat of tissue). Since organic tissues contain water up to 80%, optimal parameters strongly depend on optical properties of water at the wavelength of interest. CO_2 laser irradiation is very strongly absorbed by water and, thus it could be used for cutting and vaporizing without coagulation of almost all organic tissues. Conversely, Nd:YAG irradiation has poor absorption in water, resulting in a much larger penetration depth (2-3 mm especially for neuronal tissues) [193] and this irradiation source can be used as a coagulator.

7.2. Background

Neurosurgical applications of lasers have been studied with less excitement, compared to other medical applications of lasers [138]. The reason was the first disappointing experiments with the CO_2 laser performed at unnecessarily high power

levels. Yet, since the beginning of the 1980s, moderate power CO_2 lasers and fiber coupled Nd:YAG lasers have become popular laser sources in neurosurgical investigations. They were used in clinical applications for cutting and coagulating brain tissue [40, 192, 143, 153, 154, 41, 162, 163]. Recently, with the availability of suitable optical fibers, the 2.94 μm Er:YAG laser also became a potential surgical tool [162-163]. In the 1990s, fiber coupled high power (5-80W) diode lasers radiating in the near IR region (800-980 nm) have become commercially available with novel developments in laser technology. They are attractive for medical applications with their light-weight, portable size, lower cost, longer operating life and better operating conditions (air-cooled, silent, ready-to-use-time less than a minute) [193].

The first diode lasers used in neurosurgery operated at 800-830 nm wavelengths [157, 195]. The most important expectation of those studies were better or at least similar results in cutting and / or coagulating processes compared to Nd:YAG, CO_2 and KTP lasers [196]. According to the data reported by the early studies and some clinical applications [157,195], the 800-830 nm laser irradiation could be a better coagulation source compared to Nd:YAG; but, the results were far from being conclusive.

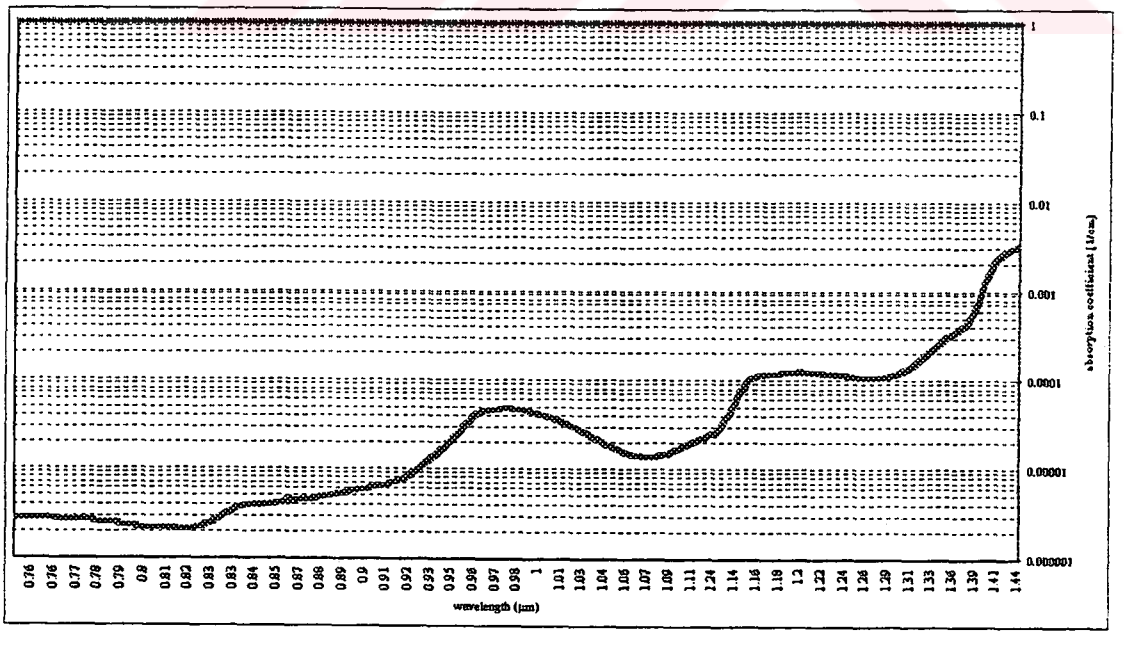

Figure 7.1. Absorption coefficient of water with respect to wavelength between 0.76-1.44 μm. There is a peak around 980 nm (Calculated from Kou et. al.'s data [197]).

7.3. Materials and Methods

The diode laser used in the present study emits radiation at 980 nm (see Appendix B.3.) and results of our early experiments showed significant differences in terms of the quality of obtained lesions compared to diode laser applications at 800-830 nm. We found that cw laser energy delivered at 980 nm vaporized the target tissue with limited coagulation zone around the target area, implying less thermal damage to surrounding tissues in the subcortical area of rat brain. It was deduced that the 980 nm laser radiation created better lesions since irradiation at 980 nm overlaps with one of the absorption peaks of water in the near infrared (IR) (see Figure 7.1.).

In the present study, stereotaxic surgical use of the 980 nm laser was investigated via histological examinations of the lesions created in rat brain. First, a predosimetry study aimed at determination of optimal lasing parameters is presented. Second, the results of the dosimetry study based on the results of the predosimetry study are summarized. Finally, the results of experiments investigating the effect of modulation will be discussed.

7.3.1. Stereotaxic Surgery

Stereotaxic surgery is a surgical method which allows the surgeon to implement an electrode or optical fiber at the desired coordinates of the brain of the subject (Figure 7.2.). It is necessary to use this method in order to perform an experiment upon a precise anatomical region of the brain. In this section the procedure of this method will be described.

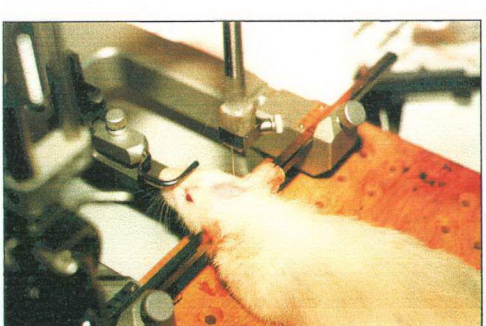

Figure 7.2. Subject placed in stereotaxic apparatus.

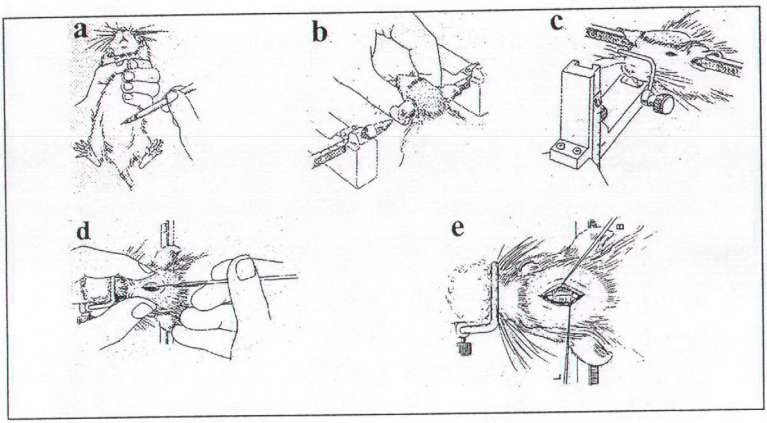

Figure 7.3. Stages of stereotaxic surgery method: (a) anesthetizing the subject by intraperitoneal injection (b-c) mounting the subject in the stereotaxic frame (d) incising the scalp (e) stereotaxic reference points bregma (B) and lambda (L) [213].

The first step was anesthetizing the rat (Figure 7.3.a). In order to determine the right anesthetic dosage, animals were weighed before the surgery. Then, they were anesthetized with ketamine (150 mg/kg ketamine; 50 mg/ml intraperitoneally). This is one of the most critical steps; overdose leads the subject to death. Ketamine was injected into the peritoneal cavity. Then, tail-pinch test was performed to determine the depth of anesthesia15 minutes after injection. The tip of the animal's tail was pinched sharply with a thumbnail. Any leg relaxation was interpreted as underdose and additional anesthetics were injected.

Second, the animal's hair from between the eyes to well behind the ears was shaven in order to minimize the possibility of infection.

Next step was mounting the animal in the stereotaxic frame. First, the fixed tip of the right stereotaxic ear bar was directed into the auditory canal of the animal's right ear by moving the head sideways against the ear-bar tip (Figure 7.3.b). Then, the loosened left ear bar was pushed into the auditory canal of the animal's left ear. After making the animal's position centered by adjusting the ear bars, animal's teeth were mounted on the incisor bar and the nose clamp was tightened (Figure 7.3.c). Afterwards, incision was done (Figure 7.3.d). The length of incision was at most 2 cm, permitting both the bone suture junctions, bregma and lambda, to be seen in the

wound (Figure 7.3.e). After the incision was made, the periosteal connective tissue which adheres to the bone was scraped off. It was necessary to dry the bone after the bleeding stopped in order to see the cranial sutures, bregma and lambda, clearly. The point bregma (B in the Figure 7.3.e) on the top of the skull is the intersection of the frontal and parietal skull plates at the midline. The point lambda (L in the Figure 7.3.e) on the top of the skull is the intersection of the parietal and interparietal skull plates at the midline. Those points were used for stereotaxic reference points. The distance between bregma and lambda was used as a correction factor for stereotaxic coordinates:

$$\text{Corrected Coordinate} = \frac{\text{Bregma} - \text{Lambda (Subject)}}{\text{Bregma} - \text{Lambda (Atlas rat)}} \times \text{atlas coordinate}$$

Coordinate points were marked and checked on the skull. Skull was drilled at those points by using a hand-held drill. Care was taken in order to eliminate the possibility of piercing the brain. Before inserting the optical fibre the dura (membrane covering the brain) was incised by using a very sharp hypodermic needle. The tip of the optical fiber was positioned on the surface of the brain and then was carefully iserted to the desired coordinates. After each laser exposure the fiber was kept in the lesion site for 2 minutes, and the next exposure followed 6 minutes after the first. Before and after each laser exposure, the tip of the fiber was checked under binocular microscope and the output power was measured. The tip of the fiber was recut by a tungsten carbide knife whenever any defect was observed. After surgery the wound was sutured and an antibiotic was applied. Behavioral observations of the animal continued to determine the time of recovery from the effects of surgery.

7.3.2. Histologic Examination

Before brain tissue can be cut into thin sections and subjected to histological examination, it was fixed and hardened. First of all, the subject was anesthetized by injection of a lethal overdose of ketamine. As soon as the the animal was anesthetized, an incision was made through the skin along the left side of the animal's sternum. The skin was peeled back and the lower blade of a pair of scissors was pushed underneath the lower boundary of the rib cage and it was cut along the sternum, through the soft ribs and muscles. A lateral incision was made along the

lower boundary of the rib cage and a flap was turned exposing the heart. This flap was cut off. As soon as the beating heart was exposed, the lower tip of the animal's right ventricle with mouse-tooth-tipped forceps and a large incision was made in it to drain the incoming venous blood. 100 to 200 ml of physiological saline was injected into the animal's left ventricle, to flush out most of the blood in the heart and brain. After the animal was perfused intracardially with 0.9% NaCl followed by 10% formaldehyde in 0.9% NaCl, it was decapitated and the brain was extracted. It was put into fixative solution (neutral buffered 10% solution of formaldehyde) in order to stabilize intercellular and intracellular substances in a state as close to the living state as possible. After 48 hours, samples were taken out of the fixative solution and rinsed in running water for two hours. Then each sample was dehydrated by 70%, 80%, 90% 100% and 100% ethyl alcohol for 18 hours, 2 hours, 2 hours, and 1 hour, respectively. After this process all water in the tissue was replaced with alcohol; the final alcohol was then replaced with a non-polar solvent, xylene. Tissue sample was then soaked in paraffin wax at a temperature above its melting point, the wax was allowed to set on cooling, and the block of wax including the tissue became ready for sectioning.

Each brain sample was sectioned in 5 μm thickness as every 100 μm throughout the lesioned part of the cortex. Six representative sections of the whole lesion were mounted onto slides and were stained by hematoxylin and eosin. Hemorrhage, fibrin exudate, coagulative necrosis, red neurons (ischemic neurons), dark neurons (atrophic neurons), macrophages and PMN (polymorphonuclear neutrophil) leukocytes were investigated.

7.4. Predosimetry Study

7.4.1. Materials and Methods

12 animals were selected from albino Wistar rats bred at Bogaziçi University's Psychobiology Laboratory. They weighed 280-320 gr at the time of surgery and were housed in their group cages before and after surgery. The rats were maintained in a temperature controlled vivarium at approximately 22°C with a 12:12 h light/dark schedule (lights on at 07:00 am.) with food and water available *ad libitum*.

Lesions were created by laser irradiation at 0.5, 1.0, 1.5, 2.0, 2.5 or 3.0 Watts. Time durations for lesion creation and lesion crater dimensions were recorded.

Surgery was performed under aseptic conditions. Animals (n=12) were anesthetized with ketamine (150 mg/kg) and put in a stereotaxic instrument. The skin was retracted and holes were drilled in the skull. Lesion coordinates were -2.8 mm posterior to bregma, ±2 mm lateral to midline, and -7.8 mm below the dura. Bilateral lesions were made in each hemisphere. Laser irradiation parameters were selected according to the results of predosimetric *in vitro* studies. The delivered power of the high power diode laser at 980 nm (Opto Power OPC-D010-980-FCPS) was controlled by a computer program developed in Superscope environment. The laser beam was delivered via a 400 μm glass fiber to the stereotaxic apparatus. Applied parameters were 2W-1.5s, 2W-2.0s, 2W-2.3s, 3W-4/3s, 3W-2s, and 3W-3s.

48 hours after the surgical procedures, animals were sacrificed by ketamin overdose and perfused intracardially with 0.9% saline followed by 10% formaldehyde in 0.9% NaCl. The brain samples were stored for 48 hr. in 10% formalin solution. 40 μm coronal sections were cut through the areas containing the lesions. Paraffin method was used during the sectioning. Every second section was mounted and stained with hematoxylin & eosin stain.

7.4.2. Results

In order to determine the optimum lasing parameters, *in vitro* experiments were performed. Power was changed gradually from 0.5 W to 3W. Dimensions of coagulation craters and exposure time were recorded (Figure 7.4). For powers below 2 W relatively long exposure time was needed to observe coagulation. 2 W laser power was found optimal to create lesions with less damage to neighbouring tissues.

Second, *in vivo* experiments were carried out within the power range of 1.5 W to 3W. The results of histologic examination showed that the 2W-2s combination was the optimum dose for good lesions with less damage to adjacent tissue (Figure 7.4 and Figure 7.5). Ablation craters surrounded with a coagulation area were observed for powers at 2 W and more; whereas only coagulation occured for less than 2 W. As exposure time increased the thermal demage created around the lesions dramatically increased. Besides, at powers greater than 2W, ablation craters obtained were much

more larger than desired and thermal damage to adjacent tissues became uncontrollable.

The shape of lesions obtained with 2W power irradiation for 2 s were quite spherical. In the center of the spherical lesion, tissues were ablated and there were coagulation zones around as expected.

The aim of this study was to investigate the applicability of 980 nm high power laser for neurosurgery. Results of *in vitro* and *in vivo* experiments and histologic examinations showed that the 980 nm laser source could be used for coagulation of neuronal tissues as an alternative to electrocoagulators and the Nd:YAG laser.

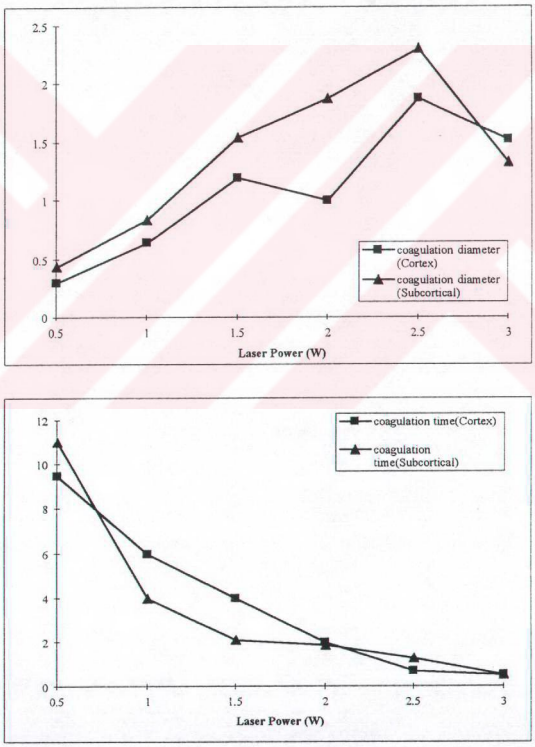

Figure 7.4. Results of in vitro experiments: coagulation time and lesion diameter as a function of laser power.

Since the 980 nm laser source can be used in neurosurgery, tissue characterization and a comprehensive dosimetry study must be performed before clinical applications. According to the collected data, 2W-2s combination is a suitable starting point for further dosimetry studies.

Previous studies showed that the diode laser at 980 nm has a lower penetration than that of the Nd:YAG laser. Irreversible damage to adjacent tissues was one of the disadvantages of Nd:YAG laser [41,162-163,193]. The current study showed that damage to peripheral tissues during diode laser irradiation was less as expected because of the higher absorption in water. Future studies should be directed towards comparing the temperature gradients created by these laser sources and electrocoagulation.

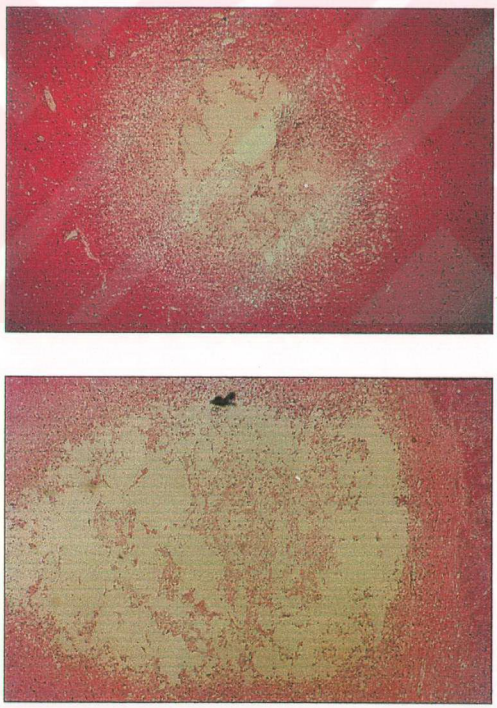

Figure 7.5. Resulting lesions by 2W-2s and 3W-2s.

7.5. Dosimetry Study

7.5.1. Materials and Methods

6 female Wistar rats weighing 180-220 gr. bred in the Animal Facility of the Psychobiology Laboratory at Bogaziçi University were used.

The diode laser (Opto Power OPC-D010-980-FCPS) emitting at 980 nm wavelength with a maximum power of 15 Watts was controlled by a personal computer (Macintosh LC). The computer program was developed in Superscope II (GW Instruments) environment as explained in Chapter 6. The program allowed the user (1) to select the output power, mode of operation (cw or modulated), modulation wave shape, and lasing duration; and (2) to monitor applied parameters (see Figure 3.2.). Control voltage (0-5 V) of the diode laser was also monitored through an oscilloscope. The laser has a maximum fiber output power of 10 W cw and was delivered through a 400 μm silica power delivery optical fiber (Spindler-Hoyer) to the stereotaxic apparatus. The output power of the fiber was measured before and after every lasing operation with a powermeter (Synrad, Powerwizard). The tip of the fiber was cut when necessary. Irradiation parameters were as follows: 2W-1.5s, 2W-2.0s, 2W-2.5, 3W-1.3s, 3W-2.0s, 3W-3.0s (238 kJ/mm^2 to 716 kJ/mm^2).

All operations were performed under aseptic conditions. The animals were anesthetized with ketamine (150 mg/kg ketamine; 50mg/ml intraperitoneally) and placed in the stereotaxic instrument. The skin was retracted and holes were drilled in the skull according to the following coordinates: -2.8 mm from bregma, ±2.0 mm lateral to midline, and -1.2 mm below the dura [198]. No changes in vital functions were expected due to lesion formation at the selected coordinates. Bilateral lesions were created in each hemisphere using the irradiation parameters determined by our previous predosimetry study [161, 211]. The time course for irradiation was in the 1.3 - 3.0 second range. The order of lesioning (left and right sides) was counterbalanced over subjects. After each exposure the fiber was kept in the lesion side for 2 minutes, and the next exposure followed 6 minutes after the last. Before and after each laser exposure, the tip of the fiber was checked under binocular microscope and the output power was measured. The tip of the fiber was recut by a tungsten carbide knife whenever any defect was observed. After surgery the wound

was sutured and an antibiotic was applied. Behavioral observations of the animal were continued to determine the time of recovery from the effects of surgery.

48 hours postoperatively, animals were sacrificed by ketamine overdose and perfused intracardially with 0.9% NaCl followed by 10% formaldehyde in 0.9% NaCl (Figure 7.6.). Brain specimens were stored in 10% formalin solution for 48 hr and blocked in paraffin. Each brain sample was sectioned in 5 μm thicknesses every 100 μm throughout the lesioned part of the cortex. Six representative sections of the whole lesion were mounted onto slides and were stained by hematoxylin and eosin. Hemorrhage, fibrin exudate, coagulative necrosis, red neurons (ischemic neurons), dark neurons (atrophic neurons), macrophages and PMN (polymorphonuclear neutrophil) leukocytes were investigated.

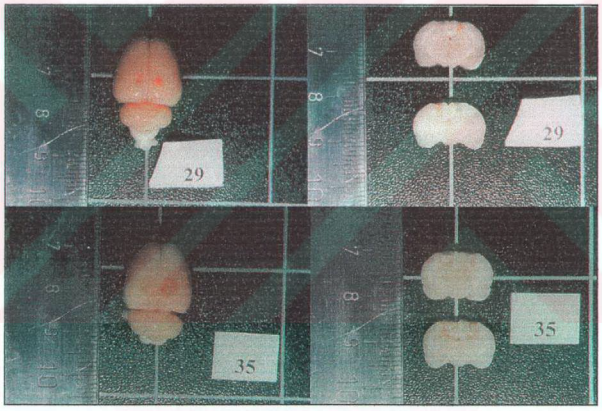

(A)

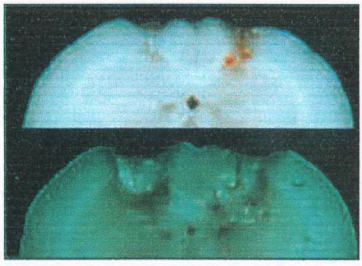

(B)

Figure 7.6. A) Typical (2W-2s and 3W-2s, 29 and 35 respectively) laser induced bilateral lesions before histological examinations. B) Magnified lesions of 29th and 35th lesions..

7.5.2. Results

Examination of the tip of the fiber revealed no tissue carbonization or adhesion. Fiber output power measurements and oscilloscope observations were also consistent with selected parameters.

The relationship between irradiation parameters (power and duration) and the dimension of created lesions in cortical tissue was examined at macroanatomic level.

Clinically, all animals recovered in less than 6 hours, and the lowest recovery time (2 hours) was observed for the animal which was subjected to the 2W-1.5s irradiation. After the recovery period, animals showed no obvious behavioral ill-effect of the surgery; their motor activities were normal and they were adequate in social interactions.

The smallest lesion was created by the 2W-1.5s irradiation whereas the greatest was created by 3W-2.0s. The diameters of the lesions were between 0.5 mm to 3.5 mm (Figure 7.7.). Diameters of lesions tended to increase with increasing power and irradiation duration. The dimensions of the lesion created by 2.0W-2.0s irradiation were found suitable. Less damage to surrounding tissue was also observed at 2.0W-2.0s irradiation. On the other hand, the lesions created at 3W power independently of irradiation duration were found too large for similar applications (Figure 7.9).

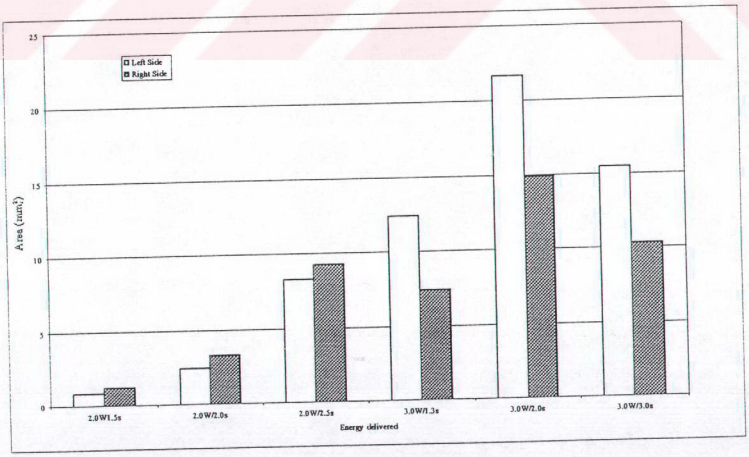

Figure 7.7. Cross-sectional areas of bilateral lesions with respect to energy delivered.

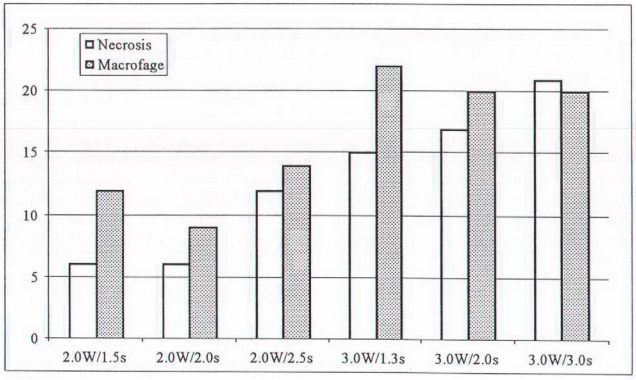

Figure 7.8. Necrosis and macrofage structures observed with respect to irradiation parameters.

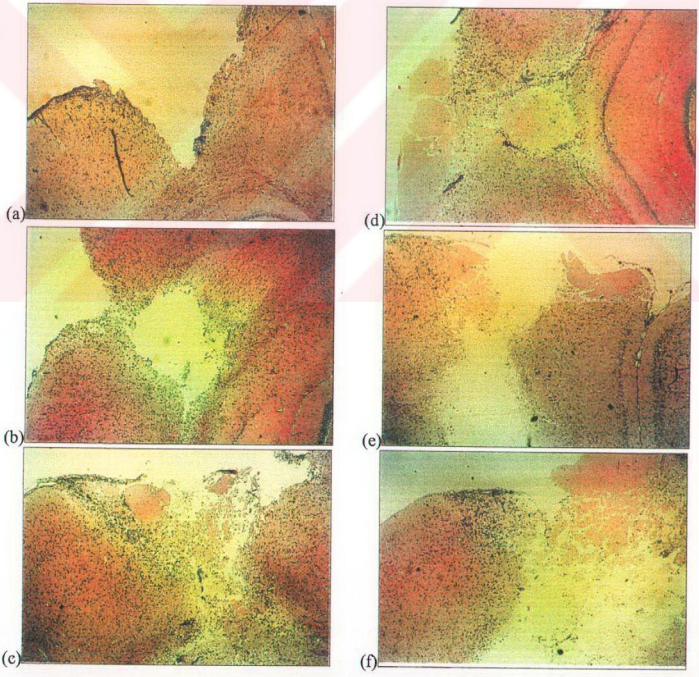

Figure 7.9. Lesions created by (a) 2W-1.5s (b) 2W-2s (c) 2W-2.5s (d) 3W-1.3s (e)3W-2s (f) 3W-3s.

The results of the histological evaluation were similar for all specimens: the target tissue was evaporated; ablated volume was surrounded by a discrete coagulation zone less than 500 μm wide; and 3rd ventricle was intact. Dark neuron formation was not observed although a limited number of the red neurons (ischemic neurons) was found. Throughout the sections, hemorrhage and fibrin exudation were absent. PMN leukocytes and macrophages were observed around the lesion sites and their numbers increased with increased amount of energy delivered (Figure 7.8.).

7.6. The Effect of Modulation

In this part, the results of the experiments done using modulated laser beam are presented.

7.6.1. Materials and Methods

14 female Wistar rats weighing 180-220 gr. bred in the Animal Facility of the Psychobiology Laboratory at Bogaziçi University were used.

Irradiation parameters were as follows: cw 2W-2.0s, cw 3W-2.0s, modulated 4J and 6J. Modulated laser irradiation consist of a series of pulses. 9W of power was delivered by 10 pulses for 4J, and 13 pulses for 6J energy, respectively, 50 ms pulse width.

All operations were performed under aseptic conditions. The animals were anesthetized with ketamine (150 mg/kg ketamine; 50mg/ml intraperitoneally) and placed in the stereotaxic instrument. The skin was retracted and holes were drilled in the skull according to the following coordinates: -2.8 mm from bregma, ±2.0 mm lateral to midline, and -1.2 mm below the dura for the first group and -2.8 mm from bregma, ±2.0 mm lateral to midline, and -1.8 mm below the dura for the second group [198]. No changes in vital functions were expected due to lesion formation at the selected coordinates. Bilateral lesions were created in each hemisphere using the irradiation parameters determined by a previous dosimetry studies [161]. The order of lesioning (left and right sides) was counterbalanced over subjects. After each exposure the fiber was kept in the lesion side for 2 minutes, and the next exposure followed 6 minutes after the last. Before and after each laser irradiation, the tip of the fiber was checked under binocular microscope and the output power was measured.

The tip of the fiber was recut by a tungsten carbide knife whenever any defect was observed. After surgery the wound was sutured and an antibiotic was applied. Behavioral observations of the animal were continued to determine the time of recovery from the effects of surgery.

48 hours postoperatively, animals were sacrificed by ketamine overdose and perfused intracardially with 0.9% NaCl followed by 10% formaldehyde in 0.9% NaCl. Brain specimens were stored in 10% formalin solution for 48 hr and blocked in paraffin. Each brain sample was sectioned in 5 μm thicknesses every 100 μm throughout the lesioned part of the cortex. Six representative sections of the whole lesion were mounted onto slides and were stained by hematoxylin and eosin. Hemorrhage, fibrin exudate, coagulative necrosis, red neurons (ischemic neurons), dark neurons (atrophic neurons), macrophages and PMN (polymorphonuclear neutrophil) leukocytes were investigated.

7.6.2. Results

Examination of the tip of the fiber revealed no tissue carbonization or adhesion. Fiber output power measurements and oscilloscope observations were also consistent with selected parameters.

Clinically, all animals recovered in less than 6 hours, and the lowest recovery time (2 hours) was observed for the animal which was subjected to the 2W-2.0s irradiation. After the recovery period, animals showed no obvious behavioral ill-effect of the surgery; their motor activities were normal and they were adequate in social interactions.

The relationship between irradiation parameters (power and duration) and the dimension of created lesions in cortical tissue was examined macroanatomically level.Among the lesions created on cortical tissue, the smallest lesion was created by the 2W-2.0s irradiation whereas the largest was created by 3W-2.0s. Volumes of lesions were between 15 mm^3 to 27 mm^3 (Figure 7.10). Diameters of lesions tended to increase with increasing power and irradiation duration. Dimensions of the lesion created by 2.0W-2.0s and pulsed 4J irradiation were found suitable. Less damage to surrounding tissue was also observed at 2.0W-2.0s and 4J irradiation. On the other hand, the lesions created at 3W-2.0s and 6J irradiation were found too large for similar applications.

For the lesions created on the subcortical tissue, the smallest lesion was created by the 2W-2.0s irradiation whereas the largest was created by 3W-2.0s. The volumes of the lesions were between 5 mm^3 to 27 mm^3 (Figure 7.11.). Diameters of lesions tended to increase with increasing power and irradiation duration. The dimensions of the lesion created by 2.0W-2.0s irradiation was found suitable. Less damage to surrounding tissue was also observed at 2.0W-2.0s irradiation. On the other hand, the lesions created at 3W-2.0s, 4J and 6J irradiation were found too large for similar applications.

The lesions created on cortical tissues were not different with respect to lasing regime. Yet, in subcortical regions modulated laser beam created bigger lesions when compared to cw irradiation.

The results of the histological evaluation were similar for all specimens: the target tissue was evaporated; ablated volume was surrounded by a discrete coagulation zone less than 500 μm wide; and 3rd ventricle was intact. Dark neuron formation was not observed although a limited number of the red neurons (ischemic neurons) was found. Throughout the sections, hemorrhage and fibrin exudation were absent. PMN leukocytes and macrophages were observed around the lesion sites and their numbers increased with increased amount of energy delivered.

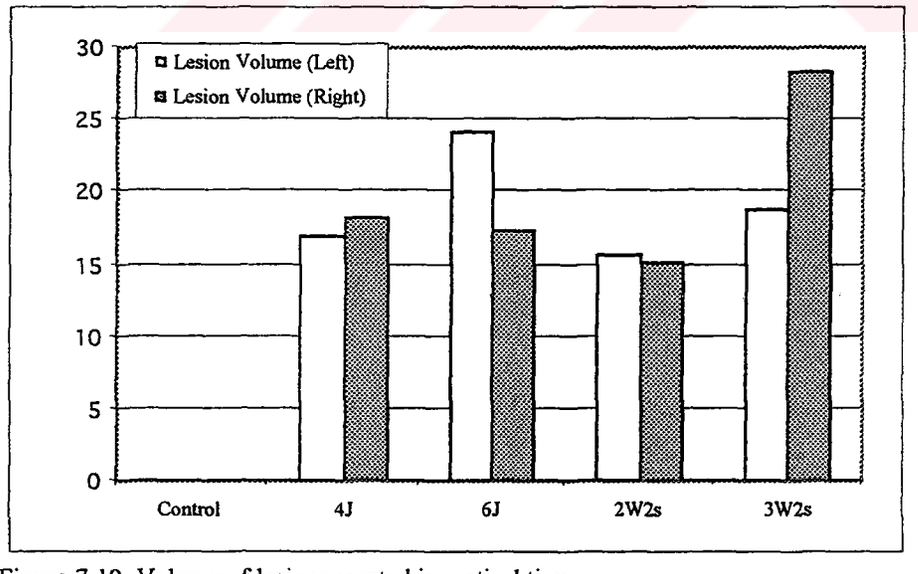

Figure 7.10. Volume of lesions created in cortical tissue.

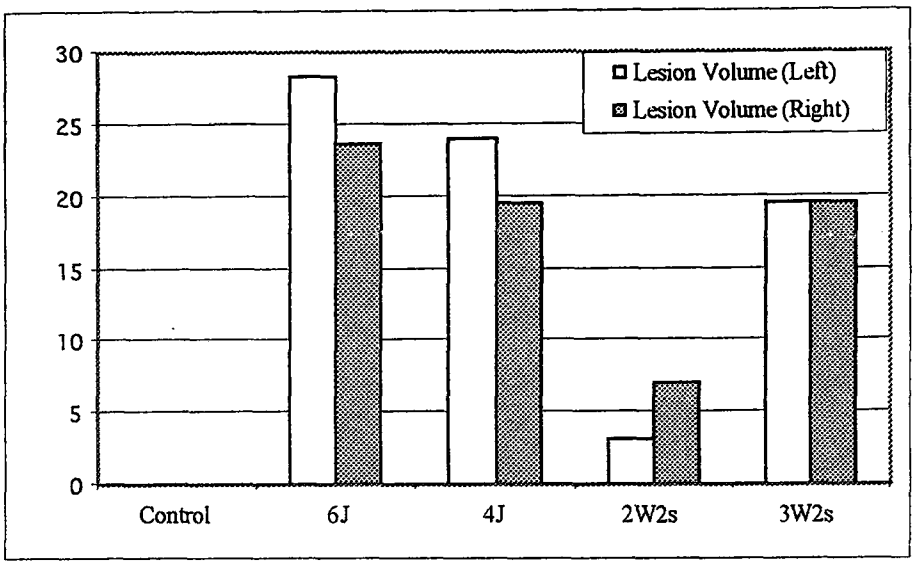

Figure 7.11. Volume of lesions created in subcortical tissue.

7.7. Discussion

In the present study, (1) the performance of the laser delivery system was tested under *in vivo* conditions; (2) optimal dose for lesion formation in rat brain tissue was estimated; and (3) histological examination showed that clearly defined lesions with minimal damage to surrounding tissue could be created with the application of the optimal dose.

We had observed earlier that the 980 nm diode laser is a promising tool for neurosurgical applications. The results of the present study supported our earlier observations. Moreover, we observed that the 980 nm irradiation created lesions with (1) less energy delivered and (2) less damage to surrounding tissues, when compared to the lesions created by the recently introduced 800-830 nm high power diode lasers [157,195]. This might be the result of the high water content of soft tissues. As seen in Figure 7.1., the 980 nm wavelength is absorbed by water better than at 800-830 nm (and also better than at 1064 nm, the wavelength of one of the most popular medical laser source, the Nd:YAG). It is necessary, however, to investigate the optical and thermal properties of target tissues before any conclusions can be reached.

An advantage of the 980 nm wavelength laser was the capability of creating lesions of similar or same dimensions with less energy delivered. This also prevented

possible damage at the tip of the fiber. No carbonization and/or destruction was observed in contrast to the report of a previous diode laser application at 800-830 nm [195]. Studies indicate that the 800-830 nm diode laser is more suitable for pigmented than non-pigmented tissues. The present study showed that the 980 nm wavelength is also suitable for non-pigmented tissues.

Previous experimental studies showed the superiority of lasers in terms of thermal effects on nervous tissue when compared to electro surgery [194]. It was well stated that surgical lasers caused less necrosis, surrounding edema and heat diffusion when compared to monopolar and bipolar electorsurgical devices (thermal effect of electrocoagulator diffused up to 3 mm). In our case, the thermal damage of 980 nm diode laser caused only a local (less than 1 mm) thermal alteration of surrounding tissue.

Results described the thermal responses of cortical and subcortical tissues due to cw and pulsed diode laser irradiation. The difference between cortical and subcortical tissues became evident for this wavelength as in the case of Er:YAG study. It is interesting that this difference can only be seen for modulated regime, i.e. short laser pulses with greater power levels. The 980 nm diode laser can be more suitable as a neurosurgical device compared to other popular lasers (Nd:YAG, KTP), with the advantage of having compact size, low weight, less setup and running expenses. It provides high efficiency and long life reliability. It could also be advantageous because of its higher absorption in water compared to the 800-830 nm diode laser.

According to the data collected, the 2.0W-2.0s irradiation parameter was a suitable starting point for comprehensive dosimetry studies. Future studies may shed light on other aspects of this new laser wavelength such as the ablative effect at high power / low exposure time regime; the optical and thermal properties of brain tissue; the effect of fiber tip geometry; may allow the 980 nm diode laser system to be used efficiently in clinical applications.

8. 980 NM DIODE LASER AS A NEW STIMULANT FOR LEP STUDIES

8.1. Introduction

The electrical activity of brain during perception of painful stimulation can be recorded through scalp electrodes and such electrical potentials are called pain-related brain potentials (PRP). In order to increase the signal to noise ratio, numerous EEG epochs during stimulation are averaged in accordance with evoked potential paradigms [199-200]. Nociceptive electrical, mechanical, chemical or thermal stimuli can evoke PRP, but, only lasers are recognized as suitable thermal stimulators. Lasers are regarded suitable stimulators whereas other electrical, mechanical, chemical or thermal stimuli may yield concurrent activation of pain and mechano-receptive fibers. Lasers are convenient thermal stimulators because they can be

1. synchronized with EEG recordings;
2. applied without physical contact, thus they do not yield multiple modalities of evoked potentials.

The evoked potentials induced by laser irradiation are called laser evoked potentials (LEP). The relationship between PRP and components of LEPs are still under investigation.

So far, different laser wavelengths were investigated [199-204]; Argon ion and CO_2 lasers were found to be best stimulators. Lasers in those experiments were used to deliver high energy pulses for short durations to record PRP, which is the electrophysiological response that occurs approximately 300 msec post-stimulus. Argon lasers were preferred because of this wavelength's relatively large penetration depth in skin and the ease of fiber coupling. On the other hand, it is a problem to afford and maintain an Argon ion laser system (cooling, weight, life time etc.).

Nd:YAG lasers were also tested, but with poor water absorption at 1064 nm, higher power levels up to 85 Watts were required. Results of comparative studies emphasized the CO_2 laser as the most efficient and practical stimulator despite the studies reporting some thermal damage seen at high energies [204-210].

In pain stimulation, the laser-tissue interaction is basically thermal. It is crucial to induce pain sensation with short pulses (10-250 msec exposures) by delivering the lowest possible energy. Fiber coupling is also an important factor for delivering energy to the desired portion of the body. Finally, the practical aspects of the laser system in use are to be considered.

The thermal effect of the 980 nm diode laser on biological tissue was investigated by our group before [161,211]. In this study, we had hypothesized that the 980 nm compact diode laser with better water absorption characteristics, thus because of better absorption by tissue when compared to the Nd:YAG laser, it can be a better stimulant for pain studies.

8.2. Materials and Methods

10 healthy subjects (5 women and 5 men) participated in our experiments voluntarily. The average age of our subjects was 30.5 (standard deviation: 7.2; range: 20 to 39). The experimental room was kept silent and dark. Subjects were calm, attentive and relaxed. They were informed about the experiment beforehand and their consent was taken.

The diode laser (Opto Power OPC-D010-980-FCPS) at 980 nm with a maximum power of 15 Watts was controlled by a personal computer and synchronized with EEG recordings. A computer program developed at the Physiology Department of Istanbul Medical School allowed the user (1) to select the output power and laser exposure duration; and (2) to record amplified EEG signals in the pre- and post-stimulus duration. Diode laser control voltage (0-5 V) was also monitored on an oscilloscope. The laser with a maximum output power of 10 W cw was delivered

through a 400 μm silica optical fiber (Spindler-Hoyer) to a collimator. Laser beam was collimated by a spherical lens and diameter of the collimated beam was 3 mm. The output power of the collimator was checked before and after every lasing operation with a powermeter (Synrad, Powerwizard). Irradiation duration was set to 200 ms. To determine the subjective pain threshold, the power of laser irradiation exposed to the right forehand of the subjects could be adjusted to 16 discrete levels in the range of 0 to 10 Watts in ascending order. Subjects were asked to report the nature of sensation at every level. The level at which the beginning of pain sensation was reported, was defined the pain threshold. During experimentation, 1.5 times the power of this level was applied as stimulus. The subjects described the stimulus presented during the EEG recording as a bearable pain sensation like pinprick perception.

EEG was recorded from scalp electrodes placed on areas Fz, Cz, Pz, C3 and C4 according to the international 10-20 system. 100 msec pre- and 900 msec post-stimulus EEG epochs were recorded at 256 Hz sampling rate after 0.1-30 Hz analog low pass filtering. 30 stimuli were presented by randomly varying the interstimulus duration between 5 and 9 seconds. Recorded EEG epochs were averaged and passed through a 0-45 Hz low pass digital filter. Latency (the time duration between stimulus and the corresponding positive or negative peak detected) and amplitude values of LEPs were measured.

8.3. Results

LEPs due to the 980 nm diode laser stimulation were recorded from 10 subjects. The average power applied was 7.55 W, with a standard deviation of 1.48 W. No irreversible thermal damage was observed on irradiated tissue.

Two negative (N1 and N2) and two positive peaks (P1 and P2) were detected in the LEP. The latencies and amplitudes of those potentials were clearly observed on the records of 8 subjects. The grand average of the LEPs recorded from those subjects

were presented in Figure 8.1. Some errors occurred at electrode locations of 2 subjects during the EEG measurement, thus only the correctly measured values were included in the analysis. The average values of latencies and amplitudes of pain related potentials were calculated and presented in Table 8.1. The variability of N1 and P1 waves, which have earlier latencies, were found to be greater than N2 and P2 waves.

Table 8.1. Average values of latencies (msec) and amplitudes (μV) of 10 subjects' PRP.

Electrode Localization	**N1**		**P1**	
	Latency	**Amplitude**	**Latency**	**Amplitude**
Fz	296.6±73.2	-3.6±2.2	358.6±71.5	2.8±2.3
Cz	303.4±78.0	-3.6±1.8	365.8±68.1	2.0±1.4
Pz	307.9±77.6	-3.6±1.6	371.4±68.3	2.4±1.9
C3	298.7±79.2	-3.3±1.7	371.8±92.0	1.7±1.7
C4	300.2±7.6	-3.5±1.5	375.9±80.2	2.7±1.9
Electrode Localization.	**N2**		**P2**	
	Latency	**Amplitude**	**Latency**	**Amplitude**
Fz	427.6±48.5	-3.2±2.6	531.0±45.6	6.1±3.3
Cz	425.3±45.3	-3.7±3.0	525.0±40.2	6.2±3.1
Pz	440.1±55.5	-3.9±2.4	526.9±38.6	6.3±3.0
C3	412.6±58.4	-3.6±2.4	524.0±39.4	6.2±2.9
C4	419.0±47.7	-3.5±2.0	516.1±40.2	6.3±3.3

Table 8.2. Variables that show significant differences due to sex of the subjects.

		Male	**Female**	**F**	***p***
C3	P2 Latency(msec)	550.0±20.3	480.7±10.0	29.3169	0.0016
C4	P2 Latency (msec)	542.0±32.9	481.7±9.6	9.0736	0.0297
C3	N2 Latency (msec)	441.1±43.4	364.7±51.3	5.1775	0.0632
C4	P1 Amplitude (μV)	1.7±0.9	3.9±2.3	4.2946	0.0769
Laser Power (Watt)		6.74±1.13	8.36±1.43	3.9572	0.0819

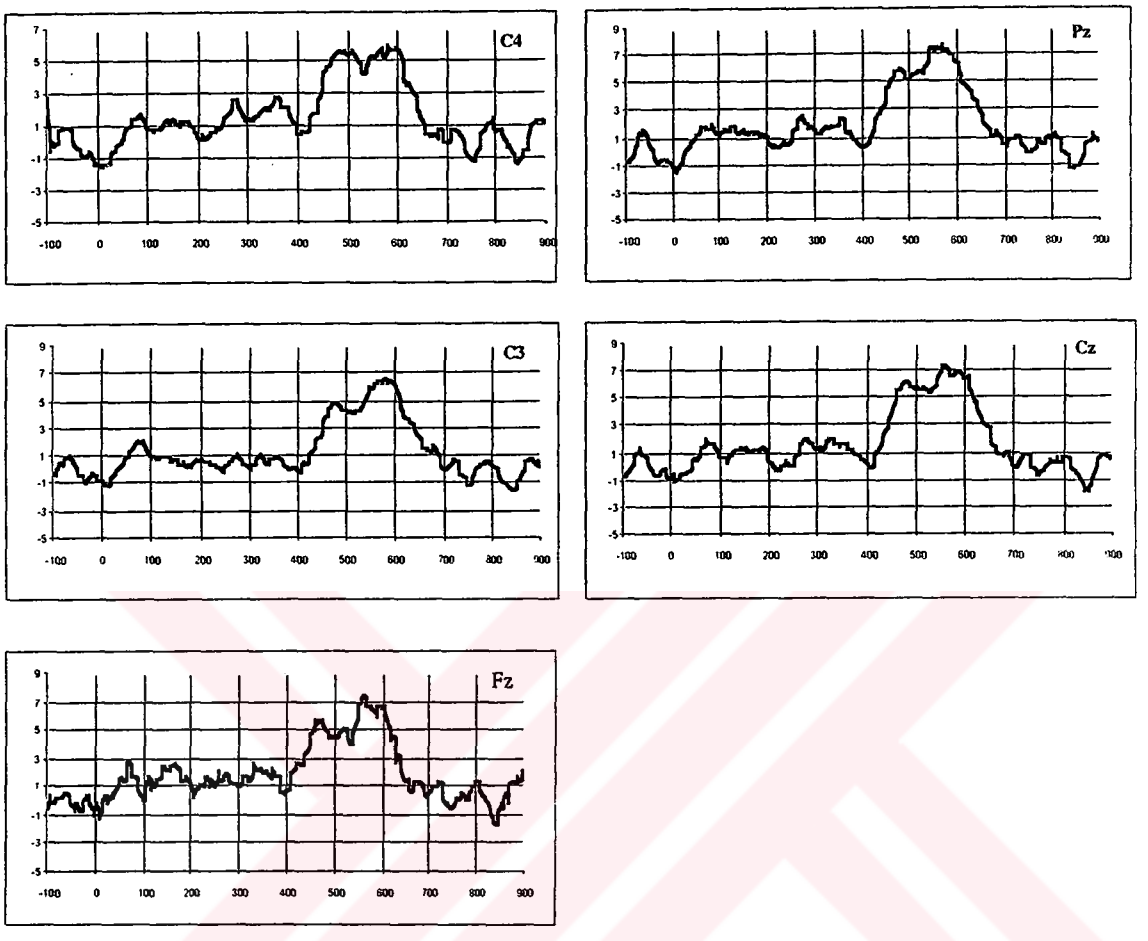

Figure 8.1. The grand average of the LEPs recorded from ten subjects (Horizontal axis shows time in ms and vertical axis shows potential in μV).

The measured values for male and female subjects were compared via ANOVA test. The latencies of P2 wave recorded from C3 and C4 standard electrode locations were found significantly different between male and female subjects ($p < 0.05$). The differences in the latencies of N2 wave at C3 location, the amplitudes of P1 wave at C4 location, and the average laser power applied as a function of sex were remarkable (see Table 8.2.).

8.4. Discussion

It is difficult to compare the N1/P1 and N2/P2 latencies and magnitude of amplitudes with the results of previous studies. There is a great latency / amplitude discrepancy due to lack of standardization in LEPs of pain research [200]. In spite of this fact,

the measured LEPs in this study are believed to be the major indicators of pain related potentials because of their wave pattern (it is similar to the LEP patterns reported in previous studies cited in 8.1. Introduction part) and acceptable values of latencies and magnitude of amplitudes. Even the differences found between male and female subjects were not consistent, the tendency of this difference was not surprising as females have higher pain thresholds than males.

Besides parameters like stimulus duration and interstimulus interval, the perception of pain and physiological response due to this perception heavily depend on the stimulator, the laser wavelength and the optical and thermal response of tissue at this wavelength. The wavelength used in this study has different characteristics when compared to those of the lasers (Argon ion, CO_2, Copper vapor, Nd:YAG) used before. Argon ion has a greater penetration depth because of low absorption in tissue but it has a drawback for the blood vessels as a consequence of high absorption of blood. The disadvantage of CO_2 is that irreversible thermal injuries may be induced during experiments. Although the 1064 nm wavelength of the Nd:YAG is very close to our laser's wavelength, the relatively larger water absorption at 980 nm may make significant differences in applications without causing any thermal injury. The results of our study showed that 7.55 W mean pain threshold for 980 nm diode laser is significantly lower than Nd:YAG laser pain threshold reported as 30-40 Watts [207].

Our preliminary results showed that the 980 nm diode laser has the capability of being a pain stimulator for LEP studies. It is worthy to test the influential parameters such as interstimulus interval, beam size, duration of stimulus and also to experiment on different sites of the body, such as oral mucosa, for different possible applications described by other researchers [208-209].

The results of this study introduced the 980 nm diode laser as a promising tool for LEP studies. The 980 nm diode laser can be more suitable stimulating device compared to other popular lasers (Argon ion, CO_2, Nd:YAG), with the advantage of having compact size, low weight, ease of coupling with optical fibers, less setup and running expenses for electrophysiology laboratories and clinical environment. It provides high efficiency and long life reliability.

9. CONCLUSIONS

Laser studies in medicine need an interdisciplinary approach as in the case of other biomedical research. After an extensive review, standard methods and well-defined procedures were followed in the studies presented in this manuscript:

i) Modelling: In order to understand laser-tissue interaction mechanisms, Monte Carlo modelling technique was applied. Laser fluence distribution in biological medium was investigated by the help of ready-to-use models. Simulation results shed light on the coagulative effect or infrared irradiation. Those simulation trials emphasize the differences in the resulting laser induced coagulation zones between tissues and underline the significance of optical characteristics of biological medium.

ii) Instrumentation: Design of the new surgical laser delivery system followed the stages of computer programming, electronic circuitry design, and controlling techniques. Two different design paradigms were folowed: (1) A quick virtual instrumentation solution and (2) A 'conventional' microcomputer based controller design. Both methods have their own advantages. Virtual instrumentation solution is heavily dependent on an enslaved personal computer whereas microcomputer based controller made the system an independent instrument. The latter one permits the researchers to use the system in clinical environment easily.

iii) Measurement: The motivation behind the experimental studies was (1) to test the developed system in real world, and (2) to investigate the physical phenomenon occurred during the application of new laser wavelengths within biological tissue. Experiments consist of *in vitro* and *in vivo* applications, histopathalogical examinations, and precise dosimetry of laser irradiation.

The methodology cited above related to various fields of biomedical research. One of the significant contribution of this study is the ability of gathering various research teams and applying different modelling, design and measurement techniques.

Interdisciplinary line of research yielded the various aspects of the subject investigated.

The original contributions of the present study are discussed below:

1. Different biological tissues were compared in terms of laser fluence distribution. The homogeneity of cardiac tissue due to Nd:YAG laser irradiation were pronounced. Experiments showed the coagulative effect of widely known Nd:YAG laser and results provided evidence for the relevancy of Monte Carlo simulation technique. The simulation results guided the rest of the study in two aspects:

   i. 1064 nm wavelength is very close to 980 nm but showed deep penetration in soft tissues. The findings reported in literature motivated the study to select 980 nm wavelength as a better candidate for surgical applications.

   ii. Great penetration depth at 1064 nm, especially in, cardiac and neuronal tissues provided evidence for questing new laser wavelengths for those applications. Thus, Er:YAG laser was taken under investigation for precise ablation in cardiovascular applications and similarly, 980 nm diode laser was preferred for neurosurgical applications.

   Besides, results of Monte Carlo simulations provided meaningful evidence for the laser-tissue interaction mechanisms:

   i. The differences in fluence distribution in radial and axial dimensions were observed in simulation results. Similar behavior was expected for cortical lesions created by 980 nm diode laser, stereotaxic coordinates were selected accordingly.

   ii. Simulations dealing with lased tissue showed significant differences due to the change in optical characteristics of lased tissue. This information was critical for experimental studies. Dosimetry was adjusted according to the carbonization treshold of tissue and tip of fiber. Consequently, carbonization was not observed.

2. Er:YAG laser was first experimented on cardiac tissue and we showed that it was a candidate for ablative purposes. Experiments were done with both Nd:YAG and Er:YAG lasers. The coagulative effect of Nd:YAG laser was studied by

simulation. Great penetration depth and homogeniety of cardiac tissue due to Nd:YAG irradiation were validated through *in vitro* experiments. On the other hand, the ablation effect of Er:YAG laser promised an application area in cardiovascular tissue. Conical ablative craters with minimal thermal damage to surrounding tissue might be preferred for selective ablation of tachicardiac foci. It is shown that, at Er:YAG wavelength, the effect of laser irradiation differed due to type of tissue. That part of the study permitted us to compare the laser-tissue interaction mechanisms of two different laser wavelengths.

3. Original data were presented dealing with the effect of the Er:YAG laser within cerebellar and cerebral tissues. Results were significant for the future applications of the Er:YAG laser within brain tissue as an ablator. Moreover, collected data reveals interesting information such as the differences in dimensions of conical ablation craters due to cortical and subcortical tissue differentiation. The major parameter in that differentiation was found as the difference in water content of tissue. Laser ablation dimensions were also found significantly different for different parts of cardiac tissue due to the different levels of water content. That property can be generalized to all soft tissues.

4. The 980 nm diode laser was presented as a new surgical device for brain tissue. The experience of simulations and experimental research dealing with various laser types (Er:YAG and Nd:YAG) versus soft tissues created a solid base for selecting diode laser wavelength and design of proper experimental procedures. A computer controlled laser delivery system for the 980 nm diode laser was designed and developed. Different instrumentation techniques contributed to biomedical instrumentation. The possibilities of virtual instrumentation resulted appreciable conveniency. That surgical laser system was adapted to stereotaxic surgical procedure and tested through *in vitro* and *in vivo* animal experiments. Experiments were carried out in a psychobiology laboratory and a well-defined laser lesioning technique was developed for the future studies of that laboratory. That was the natural outcome of interdisciplinary cooperation. All possible aspects (laser dosimetry, different regimes of laser irradiation, histological examination of thermally altered tissue) of laser-tissue interaction implications were studied and the results providing concrete evidences for the benefits of this new laser system were reported for the first time in the literature.

5. New possibilities for the use of the 980 nm laser system were researched. The interaction mechanism of 980 nm diode laser is mostly thermal as Nd:YAG laser. On the base of similar arguments for creating better thermal coagulation compared to Nd:YAG laser, 980 diode laser was investigated for LEP (Laser Evoked Potential) studies as a pain stimulant. The experiments done on human subjects showed that this new laser system can be a better candidate than the Nd:YAG laser for pain studies. Laser system was succesfully adopted to electrophysiological measurement techniques.

6. New laser systems were investigated and offered new applications in biomedicine, especially in surgery. Future studies including tissue characterization and modeling lesion formation in those biological tissues may contribute to the development of those laser systems investigated.

7. In spite of financial diffuculties, lack of sufficient technological resources and limited laboratory conditions all the original work was done sucsessfully for the first time in Turkey. Moreover, results were published in well-known international journals. The most important contribution of all is the completion of extensive fundamental scientific research covering use of medical lasers in Turkey.

REFERENCES

[1] **Maiman, T.,** 1960. Optical and microwave-optical experiments in ruby, *Phys. Rev. Lett.* **4**, 564-566.

[2] **Welch, A.J.,** 1989. Laser physics and laser-tissue interaction, *Phys. Syst. Des. Expt. Appl.*, **16** (3) 141-149.

[3] **Welch, A.J. and van Gemert, M.J.C.,** 1995. Overview of optical and thermal laser-tissue interaction and nomenclature in *Optical-Thermal Response of Laser-Irradiated Tissue*, pp. 1-12, Eds Welch A.J. & van Gemert M.J.C., Plenum Press, New York.

[4] **Letokohov, V.S.,** 1996, Some future trends of laser biomedicine in *Biomedical Optical Instrumentation and Laser-Assisted Biotechnology*, pp. 3-20, Eds. Scheggi, A.M., Martellucci, S., Chester, A.N. & Pratesi R, Kluwer Academic Publishers, Erice.

[5] **Vogel, A., Schweiger, P., Frieser, A., Asiyo, M.N. and Birngruber, R.,** 1990. Intraocular Nd:YAG laser surgery: light-tissue interaction, damage range, and the reduction of collateral effects, *IEEE J. Qu. Electron.* **QE-26**, 2240-2260.

[6] **Greenwell, T.J., Wyman, A. and Rogers, K.,** 1993. Potentiation of laser-tissue Interactions of the 805 nm laser with indocyanne green, *Laser. Med. Sci.*, **8**, 283-287.

[7] **Thomsen, S.,** 1991. Pathological analysis of photothermal and photomechanical effects of laser-tissue interactions, *Photochem. Photobiol.*, **53**, 825-835.

[8] **Zweig, A.D., Frenz, M., Romano, V. and Weher, HP.,** 1988. A comparative study of laser interaction at 2.94 μm and 10.6 μm, *Appl. Phys.*, **B47**, 259-265.

[9] **Bleir, A.R., Jolesz, F.A., Cohen, M.S., Weisskoff, R.M., Dalcanton, J.J., Higuchi, N., Feinberg, D.A., McKinstry, R.C. and Hushek, S.J.,** 1991. Real time magnetic resonance imaging of laser-tissue interactions, *Magn. Reson. Med.*, **21**, 132-137.

[10] **Niemz, M.H.,** 1996. Laser-Tissue Interactions, Heidelberg: Springer, 208-215.

[11] **Duck, F.A.,** 1990. Physical Properties of Tissue, Academic Press, London.

[12] **Jacques, S.L.,** 1996, Modelling light propagation in tissues in *Biomedical Optical Instrumentation and Laser-Assisted Biotechnology*, pp. 21-41, Eds. Scheggi A.M., Martellucci S., Chester A.N. & Pratesi R,: Kluwer Academic Publishers, Erice.

[13] **Garrison, B.J. and Srinivasan, R.,** 1985. Laser ablation of organic pollymers: microscopic models for photochemical and thermal processes, *J. Appl. Phys.*, **57**, 2909-2914.

[14] **Barr, H., Bown, S.G., Krasner, N. and Boulos, P.B.,** 1989. Photodynamic therapy for colorectal disease, *Int. J. Colorectal Dis.*, **4**, 15-19.

[15] **Barr, H., Bown, S.G., Krasner, N., Boulos, P.B., Chatlani, P. and Bown, S.G.,** 1990. Photodynamic Therapy for colorectal cancer: a quantitative pilot study, *Br. J. Surg.*, 77, 93-96.

[16] **Benson, R.C.,** 1985. Treatment of diffuse carcinoma in situ by whole bladder hemotoporphyrin hematoporphyrin derivative photodynamic therapy, *J. Urol.*, **134**, 675-678.

[17] **Camps, J.L., Powers. S.K., Beckman, W.C., Brown, J.T. and Weissmann, R.M.,** 1985. Photodynamic therapy of prostate cancer: an in vitro study, *J.Urol.*, **134**, 1222-1226.
[18] **Feyh, J., Goetz, A., Müller, W., Königsberger, R. and Kastenbauer, E.,** 1990. Photodynamic therapy in head and neck surgery, *J. Photechem. Photobiol.*, 7, 353-358.
[19] **Harty, J.I., Amin, M., Wieman, T.J., Tseng, M.T., Ackerman, D. and Broghamer, W.,** 1989. Complications of whole bladder dihematoporphyrin ether photodynamic therapy, *J. Urol.*, **141**, 1341-1346.
[20] **Karanov, S., Shopova, M. and Getov, H.,** 1991. Photodynamic therapy in gastrointestinal tumors, *Lasers Surg., Med.*, **11**, 395-398.
[21] **Marynissen, J.P.A., Jansen, H. and Star, W.M.,** 1989. Treatment system for whole bladder wall photodynamic therapy with in vivo monitoring and control of light dose rate and dose, *J.Urol.*, **142**, 1351-1355.
[22] **Moan, J. and Christensen, T.,** 1981. Photodynamic effects on human cells exposed to light in the presence of hematoporphyrin. Localisation of the active dye, *Cancer Lett.*, **11**, 209-214.
[23] **Nseyo, U.O., Dougherty, T.J., Boyle, D.G., Potter. W.R., Wolf, R., Huben, R. and Pontes, J.E.,** 1985. Whole bladder photodynamic therapy for transitionalcell carcinoma of bladder, *Urology*, **26**, 274-280.
[24] **Overholt, B., Panjehpour, M., Tefftellar, E. and Rose, M.,** 1993. Photodynamic therapy for treatment of early adenocarcinoma in Barret's esophagus, *Gastrointest. Endosc.*, **39**, 73-76.
[25] **Röder, B., Nather, D., Lewald, T., Braune, M., Freyer, W. and Nowak, C.,** 1990. Photophysical properties and photodynamic activity in vivo of some tetrapyrroles, *Biophys. Chem.*, **35**, 303-312.
[26] **Shumarker, B.P. and Hetzel, F.W.,** 1987. Clinical laser photodynamic therapy in the treatment of bladder carcinoma, *Photochem. Photobiol.*, **46**, 899-901.
[27] **Wilson, B.C. and Patterson, M.S.,** 1986. The physics of photodynamic therapy, *Phys. Med. Biol.*, **31**, 327-360.
[28] **van Best, J.A., Schuitmaker, H.J., Dubbelman, T.M., Van der Poel, C.J. and Fakkel, J.,** 1993. Near infra-red diode laser for photodynamic tumour therapy using bacteriochlorina, *Lasers Med. Sci.*, **8**, 157-162.
[29] **Baggish, M.S., Barash, F., Noel, Y. and Brooks, M.,** 1992. Comparison of thermal injury zones in loop electrical and laser cervical excisional conization, *Am J. Obstet. Gynecol.*, **166**, 545-548.
[30] **Çilesiz, İ.F. and Welch, A.J.,** 1993. Light dosimetry: effcts of dehydration and thermal damage on the optical properties of the human aorta, *Appl.Opt.*, **32**, 477-487.
[31] **Van Gemert, M.J.C. and Welch, A.J.,** 1989. Time constants in thermal laser medicine, *Lasers Surg. Med.*, **9**, 405-421.
[32] **Henriques, F.C.,** 1947. Studies of termal injury. V: The predictability and the significance of thermally induced rate processes leading to irreversible epidermal injury, *Am. J.Pathol.*, **23**, 489-502.
[33] **Romano, V., Rodriguez, R., Altermatt, H.J., Frenz, M. and Weber, H.P.,** 1994. Bone microsurgery with IR-lasers: a comparative study of the thermal action at different wavelengths, *Proc. SPIE*, **2077**, 87-97.
[34] **Svaasand, L.O., Boerslid, T. and Oeveraasen, M.,** 1985. Thermal and optical properties of living tissues, *Lasers Surg. Med.*, 5, 589-602.
[35] **Takata, A.N., Zaneveld, L. and Richter, W.,** 1977. Laser-induced thermal damage in skin, *Aerospace Med., Rep. SAM-TR-77-38*.

[36] **Welch, A.J.,** 1984. The thermal response of laser irradiated tissue, *IEEE J. Qu. Electron.*, **QE-20**, 1471-1481.
[37] **Patterson, M.S., Wilson, B.C. and Wyman, D.R.,** 1991. The propagation of optical radiation in tissue, 1. Models of radiation transport and their application, *Lasers Med. Sci.*, **6**, 155-168.
[38] **Walsh, J.T., Flotte, T.J. and Deutsh, T.F.,** 1989. Er:YAG laser ablation of tissue: effect of pulse duration and tissue type on thermal damage, *Lasers Surg. Med.*, **9**, 314-326.
[39] **Schwarzmaier, H.J., Goldback, T., Yaroslavsky, I.V., Ulrich, F., Bettag, M., Klahn, T. and Kaufmann, R.,** 1995. Optical changes of porcine brain tissue after thermal coagulation, *SPIE*, **2391**, 451-457.
[40] **Burke, L., Rovin, R.A., Cerullo, L.J. and Brown J.T.,** 1985. Thermal effects of the Nd:YAG and carbon dioxide lasers on the central nervous system, *Lasers Surg. Med.*, 5, 67-71.
[41] **Cubeddu, R., Sozzi, C., Taroni, P., Valentini, G., Bottirolli, G., and Croce, A.C.,** 1997. Study of mechanical and thermal damage in brain tissue after ablation by erbium-YAG laser, *Lasers. Med. Sci.*, **12**, 21-30.
[42] **Srinivasan, R. and Mayne-Banton, V.,** 1982. Self-developing photoetching of poly (ethylene terephthalate) films by far-ultraviolet excimer laser radiation, *Appl. Phys. Lett.*, **41**, 576-578.
[43] **Aron-Rosa, D.S., Boerner, C.F., Bath, P., Carre, F., Gross, M., Timsit, J.C., True, L. and Hufnagel, T.,** 1987. Corneal wound healing after laser keratotomy in a human eye, *Am. J. Ophthalmol.*, **103**, 454-464.
[44] **L'Esperance, F. A., Warner, J.W., Telfair, W.B., Yoder, P.R. and Martin, C.A.,** 1989. Excimer laser instrumentation and technique for human corneal surgery, *Arch. Opthalmol.*, **107**, 131-139.
[45] **Fantes, F.E. and Waring, G.O.,** 1989. Effect of excimer laser radiant exposure on uniformity of ablated corneal surface, *Lasers Surg. Med.*, **9**, 533-542.
[46] **Fjodorov, S.N. and Durnev, V.V.,** 1979. Operation of dosaged dissection of corneal circular ligament in cases of myopia of a mild degree, *Ann. Ophthalmol.*, **11**, 1885-1890.
[47] **Keates, R.H., Petrotti, L.S., Weichel, H. and Possel, W.H.,** 1981. Carbon dioxide laser beam control for corneal surgery, *Ophthalmic Surg.*, **12**, 117-122.
[48] **Marshall, J., Trokel, S., Rothery, S. and Schubert, H.,** 1985. An ultrastructural study of corneal incisions induced by an excimer laser at 193 nm, *Ophtalmology*, **92**, 749-758.
[49] **Niemz, M.H., Klancnik, E.G. and Bille, J.F.,** 1991. Plasma-mediated ablation of cornea tissue at 1053 nm using a Nd:YLF oscillator/regenerative amplifier laser, *Lasers Surg. Med.*, **11**, 426-431.
[50] **Niemz, M.H., Hoppeler, T.P., Juhasz, T. and Bille, J.F.,** 1993. Intrastromal ablations for refractive corneal surgery using picosecond infrared laser pulsed, *Lasers Light Ophthalmol.*, **5**, 149-155.
[51] **Puliafito, C.A., Steinert, R.F., Deutsch, T.F., Hillenkamp, F., Dehm, E.J. and Adler, C.M.,** 1985. Excimer laser ablation of the cornea and lens: experimental studies, *Ophthalmology*, **92**, 741-748.
[52] **Niemz, M.H., Loesel, F.H., Fischer, M., Lappe, C. and Bille, J.F.,** 1994. Surface ablation of corneal tissue using UV, green and IR picosecond laser pulsed, *Proc. SPIE*, **2079**, 131-139.

[53] **Stern, D., Schoenlein, R.W., Puliafito, C.A., Dobi, E.T., Birngruber, R. and Fujimoto, J.G.,** 1989. Corneal ablation by nanosecond and femtosecond lasers at 532 nm and 625 nm, *Arch. Ophthalmol.*, **107**, 587-592.
[54] **Wilson, S.E.,** 1990. Excimer laser (193nm) Myopic keratomileusis in sighted and blind human eyes, *Refract. Corneal Surg.*, **6**, 383-385.
[55] **Vogel, A., Busch, S., Jungnickel, K. and Birngruber, R.,** 1994. Mechanisms of intraocular photodisruption with picosecond and nanosecond laser pulses, *Lasers Surg. Med.*, **15**, 32-43.
[56] **Vogel, A., Capon, M.R.C., Asiyo-Vogel, M.N. and Birngruber, R.,** 1994. Intraocular photodisruption with picosecond and nanosecond laser pulses: tissue effects in cornea, lens, and retina, *Invest. Ophtalmol. Vis. Sci.*, **35**, 3032-3044.
[57] **Ross, B.S. and Puliafito, C.A.,** 1994. Erbium-YAG and Holmium-YAG laser ablation of the lens, *Lasers Surg. Med.*, **15**, 74-82.
[58] **Dörschel, K., Berlien, H.-P., Brodzinski, T., Helfmann, J., Müller, G.J. and Scholz, C.,** 1988. Primary results in the laser lithotripsy-clinical use and technical aspects, (Ed.:Steiner, R.) Springer-Verlag, Berlin, Heidelberg, New York.
[59] **Dretler, S.P.,** 1988. Laser lithotripsy: a review of 20 years of research and clinical applications, *Lasers Surg. Med.*, **8**, 341-356.
[60] **Hering, P.,** 1987. Limits of optical fiber systems for pulsed lasers, In: Laser lithotripsy-clinical use and technical aspects (Ed.: Steiner, R.). Springer-Verlag, Berlin, Heidelberg, New York.
[61] **Hofmann, R. and Hartung, R.,** 1987. Clinical experience with laser-induced shock wave lithotripsy. In: Laser lithotripsy-clinical use and technical aspects (Ed.: Steiner, R.). Springer-Verlag, Berlin, Heidelberg, New York.
[62] **Meyer-Schwickerath, G.,** 1956. Erfahrungen mit der Lichtkoagulation der Netzhaut und der Iris, *Doc. Ophthlmol.*, **10**, 91-131.
[63] **Zaret, M.M., Breinin, G.M., Schmidt, H., Ripps, H., Siegel, I.M. and Solon, L.R.,** 1961. Ocular lesions produced by an optical maser (laser), *Science*, **134**, 15-25.
[64] **Marshall, J. and Bird, A.C.,** 1979. A comparative histopathological study of argon and krypton laser irradiations of the human retina, *Br. J. Ophthalmol.*, **63**, 657-668.
[65] **McHugh, J.D.A., Marshall, J., Capon, M., Tothery, S., Raven, A. and Naylor, R.P.,** 1988. Transpupillary retinal photocoagulation in the eyes of rabbit and human using a diode laser, *Lasers Light Ophthalmol.*, **2**, 125-143.
[66] **Mann J.,** 1992. Surgical diode lasers, *J. Clin. Laser Med. Surg.*, **10**, 337-380.
[67] **Mc Hugh, J.D., Marcshall, J., Phytche, T.J., Hamiliton, A.M., Raven, A. and Keeler, C.R.,** 1989. Initial clinical experience using a diode laser in the treatment of retinal vascular disease, *Eye*, **3**, 516-527.
[68] **Sculpher, M.J.,** 1993. A preliminary economic evaluation of the diode laser in ophthalmology, *Lasers Med. Sci.*, **8**, 163-169.
[69] **Kelman, C.D.,** 1967. Phaco-emulsification and aspiration: a new technique of cataract extraction, *Am. J. Ophthalmol.*, **64**, 23-35.
[70] **Schwartz, L.W. and Spaeth, G.L.,** 1980. Argon laser iridotomy in primary angle-closure or pupillary block glaucoma, *Lasers Surg. Med.*, **1**, 153-164.
[71] **Pollack, I.P. and Patz, A.,** 1976. Argon laser iridotomy: an experimental and clinical study, *Ophthalmic. Surg.*, 7, 22-30.
[72] **Cotlair, A.M., Schubert, H.D., Mandek, E.R., and Trokel, S.L.,** 1985. Excimer laser radial keratotomy, *Ophthalmology*, **92**, 206-208.

[73] **Hanna, K.D., Chantang, J.C., Pouliquen, Y., Renard, G., Asfar, L., and Waring, G.O.,** 1988. Excimer laser keratectomy for myopia with a rotating-slit delivery system, *Arch. Ophthalmol.*, **106**, 245-250.
[74] **Lang, G.K., Schroder, E., Koch, J.W., Yanoff, M., and Naumann, G.O.H.,** 1989. Excimer laser keratoplasty. Part I: basic conpects, *Ophthalmic Surg.*, **20**, 262-265.
[75] **Marshall, J., Trokel, S., Rothery, S., and Krueger, R.R.,** 1986. Photoablative reprofiling of the cornea using an excimer laser: photorefractive keratectomy, *Lasers Ophthalmol.*, **1**, 21-48.
[76] **Seiler, T., Bende, T., Wollensak, J., and Trokel, S.,** 1988. Excimer laser keratectomy for correction of astigmatism, *Am. J. Ophtalmol.*, **105**, 117-124.
[77] **Taylor, D.M., L'Esperance, F.A., Del Pero, R.A., Roberts, A.D., Gigstad, J.E., Klintworth, G., Martin, C.A., and Warner, J.,** 1989. Human excimer laser lamellar keratectomy, *Ophthalmology*, **96**, 654-664.
[78] **Trokel, S.L., Srinivasan, R., and Braren, B.A.,** 1983. Excimer laser surgery of the cornea, *Am. J. Ophthalmol.*, **96**, 710-715.
[79] **Stern,, R.H., and Sognnaes, R.F.,** 1964. Laser beam effect on dental hard tissues, *J. Dent.Res.*, **43**, 873.
[80] **Hibst, R., and Keller, U.,** 1989. Experimental studies of the application of the Er:YAG laser on dental hard substances: I. Measurement of the ablation rate, *Laser Surg. Med.*, **9**, 338-344.
[81] **Hibst, R., and Keller, U.,** 1991. Removal of dental filling materials by Er:YAG laser radiation, *Proc. SPIE*, **1200**, 120-126.
[82] **Keller, U., and Hibst, R.,** 1989. Experimental studies of the application of the Er:YAG laser on dental hard substances: II. Light microscopic and SEM investigations, *Lasers Surg. Med.*, **9**, 345-351.
[83] **Melcer, J., Chaumette, M.T., and Melcer, F.,** 1987. Dental pulp exposed to CO_2 laser beam, *Lasers Surg. Med.*, 7, 347-352.
[84] **Steiger, E., Maurer, N., and Geisel, G.,** 1993. The frequency-doubled alexandrite laser: an alternative dental device, *Proc. SPIE*, **1880**, 149-152.
[85] **Visnuri, S.R., Walsh J.T.Jr., and Widgor H.A.,** 1996. Erbium laser ablation of dental hard tissue: effect of water cooling, *Lasers Surg. Med.*, 294-300.
[86] **Weichmann, G., and Johnson, J.,** 1971. Laser use in endodontics. Part II, *Oral Surg.*, **34**, 828-830.
[87] **Bastert, G., and Wallwiener, D.,** 1992. Laser in gynecology-possibilities and limitations, Springer-Verlag, Berlin, Heidelberg, New York.
[88] **Heckmann, U.,** 1992. CO_2-laser excisional conization: five years experience treating cercival intraepithelial neoplasia. In: Lasers in gynecology (Eds.: Bastert, G., Wallwiener, D.), Springer-Verlag, Berlin, G,Heidelberg, New York.
[89] **Bonney, W.W., Fallon, B., Gerber, W.L., Hawtrey, C.E., Loening, S.A., Narayana, A.S., Platz, C.E., Rose, E.F., Sall, J.C., Schmidt, J.D., and Culp, D.A.,** 1982. Cryosurgery in prostatic cancer: survival, *Urology*, **19**, 37-42.
[90] **Mulvaney, W.P., and Beck, C.W.,** 1968. The laser beam in urology, *J. Urol.*, **99**, 112.
[91] **Rosemberg, S.,** 1983. The use of CO_2-laser in urology, *Laser Surg. Med.*, **3**, 152.
[92] **Rothauge, C.F.,** 1980. Urethroscopic recanalization of urethra stenosis using argon laser, *Urology*, **16**, 158-161.

[93] **Staehler, G., Hofsteter, A., Gorisch, W., Keiditsch, E., and Müssiggang, M.,** 1976. Endoscopy in experimental urology using an argon-laser beam, *Endoscopy,* **8,** 1-4

[94] **Abergel, R.P., Meeker, C.A., Dwyer, R.M., and Lesavoy, M.A.,** 1984. Nonthermal effects on Nd:YAG laser on biological functions of human skin fibroblast in culture, *Lasers Surg. Med.,* **3,** 279-284.

[95] **Kaufmann, R., Hartmann, A., and Hibst, R.,** 1994. Cutting and skin ablative properties of pulsed mid-infrared laser surgery, *J. Dermatol. Surg. Oncol.,* **20,** 112-118.

[96] **Kaufmann, R., and Hibst, R.,** 1990. Pulsed 2.94-pm erbium-YAG laser skin ablation-experimental results and first clinical application, *Clin. Exp. Dermatol.,* **15,** 389-393.

[97] **Kaufmann, R., and Hibst, R.,** 1989. Pulsed Er:YAG-and 308 nm UV-Excimer laser: an in vitro and in vivo study of skin-ablative effects, *Lasers Surg. Med.,* **9,** 132-140.

[98] **Svensson, P., Bjerring, P., Arendt-Nielsen, L., Nielsen, J.C., and Kaaber, S.,** 1991. Comparison of four laser types for experimental pain stimulation on oral mucosa and hairy skin, *Lasers Surg. Med.,* **11(4),** 313-24.

[99] **Hibst, R., and Kayfmann, R.,** 1991. Effects of laser parameters on pulsed Er-YAG laser skin ablation, *Lasers Med. Sci.,* **6,** 391-397.

[100] **Apfelberg, D.B., Maser, M.R., and Lash, H.,** 1979. Argon laser treatment of decorative tattoos, *Br. J. Plast. Surg.,* **32,** 141-147.

[101] **Reid, R., and Muller, S.,** 1980. Tattoo removal by CO_2 laser dermabrasion, *Plast. Reconstr. Surg.,* **65,** 717-728.

[102] **Scheibner, A., Kenny, G., White, W., and Wheeland, R.G.,** 1990. A superior method of tattoo removal using the Q-switched ruby laser, *J. Dermatol. Surg. Oncol.,* **16,** 1091-1098.

[103] **Taylor, C.R., Gange, R.W., Dover, J.S., Flotte, T.J. Gonzalez, E., Michaud, N., and Anderson, R.R.,** 1990. Treatment of tattoos by Q-switched ruby laser. A dose response study, *Arch. Determatol.,* **126,** 893-899.

[104] **Charlton, A., Dickinson, M.R., King T.A., and Freemont, A.J.,** 1990. Erbium:YAG and holmium:YAG laser ablations of bones, *Lasers Med.Sci.,* **5,** 365-373.

[104] **Christ, M., Barton, T.G., Hörmann, K., and Foth, H.-J.,** 1995. A new approach to determining laser effects on bone, *Proc. SPIE,* **2327,** 394-401.

[105] **Clayman, L., Fuller, T., and Beckman, H.,** 1978. Healing of continuous-wave and rapid superpulsed carbon dioxide laser-induced bone defects, *J.Oral Maxillofac. Surg.,* **36,** 932-937.

[106] **Forrer, M., Frenz, M., Romano, V., Altermatt, H.J., Weber, H.P., Silenok, A., Istomyn, M., and Konov, V.I.,** 1993. Bone-ablation mechanism using CO_2 lasers of different pulse duration and wavelength, *Appl. Phys.,* **B56,** 104-112.

[107] **Gertzbein, S.D., de Demeter, D., Cruickshank, B., Kapasouri, A.,** 1981. The effect of laser-osteotomy on bone healing, *Lasers Surg. Med.,* **1,** 361-373.

[108] **Gonzales, C., van de Merwe, W.P., Smith, M., and Reinisch, L.,** 1990. Comparison of the erbium-yttrium aluminium garnet and carbon dioxide lasers for in vitro bone and cartilage ablation, *Laryngoscope,* **100,** 14-17.

[109] **Nelson, J.s., Orentein, A., Liaw, L.-H.L., and Berns, M.W.,** 1989. Mid-infrared erbium:YAG laser ablation of bone: the effect of laser osteotomy on bone healing, *Lasers Surg. Med.,* **9,** 362-374.

[110] **Nelson, J.S., Orentein, A., Liaw, L.-H., Berns, L., Zavar, R.B., Gianchandani, S., and Berns, M.W.,** 1989. Ultraviolet 308-nm excimer laser ablation of bone: an acute and chronic study, *Appl. Opt.*, **28**, 2350-2357.
[111] **Nuss, R.C., Fabian, R.L., Sarkar, R., and Puliafito, C.A.,** 1988. Infrared laser bone ablation, *Lasers Surg. Med.*, **8**, 381-392.
[112] **Pao-Chang, M., Xiou-Qui, X., Hui, Z., Zheng, L., and Rui-peng, Z.,** 1981. Preliminary report on the application of CO_2 laser scalpel for operations on the maxillo-facial bones, *Lasers Surg. Med.*, **1**, 375-384.
[113] **Romano, V., Rodriguez, R., Altermatt, H.J., Frenz, M., and Weber, H.P.,** 1994. Bone microsurgery with IR-lasers: a comparative study of the thermal action at different wavelengths, *Proc. SPIE*, **2077**, 87-97.
[114] **Stein, E., Sedlacek, T., Fabian, R.L., and Nishioka, N.S.,** 1990. Acute and chronic effect of bone ablation with a pulsed holmium laser, *Lasers Surg. Med.*, **10**, 384-388.
[115] **Yow, L., Nelson, J.S., and Berns, M.W.,** 1989. Ablation of bone and polymenthyl-methacrylate by an XeCl (308nm) excimer laser, *Lasers Surg. Med.*, **9**, 141-147.
[116] **Bader, M., Dittler, H.J., Ultsch, B., Ries, G., and Siewert, J.R.,** 1986. Palliative treatment of malignant stenoses of the upper gastrointestinal tract using a combination of laser and afterloading therapy, *Endoscopy*, **18**, 27-31.
[117] **Fleischer, D., and Sivak, M.V.,** 1985. Endoscopic Nd:YAG laser therapy as palliation for esophagastric cancer, *Gastroenterology*, **89**, 827-831.
[118] **Hohenberger, W., Altendorf, A., Hermanek, P., and Gall, F.P.,** 1986. The laser in gastroenterology: malignant tumors in the lower gastrointestinal tract-therapeutic alternatives, *Endoscopy*, **18**, 47-52.
[119] **Kiefhaber, P., Nath, G., and Moritz, K.,** 1977. Endoscopical control of massive gastrointestinal hemorrhage by irradiation with a high-power neodymium-YAG laser, *Prog. Surg.*, **15**, 140-155.
[120] **Mathus-Vliegen, E.M.H., and Tygat, G.N.J.,** 1990. Analysis of failures and complications of neodymium:YAG laser photocoagulation in gastrointestinal tract tumors, *Endoscopy*, **22**, 17-23.
[121] **Overholt, B., Panjehpour, M., Tefftellar, E., and Rose, M.,** 1993. Photodynamic therapy for treatment of early adenocarcinoma in Barret's esophagus, *Gastrointest. Endosc.*, **39**, 73-76.
[122] **Rutgeerts, P., Vantrappen, G., Broeckaert, L., Janssesns, J., Coremans, G., Geboes, K., and Schurmans, P.,** 1982. Controlled trial of YAG laser treatment of upper digestive hemorrhage, *Gastroenterology*, **83**, 410-416.
[123] **Sander, R., Poesl, H., Frank, F., Meister, P., Strobel, M., and Spuhler, A.,** 1988. A Nd:YAG laser with a water-guided laser beam–a new transmission system, *Gastrointest. Endosc.*, **34**, 336-338.
[124] **Sander, R., Poesl, H., Zuern, W., Spuhler, A., and Braida, M.,** 1989. The water jetguided Nd:YAG laser in the treatment of gastroduodenal ulcer with a visible vessel- a randomized, controlled and prospective study, *Endoscopy*, **21**, 217-220.
[125] **Coker, N.J., Ator, G.A., Jenklins, H.A., and Neblett, C.R.,** 1986. Carbon dioxide laser stapedotomy: a histology study, *Am. J. Otolaryngol.*, **7**, 253-257.
[126] **Gantz, B.J., Jenkins, H.A., Kishimoto, S., and Fish, U.,** 1982. Argon laser stapedotomy, *Ann. Otol.*, **91**, 25-26.
[127] **Perkins, R.C.,** 1980. laser stapedotomy for otosclerosis, *Laryngoscope*, **90**, 228-240.

[128] **Duncavage, J.A., Ossoff, R.H., and Toohill, R.J.,** 1985. Carbon dioxide laser management of laryngeal stenosis, *Ann. Otol. Rhinol. Laryngol.*, **94**, 565-569.
[129] **Frame, J.W., Das Gupta, A.R., Dalton, G.A., and Rhys Evans, P.H.,** 1984. Use of the carbon dioxide laser in the management of premalignant lesions of the oral mucosa, *J. Laryngol. Otol.*, **98**, 1251-1260.
[130] **Holinger, L.D.,** 1982. Treatment of severe subglottic stenosis without tracheotomy: a preliminary report, *Ann. Otol. Rhinol. Laryngol.*, **91**, 407-412.
[131] **Jako, G.J.,** 1972. Laser surgery of the vocal cords. An experimental study with carbon dioxide lasers on dogs. *Laryndoscope*, **82**, 2204-2216.
[132] **Parkin, J., and Dixon, J.,** 1985. Argon laser treatment of head and neck vascular lesions, *Otolaryngol. Head Neck Surg.*, **93**, 211-216.
[133] **Strong, M.S., Jako, G.J., Vaughan, C.W., Healy, G.B., and Polanyi, T.,** 1976. The use of CO_2 laser in otolaryngology: a progree report, *Trans. Am. Acad. Ophthalmol. Otolarynol.*, **82**, 595-602.
[134] **Strong M.S., Vaughan, C.W., Healy, G.B., Shapshay, S.M., and Jako, G.J.,** 1979. Transoral management of localised carcinoma of the oral cavity using the CO_2 laser, *Laryngoscope*, **89**, 897-905.
[135] **Worthen, D.M. and Wickham, M.G.,** 1974. Argon laser trabeculotomy, *Trans. Am. Acad. Ophthalmol. Otolaryngol.*, **78**, 371-375.
[136] **Herdman, R.C.D., Charlton, A., Hinton, A.E., and Freemont, A.J.,** 1993. An in vitro comparison of the erbium:YAG laser and the carbon dioxide laser in laryngeal surgery, *J. Laryngol. Otol*, **107**, 908-911.
[137] **Ohyama, M., Noberi, T., Moriyama, I., Furuta, S., and Shima, T.,** 1988. Laser thermia on head and neck malignancies: Experimental and clinical studies. *Acta Otolaryngol. Suppl.*, **458**, 7-12.
[138] **Krishnamurthy, S., and Powers, S.K.,** 1994. Lasers in neurosurgery, *Lasers Surg. Med.*, **15**, 126-167.
[139] **Ascher, P.W.,** 1979. Newest ultrastructural findings after the use of CO laser on CNS tissue, *Acta Neurochirur.*, **28**, 572-581.
[140] **Ascher, P.W., and Heppner, F.,** 1984. CO_2-Laser in Neurosurgery, *Neurosurg. Rev.*, 7, 123-133.
[141] **Ascher, P.W., Justich, E., and Schröttner, O.,** 1991. A new surgical but less invasive treatment of central brain tumours. Preliminary report, *Acta Neurochirur. Suppl.*, **52**, 78-80.
[142] **Bailes, J.E., Cozzens, J.W., Hudson, A.R., Kline, D.G., Ciric, I., Gianaris, P., Bernstein, L.P., and Hunter, D.,** 1989. Laser-assisted nerve repair in primates. *J.Neurosurg.*, **71**, 266-272.
[143] **Beck, O.J.,** 1980. The use of the Nd-YAG and the CO_2 laser in neurosurgery, *Neurosurg. Rev.*, **3**, 261-266.
[144] **Boggan, J.E., Edwards, M.S., Davis, R.L., Bolger, C.A., and Martin, N.,** 1982. Comparison of the brain tissue response in rats to injury by argon and carbon dioxide lasers, *Neurosurgery*, **11**, 609-616.
[145] **Fasano, V.A., Urciuoli, R., and Ponzio, R.M.,** 1982. Photocoagulation of cerebral arteriovenous malformations and arterial aneurysms with Nd:YAG and argon laser, *Neurosurgery*, **11**, 754-760.
[146] **Jain, K.K.,** 1984. Current status of laser applications in neurosurgery, *IEEE J. Qu. Electron.*, **QE-20**, 1401-1406.
[147] **Kelly, P.L., Alker, G.J., and Goerss, S.,** 1982. Computer asisted stereotactic laser microsurgery for the treatment of intracranial neoplasma, *Neurosurgery*, **10**, 324-331.

[148] **Neblett, C.R., Morris, J.R., and Thomson, S.,** 1986. Laser-asisted microsurgical anastomasis, *Neurosurgery,* **19**, 914-934.
[149] **Rosomoff, H.L., and Caroll, F.,** 1966. Reaction of neoplasm and brain to laser, *Arch. Neurol.*, **1**, 143-148.
[150] **Stellar, S., Polanyi, T.G., and Bredemeier, H.C.,** 1970. Experimental studies with the carbon dioxide laser as a neurosurgical instrument, *Med. Biol. Eng.*, **8**, 549-558.
[151] **Wharen, R.E., and Anderson, R.E.,** 1984. The Nd:YAG laser in neurosurgery. Part 1: Laboratory investigations-dose related biological response of neural tissue, *J. Neurosurg.*, **60**, 531-539.
[152] **Wharen, R.E., and Anderson, R.E.,** 1984. The Nd:YAG laser in neurosurgery. Part 2: Clinical studies- an adjunctive measure for hemeostasis in reactions of arterio-venous malformations, *J. Neurosurg.*, **60**, 540-547.
[153] **Beck, O.J., Wllske, J., Schonberger, J.L., and Gorsich, W.,** 1979. Tissue changes following application of lasers to the rabbit brain. Result with CO_2 and Neodymium-Yag lasers, *Neurosurg. Rev.*, **1**, 31-36.
[154] **Beck, O.J.,** 1980. The use of the Nd-YAG and the CO2 laser in neurosurgery, *Neurosurger. Rev.*, **3**, 261-266.
[155] **Boggan, J.E., Edwards, M.S., Davis, R.A., Bolger, C.A., and Martin, N.,** 1982. Comparison of the brain tissue response in rats to injury by argon and carbon dioxide lasers, *Neurosurgery*, **11**, 609-616.
[156] **Devaux, B.C., and Roux, F.X.,** 1996. Experimental and clinical standarts, and evolution of lasers in neurosurgery, *Acta Neurochir.*, **138**, 1135-1147.
[157] **Devaux, B., Roux, F.X., Merienne, L., Turak, B., Belliard, H., Leriche, B., and Cloloca, C.,** 1994. Prerequisites for the use of a high power diode laser in stereotactic neurosurgery, *Acta Neurochir.*, **129**(3-4), 230.
[158] **Roux, F.X., Merttienne, L., Cloloca, C., Devaux, B., and Chodklewicz, J.P.,** 1990. Neurosurgical lasers for tumour removal, *Lasers Med. Sci.*, 5, 241-244.
[159] **Roux, F.X.,** 1993. State of the art: neurosurgical lasers for tumour removal through conventional and stereotactical procedures, *Advances Clin. Neurosci.*, **3**, 77-91.
[160] **Gamache, F.W.S., and Morgello, L.,** 1993. The histological effects of the CO_2 versus KTP laser on the brain and spinal cord: A canine model, *Neurosurgery,* **32**, 100-104.
[161] **Gülsoy, M., Çelikel, T., Kurt, A., Canbeyli, R., and Çilesiz, İ.,** 1998. 980-nm-wavelength diode laser application in stereotaxic neurosurgery in the rat, *Proc. SPIE,* **3414**, 17-22.
[162] **Cubeddu, R., Sozzi, C., Taroni, P., Valentini, G., Bottirolli, G., and Croce A.C.,** 1997. Study of mechanical and thermal damage in brain tissue after ablation by erbium-YAG laser, *Lasers Med. Sci.*, **12**, 21-30.
[163] **Cubeddu, R., Sozzi, C., Taroni, P., Valentini, G., Bottirolli, G., and Croce A.C.,** 1994. Ablation of brain by Erbium laser: study of dynamic behavior and tissue damage, *Proceedings of SPIE*, **2077**, 13-20.
[164] **Abella, G., Norman, S., Cohen, R., Feldman, R., Geiger, F., and Conti, C.R.,** 1982. Effects of carbon dioxide, Nd-YAG and argon laser radition on coronary atheromatous plaque, *Am. J.Cardiol.*, **50**, 1129-1205.
[165] **Austin, G.E., Ratliff, N.B., Hollman, J., Tabei, S., and Phillps, D.F.,** 1985. Intimal proliferation of smooth muscle cells as an explanation for recurrent coronary artery stenosis after percutaneous transluminal coronary angioplasty, *J. Am. Coll. Cardiol.*, **6**, 369-375.

[166] **Choy, D.S.J., Stertzer, S.H., Rotterdam, H.Z., and Bruno, M.S.,** 1982. Laser coronary angioplasty; experience with 9 cadaver hearts, *Am. J. Cardiol.*, **50**, 1209-1211.
[167] **Choy, D.S.J., Stertzer, S.H., Myler, R.K., Marco, J., and Fournial, G.,** 1984. Human coronary laser recanalization, *Clin. Cardiol.*, 7, 377-381.
[168] **Grundfes, W.S., Litvack, F., Forrester, J.S., Goldenberg, T., Swan, H.J.C., Morgenstern, L., Fishbein, M., McDermid, S., Rider, D.M., Pacala, T.J., and Laudenslager, J.B.,** 1985. Laser ablation of human atherosclerotic plaque without adjacent tissue injury, *J. Am. Coll. Cardiol.*, 5, 929-933.
[169] **Grüntzig, A.,** 1978. Transluminal dilatation of coronary- artery stenosis, *Lancet*, **1**, 263.
[170] **Grüntzig, A.R., Senning, A., and Siegenthaler, W.E.,** 1979. Nonoperative dilatation of coronary stenosis, *N. Engl. J. Med.*, **301**, 61-68.
[171] **Grüntzig, A.R., and Meier, B.,** 1983. Percutaneous transluminal coronary angioplasty. The first five years and the future, *Int. J. Cardinol.*, **2**, 319- 323.
[172] **Horvath, K.A., Smith, W.J., Laurence, R.G., Schoen, F.J., Appleyard, R.F., and Cohn, L.H.,** 1995. Recovery and viability of an acute myocardial infarct after transmyocardial laser revascularization, *J. Am. Coll. Cardiol.*, **25**, 258-263.
[173] **Karsch, K.R., Haase, K.K., Wehrmann, M., Hassenstein, S., and Hanke, H.,** 1991. Smooth muscle cell proliferation and restenosis after stand alone coronary excimer laser angioplasty, *J. Am. Coll. Cardiol.*, **17**, 991-994.
[174] **Sanborn, T.A., Faxon, D.P., Kellet, M.A., and Ryan, T.J.,** 1986. Percutaneous coronary laser thermal angioplasty, *J. Am. Coll. Cardiol.*, **8**, 1437-1440.
[175] **Tierstein, P.S., Warth, D.C., Haq, N., Jenkins, M.S., McCown, L.C., Aubanle-reidel, P., Morris, N., and Ginsburg, R.,** 1991. High speed rotational atherectomy for patients with diffuse coronary artery disease, *J. Am. Coll. Cardiol.*, **18**, 1694-1701.
[176] **Waller, B.F.,** 1983. Early and late morphological changes in human coronary arteries after percutaneous transluminal coronary angioplasty, *Clin. Cardiol.*, **6**, 363-372.
[177] **Whittaker, P., Kloner, R.A., and Przyklenk, K.,** 1993. Laser-mediated transmural myocardial channels do not salvage acutely ischemic myocardium, *J. Am. Coll. Cardional.*, **22**, 302-309.
[178] **Jacques, S.L., and Wang, L.,** 1995. Monte Carlo modelling of light transport in tissues in *Optical-Thermal Response of Laser-Irradiated Tissue*, pp. 73-99, Eds Welch A.J. & van Gemert M.J.C., Plenum Press, New York.
[179] **Graaff, R., Koelink, M.H., de Mul, F.F.M., Zijlstra, W.G., Dassel, A.C.M., and Aarnoudse, J.G.,** 1993. Condensed Monte Carlo simulations for the description of light transport, *Appl. Opt.*, **32**, 426-434.
[180] **Wilson, B.C., and Adam, G.,** 1983. A Monte Carlo model for the absorption and flux distributions of light in tissue, *Med. Phys.*, **10**, 824-830.
[181] **Gülsoy, M., Kurt, A., and Çilesiz, İ.,** 1998. Monte Carlo simulation of Nd:YAG laser fluence distribution in human tissue, *Proceedings of IEEE 2nd International Biomedical Engineering Days*, Istanbul, 60-62.
[182] **Gülsoy, M., Çelikel, T., Kurt, A., and Çilesiz, İ.,** 1997. Monte Carlo Simulation of Nd:YAG Laser on Cardiac Tissue, *National Meeting of Biomedical Engineering,BIYOMUT'97*, 130-132.

[183] **Roggan, A., Albrecht, H., Dörschel, K., Minet, O., and Müller, G.,** 1995. Experimental set up and Monte Carlo model for the determination of optical tissue properties in the wavelength range 330-1100 nm, *Proc. SPIE,* **2323**, 21-36.
[184] **Splinter, R., Svenson, R.H., Littmann, L., Tuntelder, J.R., Chuang, C.H., Tatsis, G.P., and Thompson, M.,** 1991. Optical properties of normal, diseased, and laser photocoagulated myocardium at the Nd:YAG wavelength, *Lasers in Surgery and Medicine*, **11**, 117-124.
[185] **Gülsoy, M., Çelikel, T., Sennaroğlu, A., Çilesiz, I., and Kurt A.,** 1996. Coagulation of Cardiac Tissue by Nd:YAG Laser, *BIYOMUT'96 National Meeting of Biomedical Engineering*, 80-82.
[186] **Gülsoy, M., Çelikel, T., Çilesiz, I., and Kurt A.,** 1996. Ablation of Cardiac Tissue by Er:YAG Laser, *BIYOMUT'96 National Meeting of Biomedical Engineering*, 83-85.
[187] **Silverman, J.,** 1992. Integration of New Technology into General Medical Practice, *Laser Angioplasty*, Ed. Ginsburg R. & Geschwind.
[188] **Watanabe, G., Mukai, A., Misaki, T., Tsubota, M., and Iwa, T.,** 1990. Thermally controlled laser irradiation of the myocardium with intraoperative ultrasound monitoring, *Pace*, **13**, 653-662.
[189] **Splinter, R., Littmann, L., Svenson, R.H., Tuntelder, J.R., Chuang, C.H., Thompson, M., and Tatsis, G.P.,** 1992. Can cw Nd:YAG photocoagulation lesion dimensions in myocardium be predicted by Monte Carlo light propagation simulations, *J. Clin. Eng.*, **17(5)**, 409-418.
[190] **Selle, J.G., Svenson, R.H., Sealy, W.C., Gallagher, J.J., Zimmern, S.H., Fedor, J.M., Marroum, M.C., and Robicsek, F.,** 1986. Successful clinical laser ablation of tachycardia: a promising new therapeutic method, *Ann. Thorac. Surg.* **42**, 380-384.
[191] **Splinter, R., Semenov, S.Y., Nanney, G.A., Littmann, L., Tuntelder, J.R., Svenson, R.H., Chuang, C.H., and Tatsis G.P.,** 1995. Myocardial temperature distribution under cw Nd:YAG laser irradiation in in vitro and in vivo situations: theory and experiment, *Appl. Opt.*, **34 (3)**, 391-399.
[192] **Burke, L., Rovin, R.A., Cerullo. L.J., and Brown, J.T.,** 1985. Thermal effects of the Nd:YAG and carbon dioxide lasers on the central nervous system, *Lasers Surg. Med.*, 5, 67-71.
[193] **Cecchetti, W., Guazzieri, S., Tasca, A., and Martelucci, S.,** 1996. 980 nm High Power Diode Laser in Surgical Applications, in *Biomedical Optical Instrumentation and Laser-Assisted Biotechnology*, pp. 227-230, Eds. Scheggi, A.M., Martellucci, S., Chester, A.N., and Pratesi, R., Kluwer Academic Publishers, Erice.
[194] **Lombard, G.F., Benech, F., Tealdi, S., and Ponzio, R.M.,** 1982. Thermal effects on nervous human tissues under electro or laser surgery, *J. Neurosurg. Sci.*, **26**, 265-271.
[195] **Devaux, B.C., Roux, F.X., Nataf, F., Turak, B., and Cioloca, C.,** 1988. High-power diode laser in neurosurgery: clinical experience in 30 cases, *Surg. Neurol.*, **50**, 33-40.
[196] **Nagatani, T., Saito, K., and Yoshida, J.,** 1997. Experimental use of semiconductor diode laser for neuroendoscopic surgery, *Minim. Invas. Neurosurg.*, **40**, 98-100.
[197] **Kou, L., Labrie D., and Chylek, P.,** 1993. Refractive indices of water and ice in the 0.65-to 2.5μm spectral range, *Applied Optics*, **32**(19), 3531-3540.
[198] **Paxinos, G., and Watson, C.,** 1986. The Rat Brain, in *Stereotaxic Coordinates*, Academic Press, New York.

[199] **Bromm, B., and Lorenz, J.,** 1998. Neurophysiological evaluation of pain. *Electroencephalography and clinical Neurophysiology*, **107**, 227-253.
[200] **Chen, A.C.N., Arendt-Nielsen, L., and Plaghki, L.,** 1998. Laser evoked potentials in human pain. I. Use and possible misuse, *Pain Forum*, **7(4),** 174-184.
[201] **Chen, A.C.N., Arendt-Nielsen, L., and Plaghki, L.,** 1998. Understanding of human pain in the brain through topographic mapping and quantification of laser-evoked potentials. An integration, *Pain Forum*, **7(4),** 196-200.
[202] **Kakigi, R., and Watanabe, S.,** 1998. Pain-related somatosensory-evoked potentials following CO_2 laser stimulation, *Pain Forum*, **7(4),** 185-187.
[203] **Towell, A.D., and Boyd, S.G.,** 1993. Sensory and cognitive components of the CO_2 laser evoked cerebral potential, *Electroencephalography and clinical Neurophysiology*, **88**, 237-239.
[204] **Treede, R.-D., Magerl, W., and Baumgartner, U.,** 1998. Laser-evoked potentials for assessment of nociceptive pathways in humans. *Pain Forum*, **7(4)**, 191-195.
[205] **Treede, R.-D.,** 1994. Evoked potentials related to pain. Touch, temperature and pain in Health and disease: Mechanisms and Assessments, in *Progress in pain research and management*, Vol. 3., pp. 473-489, eds, Bovie, J., Hansson, P., and Lindblom, U., IASP Press, Seattle.
[206] **Zaslansky, R., Sprecher, E., and Yarnitsky, D.,** 1998. What do pain-evoked potentials really measure? Revisited, *Pain Forum*, **7(4),** 188-190.
[207] **Towell, A.D., Purves, A.M., and Boyd, S.G.,** 1996. CO_2 laser activation of nociceptive and non-nociceptive thermal afferents from hairy and glabrous skin, *Pain*, **6**, 79-86.
[208] **Svensson, P., Bjerring, P., Arendt-Nielsen L., and Kaaber, S.,** 1992. Quantitative determinations of sensory and pain thresholds on human oral mucosa by argon laser stimulation, *Pain*, **49**, 233-239.
[209] **Svensson, P., Beydoun, A., Morrow, T.J., and Casey K.L.,** 1997. Human intramuscular and cutaneous pain: psychophysical comparisons, *Exp. Brain. Res.*, **114**, 390-392.
[210] **Svensson, P., Rosenberg, B., Beydoun, A., Morrow, T.J., and Casey, K.L.,** 1997. Comparative psychophysical characteristics of cutaneous CO_2 laser and contact heat stimulation, *Somatosensory & Motor Res.*, **14(2)**, 113-118.
[211] **Gülsoy, M., Çelikel, T., Kurtkaya, Ö., Sav, A., Kurt, A., Canbeyli, R., and Çilesiz, İ.,** 1999. Application of the 980 nm diode laser in stereotaxic surgery, *IEEE Selected Topics in Quantum Electronics*, **5(4)**, 1090-1094.
[212] **Schwab, M., Bauer, R., and Zwiener, U.,** 1997. The Distribution of normal brain water content in Wistar rats and its increase due to ischemia, *Brain Res.*, **21**; 749(1), 82-87.
[213] **Skinner, J.E.,** 1971. Neuroscience: A Laboratory Manual, Saunders Company, Toronto.

APPENDIX A: MONTE CARLO SIMULATION TECHNIQUE

The transport of an infinitely narrow photon beam incident on an infinitely wide tissue in the cylindrical coordinates (r,z) was simulated by Monte Carlo Simulation Program. This program available over the internet (www.laser.mda.uth.tmc.edu/lihong.htm) calculates the statistical distribution of photon propagation at a specific wavelength by simulating the the random walk of a finite number of photons. The photon fluence is obtained by convolving the photon absorption. The theoretical background of the model applied was described by Jacques et al. [178] and utilized by various researchers in previous studies [179-180].

Monte Carlo method is a numerical solution to the following transport equation.

$$\frac{dJ(\mathbf{r},\mathbf{s})}{ds} = -\alpha_t J(\mathbf{r},\mathbf{s}) + \frac{\alpha_s}{4\pi}\int_{4\pi} p(\mathbf{s},\mathbf{s}')\, J(\mathbf{r},\mathbf{s}')\, d\omega' \qquad (A.1)$$

$J(\mathbf{r},\mathbf{s})$ is the power flux density in a specific direction **s** within a solid angle $d\omega$ and called radiance in units of W cm^{-2} sr^{-1}. The total attenuation coefficient and scattering coefficient are denoted by μ_t and μ_s respectively. Thus the change in radiance due to an infinitesimal path length ds is the sum of radiance in a solid angle dw in proportion with $p(\mathbf{s}, \mathbf{s}')$, the phase function of a photon to be scattered from direction **s'** into **s**.

In Figure A.1. the flow chart of Monte Carlo simulation is given. First, photons are generated at the surface of the medium with a weight of unity first. In the second step, the distance to the first collision is determined and the photon is moved in the medium containing randomly distributed absorbing and scattering particles. Then program checks wether the photon is still in the medium or not. If it is not in the medium, there are two alternatives: (1) photon may escape from the medium then the program updates the reflection or transmission and goes to the end of the routine, if it is the last photon task ends, if it is not, another photon is initialized. (2) the photon

may be internally reflected, then, it means that the photon is in the medium. If it is decided that the photon is in the medium, weight of the photon is decreased due to absorption. The remaining photon weight is scattered and the same procedure is held until the weight becomes less then a certain treshold value. Program runs until the last photon is "extinguished".

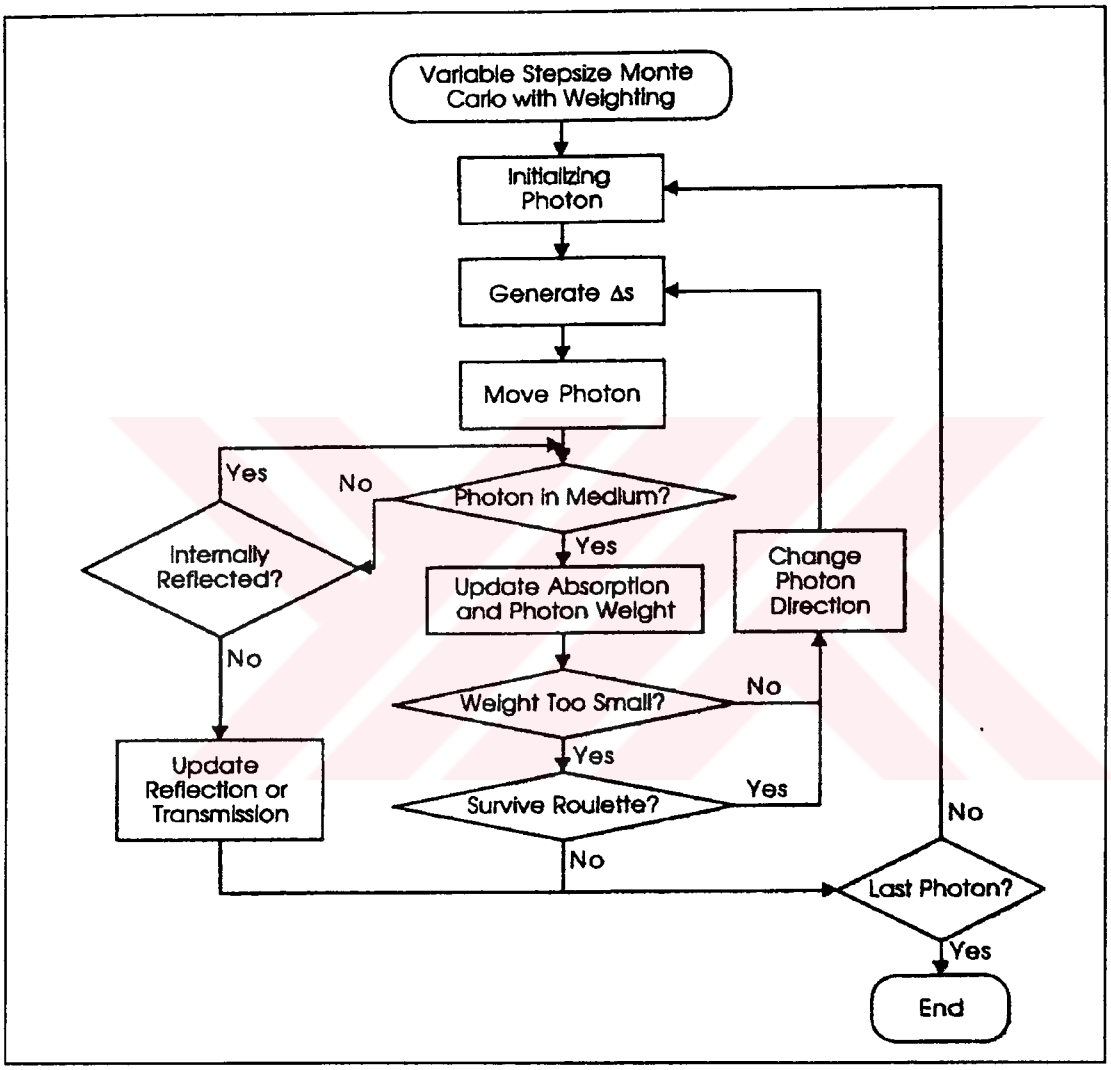

Figure A.1. Flow chart of the Monte Carlo simulation program [178].

Semi-infinite tissue layer is described by the following parameters: thickness (d), refractive index (n), absorption coefficient (μ_a), scattering coefficient (μ_s), and anisotropy factor (g). Absorption coefficient is defined as the probability of photon absorption per unit infinitesimal pathlength, and scattering coefficient is defined as the probability of photon scattering per unit infinitesimal pathlength. The anisotropy factor is the average cosine value of the deflection angle.

Besides the parameters describing the tissue, the following data are input parameters of the program:

- Number of photons,
- Grid line separations (Δr, Δz)
- Number of grid elements (#Δr, #Δz, #Δa).

In Monte Carlo method applied in the present studies, the response to an infinitely narrow photon beam on the surface of a tissue is calculated for simplicity. However, in real cases laser beam has always a finite size. Because this system is linear (i.e. if the input intensity is multiplied by a factor then the responses will be multiplied by the same factor) and invariant (i.e. when the input beam is shifted horizontally by a distance in a certain direction then the responses will be shifted in the same way), the response of the finite size photon beam can be calculated by the convolution of the response to the infinitely narrow photon beam which is assumed as a Green's function of the tissue system. So the resulting fluence distribution can be calculated by inputting the source function (e.g. Gaussian beam).

In the present study the Monte Carlo simulation and convolution programs developed by Wang and Jacques is used [178].

APPENDIX B: LASER SYSTEMS

B.1. Nd:YAG Laser

The Nd:YAG laser (Quantronix Series 100 Lasers) located in the Laser Laboratory of the Physics Department in Koç University was used. It is configured for CW (continuous wave), 1064 nm wavelength laser emission. The laser uses an Nd:YAG crystal rod as the source of photon emissions. Yttrium Aluminum Garnet (YAG) is the host material for the active element, neodymium, whose Nd ions emit 1064 nm wavelength photons. The maximum power output is 12 Watts at TEM_{00} mode. The Nd:YAG crystal is placed between two adjustable mirrors. A water cooling unit serves to cool down the laser system.

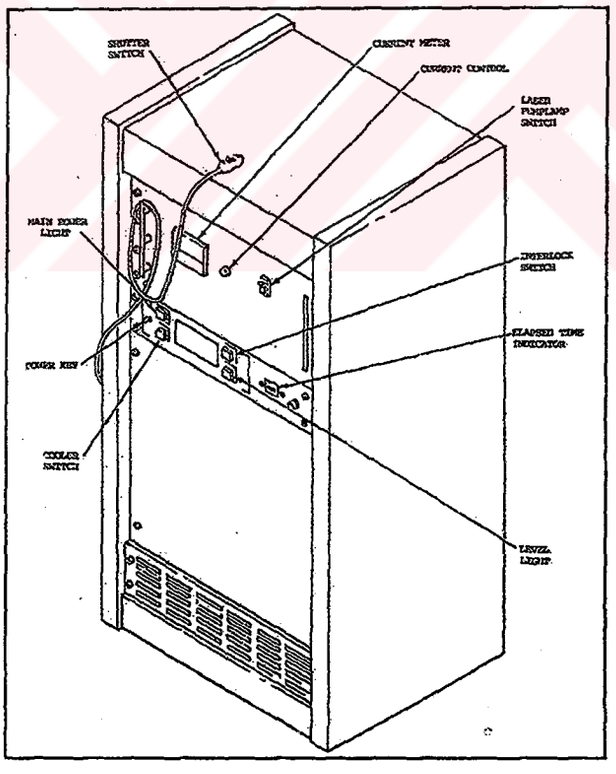

Figure B.1. Front panel controls of Quantronix Series 100 Lasers.

The laser system is adjusted via front panel controls: When the power key is turned on it applies 117 VAC to the front panel lamps and to the interlocks via the cooler switch (Figure B.1.). Cooler switch, switches power to the interlock relays. When it is pressed, its lamp illuminates and 117 VAC is applied to the interlock switch.

Interlock switch starts the cooler pump, overrides the system interlocks when pressed. This allows the pump to develop sufficient flow to satisfy the flow switch. After the flow switch satisfied, the pump will run even when the interlock switch is released, and the interlock switch lamp will go out. If the lamp illuminates during normal operation, it indicates either a water flow, level or temperature malfunction. Level light illuminates when the water level in the reservoir is too low. Elapsed time indicator provides an indication of the number of hours the pump has been running, but not necessarily the number of hours the system has been lasing. Shutter switch opens and closes the intracavity shutter to interrupt lasing. Laser pumplamp switch turns on the power supply for the laser pump. Current control adjusts laser power level by altering the current to the pumplamp. Current meter monitors current applied to the pumplamp.

B.2. Er:YAG Laser

The Er:YAG laser system used was supplied by Teknofil Ltd. Sti. for the studies presented in this manuscript. The Er:YAG laser (TULAMASHZAVOD, Ertula Surgical Based Device) emits radiation at 2.94 μm wavelength. Laser pulses have the energy levels of 0.3, 0.5, and 1.0 J as set by the manufacturer; exposure time per pulse is 150 μsec. The The corresponding average power densities are 37.7 J/cm^2, 62.9 J/cm^2, and 125.8 J/cm^2, respectively.

Er:YAG laser system basically consists of a resonant cavity, the erbium crystal between two adjustable mirrors and the pumping flash lamp located inside the cavity (Figure B.2). There is a power supply to deliver energy to the flash lamp and an optical system for focusing the laser light. Optical system consists of a cylindrical lens and two guiding light sources. diameters of the eliptical spotsize are 0.75mmx1.35mm.

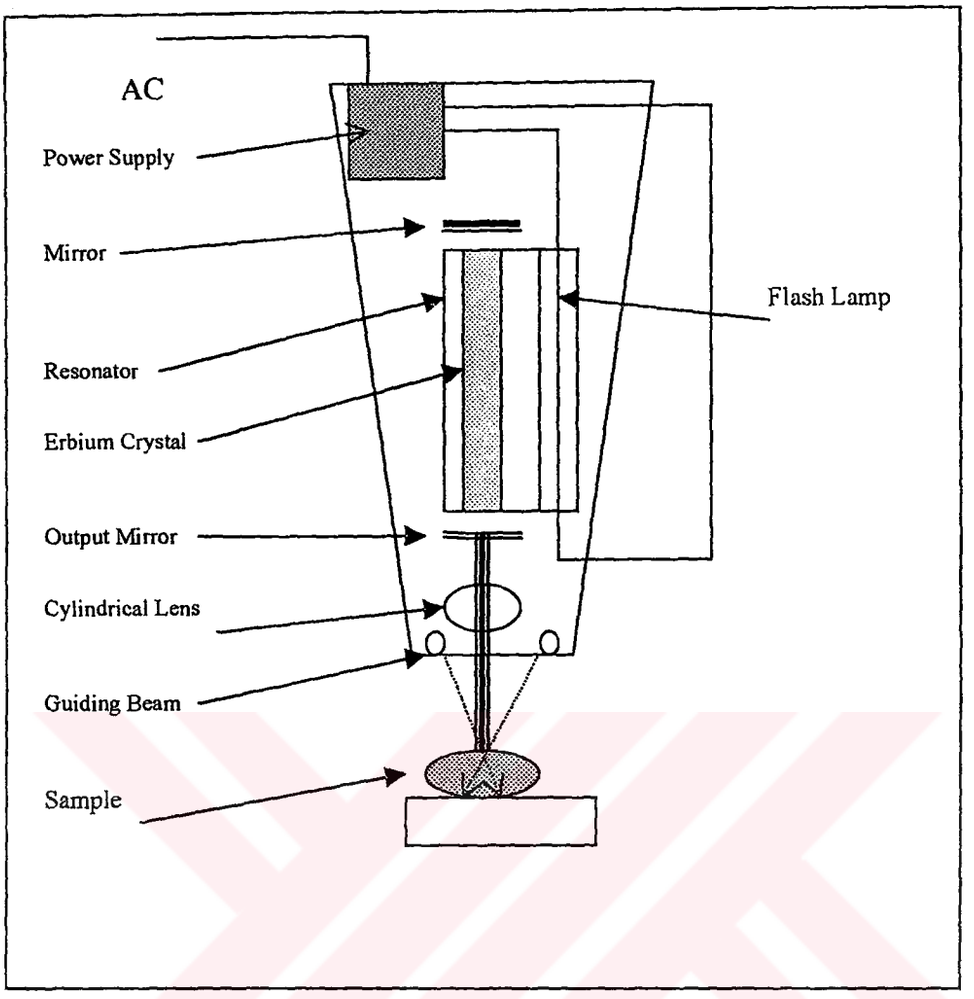

Figure B.2. Er:YAG Laser set up.

B.3. Diode Laser

In this part the technical specifications of the Opto Power OPC-D010-980-FCPS laser is given.

The Opto Power OPC-D010-980-FCPS is a custom ordered high power diode laser system capable of emitting 10 Watts (up to 15 Watts) of continuous wave (cw) near-infrared energy at 980 nm. The OPC system provides output through a 1 m. fiber optic cable. Technical specifications are given in Table B.1.

The Opto Power OPC-D010-980-FCP has a controller module (The OPC Remote Control) which allows the user to set diode temperature and diode current (Figure B.3.).

Laser beam can be turned on and off from this controller manually. Actual temperature and diode current values can be monitored through two liquid crystal displays on the controller.

Table B.1. Technical specifications of the Opto Power OPC-D010-980-FCPS (Integrated Diode Laser Units with OPC Model Numbers FCPS, HBPS, CSPS, FCHS & HBHS User's Manual, October 1997, Opto Power Corporation)

Output power	10 W, nominal	**Humidity**	5% to 95%
Weight	12 pounds, nominal	**Input Power**	220Vac, 50 Hz; 6A (<175 W)
Cooling Requirements	None required	**Beam Characteristics**	Semiconductor, multimode
Delivery Optical Fiber Bundle	250μm diameter	**Beam Divergence ($1/e^2$)**	21° cone
Delivery Fiber Length	1 m	**Diode Laser Center Wavelength**	980 nm
Delivery Fiber Termination	SMA 905 connector	**Center Wavelength Tolerance**	± 5 nm
Typical Operating Temperature	15°C to 35°C	**Center Wavelength; User Adjustable**	± 3 nm
Typical Storage Temperature	-30°C to 80°C	**WavelengthTemperature Coefficient**	0.27 to 0.30 nm/°C
Emission Bandwidth (FWHM)	< 3 nm		

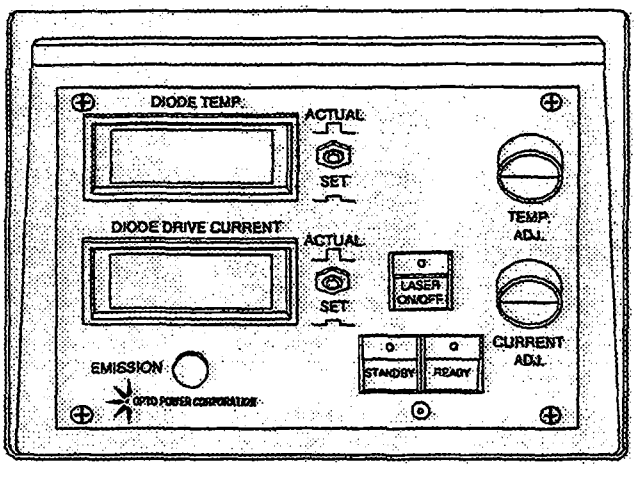

Figure B.3. OPC Remote Control module of the diode laser system

C. Power Measurements

Two types of powermeters are used during the experiments:

1. Synrad Powerwizard: It is a small size powermeter with a measurement range of 0-250 W. Laser output power was measured before and after all trials of laser shot. It is important to check the output because of possible damage that may occur on the tip of the optical fibers used. In the case of inefficiency, the damaged tip of fiber is cut by a tungsten knife.

2. Coherent Ultima Labmaster: It is a power and energy measuring and analyzing system for cw, single pulse and repetitive pulse laser systems coupled with one of the Coherent Smartsensors detector head. This system measures the irradiating power in a spectral range of 0.25-10.6 μm, with an accuracy of ±4%, with a power resolution of 0.1 W within the range of 1-100 W. The range of measured energy is between 0.5-50 J with maximum pulse length of 0.3 s. This system was used to measure the diode laser fiber output power and to calibrate the output power with respect to diode laser driver current (Figure C.1.).

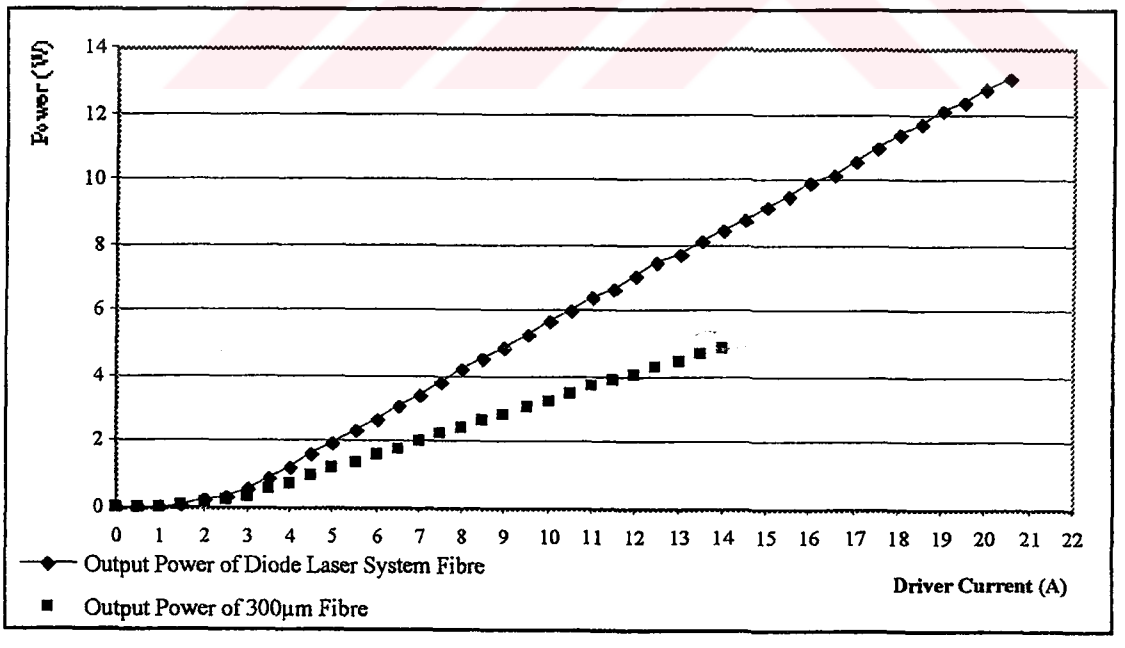

Figure C.1. The measured output power of diode laser system.

VITAE

Murat Gülsoy received his BS and MA degrees in electrical engineering and in psychology from Boğaziçi University, Istanbul, TURKEY, in 1989 and 1992, respectively. He studied evoked brain potentials for his Master's research. He completed his doctoral research on thermal aspects of laser-tissue interactions in the Biomedical Engineering Program at Istanbul Technical University, in January 2000. He is also a lecturer with the Institute of Biomedical Engineering at Boğaziçi University.